

# Mobile Robots with In-Situ and Remote Sensors for Real World Gas Distribution Modelling

*To my parents, my sister and  
all the rest of my family*

*Örebro Studies in Technology 64*



VÍCTOR MANUEL HERNÁNDEZ BENNETTS

**Mobile Robots with In-Situ and Remote Sensors for Real  
World Gas Distribution Modelling**

© Víctor Manuel Hernández Bennetts, 2015

*Title:* Mobile Robots with In-Situ and Remote Sensors for Real World Gas  
Distribution Modelling

*Publisher:* Örebro University 2015  
[www.publications.oru.se](http://www.publications.oru.se)

*Print:* Örebro University, 12/2014

ISSN 1650-8580  
ISBN 978-91-7529-055-3

## Abstract

Víctor Manuel Hernández Bennetts (2015): Mobile Robots with In-Situ and Remote Sensors for Real World Gas Distribution Modelling. Örebro Studies in Technology 64.

This thesis work addresses the task of gas distribution modelling using mobile robots equipped with gas sensors. Gas Distribution Modelling (GDM) is the artificial olfaction task of creating spatio temporal representations of the observed gas distribution from a set of relevant variables such as gas concentration measurements. The use of mobile robots in gas sensing related tasks can bring several advantages over conventional methods such as manual inspection routines or fixed sensing networks. For example, the collection of measurements at industrial facilities can be automatized, hazardous areas can be inspected without exposing human personnel and in emergency scenarios, mobile robots can be rapidly deployed to assist first responders. In these scenarios, GDM is highly relevant since the estimated models can be used to locate gas leaks, identify hazardous areas with high concentration levels and they can be used as inputs for models that predict long term emission patterns at a given facility.

The contributions presented in this thesis are three-fold. First, a set of algorithms is proposed for GDM with in-situ sensors. These algorithms are designed for real world environments, where multiple chemical compounds are commonly present. The limitations of the sensors are addressed by combining different sensing technologies such as metal oxide sensors and photo ionization detectors. In this way multiple distribution models, one for each identified compound, are generated. Second, the use of emergent gas sensing technologies is explored in the context of GDM. Robot assisted gas tomography, which combines tomographic reconstruction algorithms with a mobile robot equipped with remote sensors is first proposed in this thesis. Third, the feasibility of using mobile robots to monitor methane emissions from landfill sites is evaluated. A proof of concept platform that implements robot assisted gas tomography was developed to inspect large environments in order to estimate gas distribution models. The results of this evaluation show that the algorithms presented in this thesis work represent a major step towards a fully autonomous robot that can operate in complex, real world environments.

*Keywords:* Mobile Robotics Olfaction, Gas Sensors, Gas Discrimination, Gas Distribution Mapping, Tomography of Gases, Service Robots, Environmental Monitoring.

Víctor Manuel Hernández Bennetts, School of Science and Technology  
Örebro University, SE-701 82 Örebro, Sweden, victor.hernandez@oru.se



# Acknowledgments

First, I would like to express my gratitude to my supervisor, Prof. Achim Lilienthal, for his valuable comments, guidance and for giving me the opportunity to conduct my PhD studies at the MRO lab. I would also like to thank my co-supervisors, Dr. Marco Trincavelli and Dr. Erik Schaffernicht, for all the advices, guidance and feedback they provided me during my studies.

Certainly this thesis would not have been possible without the support of many of my colleagues. Many thanks to Per Sporrong and Bo Lennart Silfverdal, for their extraordinary technical support; to Dr. Todor Stoyanov and Dr. Henrik Andreasson for sharing their robot localisation expertise; to Ali Abdul Khaliq, for his outstanding effort during the preparation of the 2012 Gasbot Demo and to Ingela Fransson, Jenny Tiberg and Barbro Alvin, for helping me with the administrative side of my studies. A special recognition goes to Dr. Patrick Neumann, Dr. Matthias Bartholmai and Dr. Víctor Pomareda Sesé, with whom I co-authored several publications.

Many thanks to my closest friends Athanasia, Pieter, Ahmed, Prashanth, Lía, Eirini, Angy, Erik and Mehmet for the great moments, moral support and fruitful discussions.

Finally, I would like to thank my family, for the unconditional support they have always provided me with. No matter the distance, I can always count with them.

This work was financed by Robotdalen (Gasbot, project number 8140) and supported by Clearpath Robotics, through its 2012 Partnerbot Programme. The Partnerbot programme provided the Gasbot research team with a Husky A-200 robotic platform.





# Contents

<b>1</b>	<b>Introduction</b>	<b>1</b>
1.1	Mobile Robotics Olfaction . . . . .	1
1.2	Towards Real World Applications with MRO Systems . . . . .	3
1.2.1	An Example Scenario . . . . .	4
1.3	Scope of this Thesis . . . . .	5
1.3.1	Outline . . . . .	6
1.3.2	Contributions . . . . .	7
1.3.3	Publications . . . . .	7
<b>2</b>	<b>Mobile Robotics Olfaction</b>	<b>11</b>
2.1	Gas Sensing Technologies . . . . .	13
2.1.1	In-situ Gas Sensors . . . . .	13
2.1.2	Remote gas sensors . . . . .	16
2.2	Mobile Robotics Olfaction Tasks . . . . .	19
2.2.1	Gas Detection . . . . .	20
2.2.2	Gas Quantification . . . . .	22
2.2.3	Gas Discrimination . . . . .	23
2.2.4	Gas Distribution Modelling . . . . .	24
2.3	Gas Source Localisation . . . . .	24
2.3.1	Early Works and Diffusion Dominated Approaches . . . . .	25
2.3.2	Turbulence Dominated Algorithms . . . . .	25
2.4	Are Bio-inspired MRO Algorithms Suitable for Realistic Applications? . . . . .	30
2.4.1	Robotic Platforms . . . . .	30
2.4.2	Experimental Scenarios . . . . .	32
2.4.3	Environment and Sensor Characterization . . . . .	34
2.4.4	A Statistical Approach to Detect Gas Leaks . . . . .	39
2.5	Conclusions . . . . .	41

<b>3</b>	<b>Gas Discrimination with Mobile Robots</b>	<b>43</b>
3.1	E-Nose Architecture . . . . .	44
3.1.1	Sampling and Delivery System . . . . .	45
3.1.2	Sensor Array . . . . .	46
3.1.3	Pattern Recognition Block . . . . .	47
3.1.4	Feature Selection . . . . .	48
3.1.5	Classification . . . . .	49
3.2	Applications of E-Nose Technologies . . . . .	49
3.2.1	Gas Discrimination Under Laboratory Conditions . . . . .	49
3.2.2	Gas Discrimination in uncontrolled environments . . . . .	50
3.2.3	Gas Discrimination with Mobile Robots . . . . .	52
3.3	A Gas Discrimination Algorithm for Uncontrolled Environments	53
3.3.1	Signal pre-processing . . . . .	56
3.3.2	Feature Extraction . . . . .	56
3.3.3	Feature Selection . . . . .	56
3.3.4	Classification Algorithm . . . . .	57
3.3.5	Experimental validation . . . . .	59
3.4	Conclusions . . . . .	65
<b>4</b>	<b>Gas Distribution Modelling With In-Situ Gas Sensors</b>	<b>67</b>
4.1	Model Based GDM Approaches . . . . .	68
4.2	Model Free GDM Approaches . . . . .	69
4.3	The Kernel DM+V Algorithm . . . . .	71
4.4	Towards Online Parameter Selection for Gas Distribution Map- ping . . . . .	73
4.4.1	Parameter Selection for Kernel DM+V . . . . .	73
4.4.2	Virtual Leave One Out CV for Bandwidth Selection . . . . .	74
4.4.3	Evaluation . . . . .	75
4.5	Gas Distribution Mapping of Multiple Heterogeneous Chemical Compounds . . . . .	78
4.5.1	Parameter Selection for Multi Compound Gas Distribu- tion Maps . . . . .	81
4.5.2	Evaluation . . . . .	82
4.6	Conclusions . . . . .	86
<b>5</b>	<b>Gas Distribution Modelling With Remote Gas Sensors</b>	<b>89</b>
5.1	Computed Tomography of Gases . . . . .	90
5.2	Towards Robot Assisted Gas Tomography . . . . .	94
5.3	Gasbot: Robot Assisted Gas Tomography for Landfill Monitoring	96
5.3.1	Landfill Site Monitoring . . . . .	96
5.3.2	The Robotic Prototype Gasbot . . . . .	98
5.3.3	Evaluation . . . . .	105
5.4	Conclusions . . . . .	112

<b>6</b>	<b>Conclusions</b>	<b>115</b>
6.1	Contributions . . . . .	115
6.2	Limitations . . . . .	117
6.3	Future Research Directions . . . . .	118
<b>A</b>	<b>Experimental Scenarios</b>	<b>121</b>
A.1	Experiments with In-Situ Sensors . . . . .	121
A.1.1	Robot Arena . . . . .	121
A.1.2	Indoor Corridor . . . . .	122
A.1.3	Outdoor Courtyard I . . . . .	122
A.1.4	Open Field . . . . .	123
A.1.5	Outdoor Courtyard II . . . . .	123
A.2	Experiments with Remote Sensors . . . . .	124
A.2.1	Underground Corridor . . . . .	124
A.2.2	Decommissioned Landfill Site . . . . .	124
A.2.3	Large Open Field . . . . .	125
	<b>References</b>	<b>127</b>



# Chapter 1

## Introduction

In recent years, the use of mobile robots in different fields of application has grown considerably. Mobile robots equipped with perception modalities, such as cameras, range sensors and global positioning systems have been successfully brought to mining [1], construction [2] and logistics [3] among other applications. In these scenarios, the different perception modalities are used to construct spatial representations of the scene, detect and identify specific objects and to estimate the robot's pose in the environment.

The use of gas sensing modalities in mobile robotics can be of high importance in different industrial, safety and security applications. However, the incorporation of gas sensors in robotic platforms has not been fully realised due to the challenges associated with gas sensing in uncontrolled environments and the comparatively slow development of chemical sensing technologies [4].

### 1.1 Mobile Robotics Olfaction

Mobile Robotics Olfaction (MRO) is the line of research that addresses the task of integrating gas sensing modalities on mobile robotic platforms. MRO requires the fusion of different disciplines such as signal processing, machine perception, autonomous navigation and pattern recognition.

Robots with gas sensing capabilities can be brought to different application areas. For example, gas sensitive robots can be used in industrial facilities (Figure 1.1(a)) to carry out routine inspection tours that aim to locate gas leaks and to monitor emission levels [5]. In this application scenario, robots can relieve plant personnel from repetitive inspection routines by automating the measurement collection process.

For civil authorities, the detection of gas leaks is critical due to safety concerns. MRO systems can be used to routinely inspect public areas and pipelines and in case of a contingency, where e.g. a leak of a toxic chemical has occurred, MRO systems can be used to minimize the exposure of crew personnel and first aid responders. An example of an application scenario is the 2011 incident in

the Nynäsham refinery in Sweden (Figure 1.1(b)), where significant amounts of hydrogen sulphide ( $\text{H}_2\text{S}$ ), which is a highly poisonous gas, were released. In similar emergency scenarios, a MRO system can collect useful information that allows the first response teams to assess the severity of the situation without deploying crew personnel in hazardous locations.

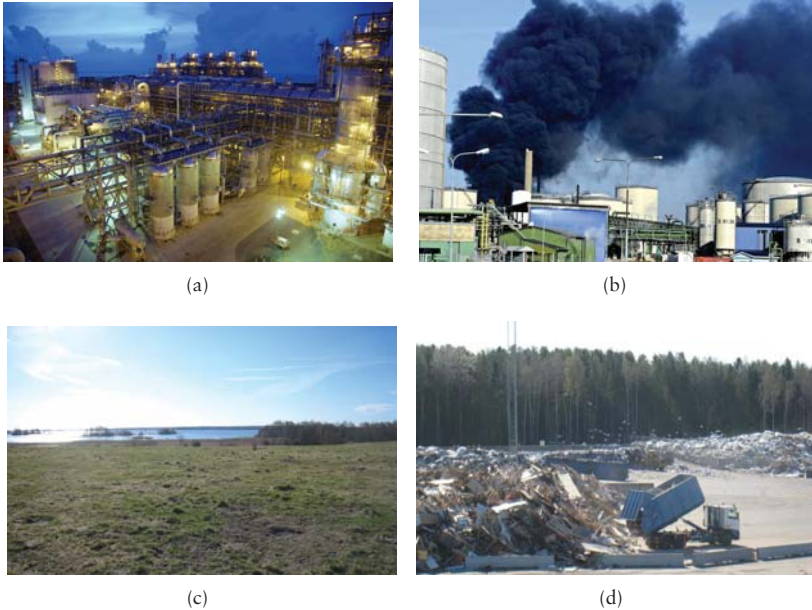


**Figure 1.1:** Examples of application scenarios for MRO systems. (a) Inspection of industrial facilities, such as the Darwing LNG plant in Australia<sup>1</sup>. (b) Emergency scenarios. Such as the Nynäsham incident in Sweden, 2011<sup>2</sup>. (c) and (d) Decommissioned and active landfill sites located in the municipality of Örebro, Sweden, where  $\text{CH}_4$  fugitive emissions are common.

Emission monitoring is another target application for MRO systems. A particular example is Natural Gas (NG) and Bio-Gas (BG) emission monitoring in production facilities (Figures 1.1(c) and 1.1(d)). NG and BG are composed mostly of methane ( $\text{CH}_4$ ) and thus, strict monitoring approaches are required due to the global warming potential of  $\text{CH}_4$  [6, 7]. By regulation, BG producers are required to issue monthly emission reports but in practice, measurements are sparsely collected, only at a few predefined locations. These inadequate monitoring practices can lead to unnoticed leaks that can release significant

<sup>1</sup><http://www.hydrocarbons-technology.com/projects/darwin/>.

<sup>2</sup><http://www.aftonbladet.se/nyheter/article13825662.ab>.

amounts of  $\text{CH}_4$ . Civil authorities, such as the the U.S. Department of Energy (DoE), have allocated resources to improve sensing technologies and deliver an order-of-magnitude reduction on the cost of  $\text{CH}_4$  sensing [8]. In this context, MRO systems can be used to detect leaks, automatise monitoring processes and to collect dense datasets for the characterization of  $\text{CH}_4$  emission patterns.

## 1.2 Towards Real World Applications with MRO Systems

The origins of MRO can be traced back to the early 1990s, where the predominant approach was to construct gas sensitive robots equipped only with a single chemical sensor. During this early development stage, the goal was to design biologically inspired algorithms that mimicked the exceptional gas sensing capabilities of insects and other animals. These bio-inspired algorithms implemented reactive behaviours that allowed robotic prototypes to track gas plumes towards the location of an emitting source. These algorithms did not consider aspects such as the limitations of the gas sensors (described below) and they often assumed laminar wind flow conditions. In addition, validation was almost exclusively carried out with *toy-like* robots in simplified scenarios of a few square meters and under tightly controlled environmental conditions. Due to the above mentioned limitations, these early MRO prototypes were not suitable to address practical, real world applications, such as the examples presented in Figures 1.1(a) to 1.1(d).

The development of MRO systems aimed for practical applications should consider the challenges of gas sensing in unstructured natural environments. In natural environments, gas dispersion is determined by changing wind flow patterns, heat distribution, pressure, humidity and the topology of the environment. These environmental conditions produce complex gas structures of fluctuating concentration levels. Under these conditions, MRO systems need to be able to extract meaningful information from the acquired gas concentration measurements.

In addition to the environmental conditions, further challenges arise due to the fact that most of the currently available sensors were designed for laboratory applications, where concentration levels and ambient conditions are controlled. Furthermore, the specific shortcomings of the used sensing technologies have to be addressed. For example, metal oxide sensors, which are widely used in MRO research, suffer from ambient drift and have to be recalibrated on a regular basis [9]. Moreover, these sensors are partially selective, which means that they react to different gas interferents, in addition to the target compound specified by the manufacturer. While more robust sensors have been developed for field inspection, these devices are considerably more expensive than other available sensors and, in some cases, their operational principle prevents them from being used on mobile platforms.

### 1.2.1 An Example Scenario

By considering the above mentioned challenges, we can illustrate in Figures 1.2(a) and 1.2(b) how MRO systems can address gas sensing in an example scenario. In this scenario, a wheeled robot equipped with a set of commercial gas sensors and other perception modalities is commanded to inspect an outdoor location to measure methane ( $\text{CH}_4$ ) concentrations. In the target area, an emitting gas source releases  $\text{CH}_4$  over a background concentration of carbon dioxide ( $\text{CO}_2$ ), which is considered an interferent gas in this particular example.

The overall problem of gas sensing can be decomposed in a set of sub-tasks as follows. The first task to address is **gas detection**. This means that given a set of measurements acquired with the gas sensors, it should be determined whether or not a gaseous compound is present in the exploration area. This task is particularly challenging in unstructured environments where gas concentration measurements are given as time series composed mostly of intermittent transient responses [10].

Once the presence of a gaseous compound has been determined, the robot's sensing modalities should allow to discriminate between the target compounds and possible interferents (in the example,  $\text{CH}_4$  and  $\text{CO}_2$  respectively). Selectivity limitations can be addressed using **gas discrimination** algorithms. These algorithms combine arrays of partially selective sensors with pattern recognition algorithms to estimate a label (or a posterior probability) of the measurement's identity [11]. The subsequent task of **gas quantification** allows to express the acquired measurements in terms of absolute gas concentrations, for example, parts per million (ppm). When gas sensors cannot deliver calibrated concentration measurements, gas quantification algorithms are used. These algorithms allow to estimate a calibrated concentration value from measurements acquired with non calibrated gas sensor and other relevant modalities [12].

Additional tasks in MRO can include **gas source localisation** and **sensor planning**. Gas source localisation is the process of estimating the position of an emitting source based on gas concentration measurements and other relevant environmental information (e.g. wind data) [13]. Sensor planning algorithms suggest measurement locations based on the current knowledge about the environment [14], with the aim of producing efficient exploration trajectories that provide full coverage of the inspection area and the most informative locations for gas sensing.

From the acquired information (e.g. calibrated concentration readings, gas identity), it is then possible to create spatio-temporal representations of the gas distribution for each of the detected gas compounds. The task of deriving these representations is commonly referred to as **gas distribution modelling** [15]. It is of high importance not only to present the acquired information to human operators in an intuitive form. The computed models can also be used in related tasks such as gas source localisation [16] or in sensor planning algorithms [14].



Gas distribution modelling can be performed using *model-based* or *model-free* algorithms [17]. The first set of algorithms assume an underlying functional form to explain the spatial distribution of the gas concentrations. However a key limitation of this approach is that inaccurate gas distribution maps are generated when an overly simplistic model is assumed or when boundary conditions for sophisticated models are not known. On the other hand, *model-free* algorithms, do not make strong assumptions regarding the functional form of the gas distribution, but rather treat the acquired sensor measurements as random variables and derive statistical representations of the observed gas dispersion.

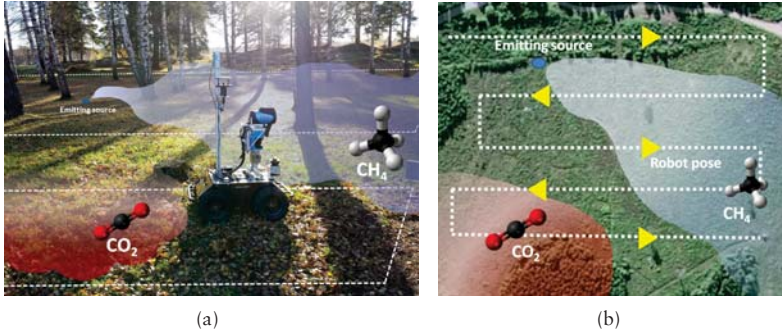


**Figure 1.2:** An example scenario of a MRO system performing gas sensing. The estimated gas distribution model of CH<sub>4</sub> is depicted by shades of blue while the CO<sub>2</sub> model is represented by shades of red. The dashed white lines denote the exploration trajectory and the yellow triangles represent the robot's pose. (a) 3D view. (b) Top-down view.

### 1.3 Scope of this Thesis

This thesis work presents a set of contributions towards the development of MRO systems for real world applications. More specifically, the task of Gas Distribution Modelling (GDM) is addressed using *model-free* algorithms in real world applications. This means that sensor shortcomings, such as partial selectivity are considered while many simplifying assumptions, such as uniform wind flow patterns and a predefined gas dispersion model are avoided.

GDM is thus performed using two different approaches. First, we combine non selective and partially selective sensors to generate gas distribution maps under the presence of multiple chemical compounds. The presence of a single chemical has been largely assumed by state of the art GDM algorithms before this thesis.

Multi-compound GDM implies that the task of gas discrimination has to be addressed. In this context, we propose a novel algorithm that uses arrays

of partially selective sensors to estimate the identity of the gas measurements. Once the identity of the measurements has been estimated, it is then possible to construct calibrated gas distribution maps, one for each of the identified compounds. The sensors used in this approach are *in-situ*, which means that measurements are reported as point concentrations and they cover only a few centimetres around the sensor.

In addition, we explore the use of emerging gas sensing technologies that can provide high selectivity and calibrated concentration readings. More specifically, we evaluate the use of absorption spectroscopy based sensors for the task of GDM. The distinctive characteristic of this sensing technology is that the reported measurements are spatially unresolved (i.e. integral concentrations in  $\text{ppm} \cdot \text{m}$ ), with no information regarding the length of the optical beam emitted by the sensors or the spatial distribution of the concentrations along the optical path. In the context of GDM, the use of integral concentration measurements, instead of point concentrations, requires algorithms that are radically different to the ones proposed in current state of the art. In literature, the task of creating gas distribution models from integral measurements is commonly referred to as Computed Tomography of Gases (CTG) [18].

### 1.3.1 Outline

The remaining chapters of this thesis are structured as follows:

**Chapter II** presents an overview of the different tasks that are addressed in MRO as well as the most commonly used gas sensing technologies in this area of research. In addition, the particular challenges of MRO are identified through a set of experiments in prototypical scenarios, using different robotic platforms and gas sensing technologies.

**Chapter III** is focused on the task of gas discrimination with mobile robots. The first part of this chapter presents the state of the art in this particular area. The second part presents an algorithm for gas discrimination in uncontrolled environments.

**Chapter IV** is focused on gas distribution modelling with *in-situ* sensing technologies. First, a review on related work is presented. The key contribution presented in this chapter is a statistical approach to compute gas distribution maps of multiple heterogeneous substances. The presence of a single chemical has been largely assumed by state of the art approaches.

**Chapter V** evaluates the use of remote sensing technologies for gas distribution modelling using mobile robots. More specifically, we propose the use of robotic platforms to perform tomography of gases. The concept of Robot Assisted Tomography of Gases is then validated with the design and testing of a *proof of concept* mobile robotic system intended for emission monitoring at landfill sites.

Chapter VI concludes this thesis with final remarks and suggests directions for future research work.

### 1.3.2 Contributions

The contributions presented in this thesis work can be summarized as follows:

- Introduction of the concept of Robot Assisted Gas Tomography (RAGT), a technique that uses spatially unresolved measurements acquired with mobile platforms to generate gas distribution maps.
- Design, development and validation of a *proof of concept* mobile robotic platform for the task of emission monitoring on landfill sites.
- Design of a statistical gas distribution mapping algorithm that considers the presence of multiple chemical compounds.
- Implementation of an algorithm for online parameter selection for gas distribution modelling. This algorithm considers the particular characteristics of gas sensing in open environments in order to decrease the computation time by avoiding the training and testing of multiple models.
- Design of a gas discrimination algorithm tailored to address the challenges of gas sensing in unstructured environments.
- Collection of large datasets in different prototypical environments, where MRO robots are expected to operate. These datasets were collected with different robotic platforms (e.g. ground and aerial robots) as well as with different gas sensing technologies such as metal oxide sensors, photo ionization detectors and spectroscopy based remote sensors.

### 1.3.3 Publications

The contributions of this thesis work have been presented in different peer reviewed journal articles or conference papers. The articles are either published or under review at the time of writing. The major results from this dissertation were published in the following articles:

- V. Hernandez, A. Lilienthal, P. Neumann and M. Trincavelli. Mobile robots for localizing gas emission sources on landfill sites: is bio-inspiration the way to go?. Front. Neuroeng. 4:20.

Part of Chapter 2

- V. Hernandez, E. Schaffernicht, V. Pomareda, A. Lilienthal and M. Trincavelli. A Novel Approach for Gas Discrimination in Natural Environments with Open Sampling Systems. Sensors, 2014 IEEE. (to appear).

Part of Chapter 3

- *V. Hernandez, V. Pomareda, A. Lilienthal, E. Schaffernicht and M. Trincavelli. Combining Non Selective Gas Sensors on a Mobile Robot for Identification and Mapping of Multiple Chemical Compounds. Sensors* 2014, 14, 17331-17352.

Part of Chapter 3 and Chapter 4

- *V. Hernandez, A. Lilienthal and M. Trincavelli. Creating true gas concentration maps in presence of multiple heterogeneous gas sources. Sensors, 2012 IEEE , vol., no., pp.1,4, 28-31 Oct. 2012.*

Part of Chapter 4

- *V. Hernandez, M. Trincavelli, A. Lilienthal and E. Schaffernicht. Online Parameter Selection for Gas Distribution Mapping. Sensor Lett., no. 12, pp. 1147-1151 (2014).*

Part of Chapter 4

- *M. Trincavelli, V. Hernandez and A. Lilienthal. A least squares approach for learning gas distribution maps from a set of integral gas concentration measurements obtained with a TDLAS sensor. Sensors, 2012 IEEE , vol., no., pp.1-4, 28-31 Oct. 2012. Contributed mostly in the experimental validation.*

Part of Chapter 5

- *V. Hernandez, A. Lilienthal, A. Khaliq, V. Pomareda and M. Trincavelli. Towards real-world gas distribution mapping and leak localization using a mobile robot with 3d and remote gas sensing capabilities. Robotics and Automation (ICRA), 2013 IEEE International Conference on , vol., no., pp. 2335-2340, 6-10 May 2013.*

Part of Chapter 5

- *V. Hernandez, E. Schaffernicht, T. Stoyanov, A. Lilienthal and M. Trincavelli. Robot Assisted Gas Tomography - Localizing Methane Leaks in Outdoor Environments. Robotics and Automation (ICRA), Robotics and Automation (ICRA), 2014 IEEE International Conference on, pp. 6362-6367, 31 May-7 June 2014.*

Part of Chapter 5

The following publications are not in the core contributions of this dissertation. However, they correspond to work performed during this thesis, mostly in the form of data collection and co-authoring of the articles:

- *P. Neumann, V. Hernandez, A. Lilienthal, M. Bartholmai and J. Schiller. Gas source localization with a micro-drone using bio-inspired and particle filter-based algorithms. Advanced Robotics, 27:9, 2013, pp. 725-738.*

- *P. Neumann, M. Schnürmacher, V. Hernandez, A. Lilienthal, M. Bartholmai and J. Schiller.* **A Probabilistic Gas Patch Path Prediction Approach for Airborne Gas Source Localization in Non-Uniform Wind Fields.** 5th International Symposium on Olfaction and Electronic Nose (ISOEN), 2013.
- *V. Pomareda, V. Hernandez, A. Khaliq, M. Trincavelli, A. Lilienthal, and S. Marco.* **Chemical source localization in real environments integrating chemical concentrations in a probabilistic plume mapping approach.** 5th International Symposium on Olfaction and Electronic Nose (ISOEN), 2-5 July 2013.
- *P. Neumann, S. Asadi, V. Hernandez, A. Lilienthal and M. Bartholmai.* **Monitoring of CCS Areas using Micro Unmanned Aerial Vehicles (MUAVs).** Energy Procedia, 37, 2013, pp. 4182-4190.



## Chapter 2

# Mobile Robotics Olfaction

As introduced in Chapter 1, Mobile Robotics Olfaction (MRO) is the line of research that addresses the task of integrating gas sensing modalities with mobile platforms. Performing gas sensing on-board robotic platforms requires the fusion of different disciplines, such as signal processing, artificial olfaction, machine perception, autonomous navigation and pattern recognition.

In early MRO research, the focus was on the development of algorithms that implemented reactive behaviours to track odour cues, in an attempt to mimic the biological sense of smell. These early algorithms were designed under unrealistic assumptions that for example, considered laminar wind flow and an underlying model for the gas dispersion phenomenon (e.g. Gaussian-like plume structures [19]). In addition, experimental validation was successfully carried out only in small, tightly controlled scenarios that did not properly capture the complex conditions of real world scenarios [4, 13].

MRO systems intended for practical applications should consider the challenges of gas dispersion in realistic environments. Gas dispersion is caused by diffusion and turbulence. Diffusion is the process where the random movement of gaseous particles lead to concentration equalization in a given scenario [20]. Turbulence on the other hand, causes the formation of eddies and vortices of different size and concentration that create patchy and intermittent plume structures. Additionally, intermittent wind flow patterns can meander, dilute and spread gas concentration patches.

Gas dispersion is quantified by the Reynolds number [21], which is a dimensionless value that characterizes the flow pattern at a given location. At low Reynolds numbers, diffusion produces smooth, Gaussian concentration profiles where the highest concentration level is measured at the location of the emitting source. At medium to high Reynolds number, dispersion is dominated by turbulence and thus, irregular concentration patterns are generated (Figures 2.1(a) and 2.1(b)).

Designing algorithms able to operate in turbulent environments (i.e. environments with high Reynolds numbers) is a complex task. Due to the dynamics

of turbulent environments, the sensors readings are noisy, intermittent time series. In addition, it is hard to collect representative datasets due to the large amount of variables that influence the gas dispersion phenomenon. Thus, it is not feasible to design experiments under exhaustive environmental and topographic conditions. Repeatability becomes an issue, since even slight variations in the environmental conditions can considerably affect the outcome of a given validation trial.

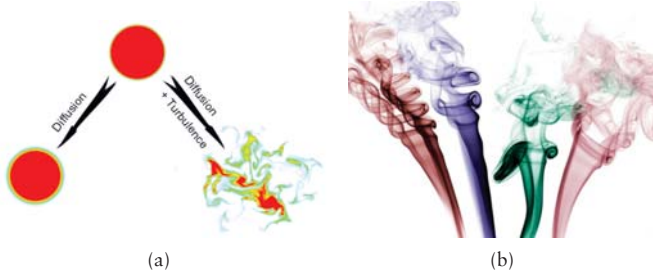


**Figure 2.1:** (a) State diagram that illustrates the effects of turbulence dominated and diffusion dominated gas dispersion. The top state is a gas circular patch with homogeneously distributed concentration. The left state represents a diffusion dominated dispersion pattern where only random molecular motions occur. The right state represents a turbulent dominated dispersion pattern[21]. (b) Turbulent dispersion with irregular concentration patterns at the end of the gas plumes<sup>1</sup>.

However, considerable success has been achieved when simplifying assumptions are removed and when an engineering, statistically driven perspective is adopted. This perspective, along with more reliable gas sensing mechanisms, has allowed to develop *proof of concept* prototypes that have successfully carried out tasks such as environmental monitoring [22], inspection of industrial facilities [5] and detection of hazardous and warfare agents<sup>2</sup> in more realistic experimental scenarios.

In the remaining of this chapter, we present an overview of the research area of MRO. First, in Chapter 2.1, gas sensing technologies that are relevant for MRO are introduced. In Chapter 2.2, we identify the different tasks that have to be addressed when designing MRO systems. For its relevance in this dissertation, the task of gas source localisation is thoroughly described in Section 2.3. In Section 2.4, we present a set of example scenarios, where the task of finding an emitting gas source with a mobile robot is performed. Through the characterization of the different experimental configurations, we identify

<sup>1</sup><http://gizmodo.com/5661918/shooting-challenge-smoke-gallery-1>

<sup>2</sup><http://www.foi.se/en/Customer--Partners/Projects/LOTUS/LOTUS/>



some of the challenges to address and we propose a solution to locate the gas source. Section 2.5 closes this chapter with final remarks and conclusions.

## 2.1 Gas Sensing Technologies

Gas sensors are transducers that respond to stimuli produced by chemicals in gaseous phase [23]. These sensors are intended for the identification and quantification of target compounds and they are a critical component of safety and security systems. Key requirements for gas sensors in MRO applications are high sensitivity and selectivity to target compounds, low sensitivity to environmental conditions and interferents, rapid response/recovery times, low power consumption and compact sizes [24].

Gas sensors can be classified according to different taxonomies that are mostly based on the physical principles of the transduction mechanisms [25]. For the scope of this thesis we identify two major branches namely *in-situ* gas sensors and remote gas sensors. In the following sections we describe these two different sensor families and while an exhaustive review is out of the scope of this thesis, we introduce a set of sensors that are relevant to MRO related tasks.

### 2.1.1 In-situ Gas Sensors

*In-situ* sensors require a direct interaction between the sensitive layer of the sensor and the target gas compound. This means that each reported measurement corresponds to the concentration level of an area of few square centimetres around the sensor itself. Gas measurements can be reported in the form of voltage, current, conductance, frequency and thermal changes.

#### Conductometric Sensors

Conductometric devices report the presence of gaseous compounds in the form of conductance changes due to chemisorption and redox reactions in the sensitive layer of the device [26]. There are different technologies based on conductometric principles, among others chemical field effect transistors, electrochemical cells, and Metal Oxide (MOX) sensors [23].

MOX sensors (Figure 2.2(a)) are perhaps the most popular conductometric sensor in MRO due to their widely commercial availability, low cost, relatively fast response times and high sensitivity. For a MOX sensor, the logarithm of the change in resistance over a certain range is approximately linearly proportional to the logarithm of the concentration of the gas [26]. MOX sensors can be broadly divided into two categories, namely n-type and p-type sensors. n-type sensors can be fabricated with SnO<sub>2</sub> and ZnO sensitive layers and they respond to reducing gases such as H<sub>2</sub>, CH<sub>4</sub>, CO, C<sub>2</sub>H<sub>5</sub>, C<sub>2</sub>H<sub>5</sub>OH, (CH<sub>3</sub>)<sub>2</sub>CHOH. On the other hand, p-type sensors can be fabricated with NiO and CoO substrates and respond to oxidizing gases such as O<sub>2</sub>, NO<sub>2</sub>, and Cl<sub>2</sub> [27].

However, MOX sensors have several drawbacks that have to be considered when designing MRO systems. First, the sensing surface has to be heated to temperatures up to 500°C in order to operate. This translates into a relatively high power consumption. Second, they show poor selectivity. MOX sensors react to different interferent gases and not only to the target compound specified by the manufacturer. Third, the slow response and recovery times of a MOX sensor are a factor to consider. When exposed to a target compound, MOX sensors will show a transient response of a few seconds, before reaching a steady response level. When the sensor is no longer exposed to the target compound, the sensor response will gradually recover the baseline level only after a few minutes. The baseline level represents the sensor output in the absence of chemical compounds [26].

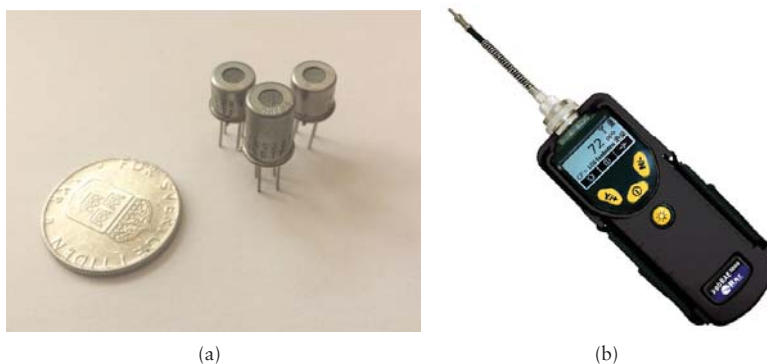


Figure 2.2: (a) A set of *Taguchi-type* MOX sensors. (b) A ppbRAE 3000 PID<sup>3</sup>.

### Photo Ionization Detectors

In Figure 2.2(b), a Photo Ionization Detector (PID) shown. PIDs are sensors that use high energy photons, typically in the ultraviolet range (UV), to break gas molecules into positively charged ions. As a compound enters the PID it is ionized when it absorbs high-energy UV light. In commercial PID detectors the UV light is normally provided with a 10.6 eV UV lamp. The UV light excites the molecules, which temporarily lose an electron and thus become positively charged ions. The ions produce an electric current, which is the signal output from the detector. The output signal of a PID is linearly proportional to the concentration of the chemical compound being analysed.

As a standalone detector PIDs are broad band detectors and are not selective, as the UV light ionizes all molecules that have an ionization energy less

<sup>3</sup><http://www.raesystems.com/products/ppbrae-3000>

than or equal to the lamp output. Unlike MOX gas sensors, if the chemical compound is known, PIDs can provide true concentration measurements, by multiplying the sensor's reading by a correction factor, which is provided by the manufacturer. Moreover, the response dynamics of a PID is much quicker compared to the one of MOX sensors. However, PIDs are relatively expensive devices and their weight and size can limit their use in applications with robots of limited payload. In addition, PID's cannot detect methane, which is of high economical and environmental interest [28].

### Chromatography Based Sensors

While sensors based on analytical chemistry, such as chromatography, are often bulky and suitable for laboratory applications only, recent developments have allowed to bring these devices to field inspection in the form of portable measurement systems. A chromatography sensor is a device that separates complex gas mixtures into individual components [29]. The gas sample is injected into a column, where a carrier gas transports it towards the location of a set of detectors down the column. The sample is dissolved due to the different speeds of its various constituents due to which they reach the end of the column and the detectors at different times. The detectors measure the concentrations of the individual components of the mixture, eluted from the column.

Gas chromatography is a well established technology and there are several hand-held devices that are commercially available. An example of such devices is the *Frog-4000* (Figure 2.3(a)) from Defiant Technologies. These devices can perform chromatography analysis on-site and their use is not restricted to laboratory environments. The *Frog-4000* can discriminate chemicals such as Benzene and Toluene and compared to laboratory chromatographs, it does not require a carrier gas to process the samples. However, the *Frog-4000* does not return calibrated concentration readings. While portability is not an issue for these devices, the main constraint that prevents them to be used on-board mobile robots is their *cycle times*. It takes up to 5 minutes to process a single gas sample.

### Spectroscopy Sensors

Ion Mobility Spectroscopy (IMS) sensors are based on the measurement of the Time of Flight (ToF) of ionized gas samples. When a sample enters the IMS device, it is then ionized by e.g. a radioactive source. The resulting positive and negative charged species will be accelerated over short distances and their ToF is measured. Then, the measured ToF is compared against the mobility profiles of known compounds in order to find a match. IMS devices can operate in atmospheric conditions and thus they do not require vacuum pumps.

There exist a wide variety of sensors and devices based on IMS. An example of an IMS based device is the Multi-Mode Threat Detector (MMTD) from

Smiths Detection. The MMTD (Figure 2.3(b)) is a hand held device that has a wide spectrum of narcotics, explosives and chemical warfare agents mobility profiles and thus can be used for military and security applications. The MMTD can process a single gas sample under 10 s.

Optical spectroscopy can also be used as a sensing mechanism. An example of an optical spectroscopy sensor is the Picarro's G2301 (Figure 2.3(c)). The G2301 is based on Cavity Ring-Down Spectroscopy (CRDS), which is an optical spectroscopy technique that quantifies the spectral features of gas molecules by measuring the absorption and scattering of a laser beam, modulated at a specific wavelength. This sensor is aimed for environmental monitoring and is capable of measuring green house gases such as carbon dioxide, methane and water at the parts-per-billion range with a response time under 5 s.

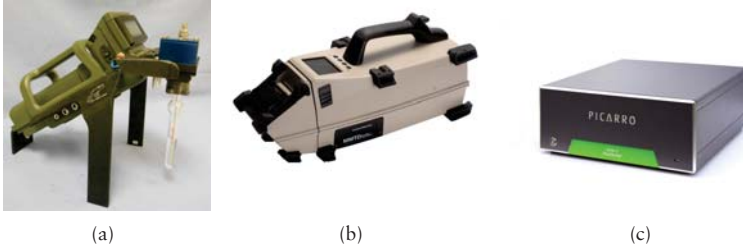


Figure 2.3: (a) The Frog-4000 chromatograph<sup>4</sup>. (b)The MMTD IMS sensor, manufactured by Smith Detection<sup>5</sup>. (c) The G2301, manufactured by Picarro<sup>6</sup>.

### 2.1.2 Remote gas sensors

As implied by its name, remote sensing can be defined as the distant measurement of a phenomenon of interest through propagated signals such as optics, acoustics or microwaves [30]. Regarding gas sensing, concentration readings are acquired by measuring the interaction between gaseous particles and electromagnetic energy emitted from an artificial or natural source. Broadly speaking, remote gas sensing can be classified into active and passive principles [31]. Active sensors generate electromagnetic radiation under controlled conditions (e.g. xenon lamps, infra-red diodes) over long distances in open air settings, while passive sensors do not require an artificial emitting source and measurements are carried out by using a natural source such as sunlight.

The operating principle behind most active sensors is absorption spectroscopy. Gas molecules absorb energy in narrow bands surrounding specific wavelengths

<sup>4</sup><http://www.defiant-tech.com>.

<sup>5</sup><http://www.smithsdetection.com>.

<sup>6</sup>[http://www.picarro.com/products\\_solutions/gas\\_analyzers/co\\_co2\\_ch4\\_h2o](http://www.picarro.com/products_solutions/gas_analyzers/co_co2_ch4_h2o).

in the electromagnetic spectrum. Outside this narrow bands, there is practically no absorption. When the emitting source is modulated in the particular absorption band of a target gas molecule, the beam is attenuated along the optical path when it enters in contact with patches of the target gas. In this way, a high degree of selectivity can be achieved and concentration measurements can be estimated by using the Beer-Lambert law [32, 33].

The target gaseous compound and the maximum sensor range are largely determined by the nature of the sensor's emitted beams. Differential Optical Absorption Spectroscopy (DOAS) for example, quantifies gas concentrations by measuring the absorption of UV light by chemical compounds such as Nitrogen and Oxygen. DOAS sensors are ideal for compounds that do not have narrow absorption bands and they can measure concentration levels in the range of *parts per trillion* (ppt). In addition, DOAS sensors can acquire measurements with remarkably long optical paths, in some cases up to 10 km [34]. However, due to their wide absorption bands, DOAS cannot accurately quantify different molecular species.

The main application for Differential LiDAR (DIAL) sensors is the measurement of aerosols, dust and gases in the lower few Kilometres of the atmosphere. DIAL devices acquire concentration measurements from the reflected or backscattered light from two sources of different wavelength, one located at the absorption band of the target compound ("on" beam) and the second one is located just outside the absorption band ("off" beam). When emitted, both lasers are scattered by molecules and particles located in the optical paths. During their trajectories, the "on" beam is absorbed by the target gaseous compounds, which can be used to determine the identity and the concentration of the compound. The "off" beam is scattered by atmospheric particles and, by measuring the intensity of the backscattered rays and their time delay, it is possible to determine the spatial location of the measured gas [35].

In Figure 2.4, a schematic diagram of a Tunable Diode Laser Spectroscopy (TDLAS) sensor is shown. In the figure, a diode emits a beam that traverses a given gas cloud. The emitted beam is backscattered when it hits a given surface and the reflected rays are measured by the device. The emitting diode is chosen to optimize the sensitivity to the target gaseous compound and the diode's wavelength is thus set to the corresponding absorption band. The diode is then driven on and off of the absorption band. During this process, the power of the beam is measured continuously and, by comparing the measurements when the beam is on the target wavelength against the measurements when the beam is off, it is possible to determine, with high degree of selectivity, whether the emitted beam has traversed a target gas patch or not [33]. In Figure 2.5, an absorption profile for different chemical compounds is shown. It can be noticed from the example that a modulation frequency (i.e. wavelength) can be chosen to optimize the methane ( $\text{CH}_4$ ) selectivity of the device over different interferent chemical compounds.

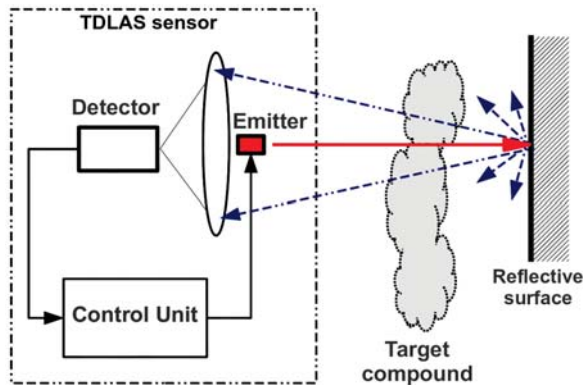


Figure 2.4: (a) Block Diagram of a TDLAS remote sensor.

TDLAS sensors are available for a large variety of target compounds, among others, ammonia, carbon monoxide, methane, oxygen, water and hydrogen sulphide. TDLAS sensors are compact, light devices that can be carried by human operators performing manual scans. These devices can achieve a high degree of selectivity, require low maintenance and they are relatively inexpensive, compared to other remote gas sensing technologies. On other hand, the selectivity of the device is limited to only one compound per diode and beams blocked by e.g. dust, result in faulty readings [31].

While most of the techniques described above are able to detect and quantify a single compound, Fourier Transform Infra-Red (FTIR) spectroscopy devices can detect multiple compounds by using principles of interferometry and spectral analysis. An FTIR consist of an emitter and a transceiver. The emitter generates an interference pattern using artificial or background infra-red sources, which are then transmitted to a receptor that is place up to 500 m away [34]. The Fourier transform is then applied to the received beam in order to acquire its frequency pattern. The receiver then correlates this pattern to stored frequency fingerprints of different known compounds. In this way, multiple gases can be detected with a single FTIR device. Perhaps one of the biggest drawbacks of FTIR devices is their high sensitivity to carbon monoxide, which turns into interferences that disrupt the sensor's accuracy. In addition, FTIR devices might not be sensitive enough to comply with ambient data quality standards.

Image Multi-Spectral Sensing (IMSS) cameras capture spectral signatures and chemical compositions within the sensor's line of sight. In other words, the electromagnetic spectrum is divided into a number of bands and data is collected within each of these bands. IMSS sensors can use as well interferometry principles, similar to FTIR devices [36, 37], capturing interferographic infor-

mation in each pixel of the acquired image. The ability to capture images is one of the main advantages of IMSS systems. This means that multiple gas identification is not only possible but also, their spatial distribution can be captured. IMSS systems have on the other hand, a low accuracy and they are heavily influenced by weather conditions.

Thermal Infra-Red (IR) cameras use IR radiation to form images in an analogous way as photographic cameras use visible light. IR cameras are mostly used to detect leaks that are not visible to the human eye for example. IR cameras can highlight the source and the trail of a gas leak in a wide variety of applications, for example inspection of tank vents [38]. While IR cameras have remarkable advantages such as portability and a wide field of view, one of the major limitation of this technology is its inability to quantify the detected gas plumes.

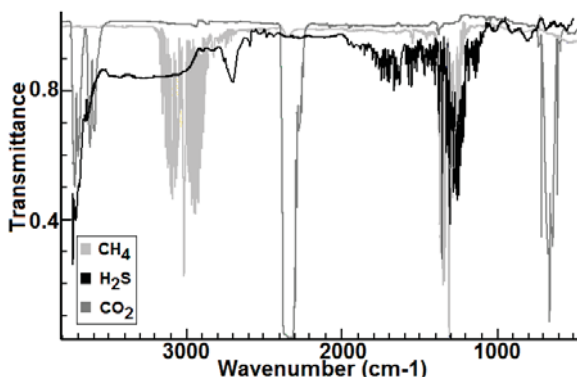


Figure 2.5: Absorption profiles for different gases.

## 2.2 Mobile Robotics Olfaction Tasks

Figure 2.6 presents a general overview of the different tasks related to MRO. The arrows denote how the outputs generated by one task (or a block thereof) can be used as inputs for subsequent tasks. MRO can thus be seen as the intersection between three broad disciplines namely chemical sensing, artificial olfaction and mobile robotics. At the lower level in the diagram, gas sensing is located. This means that the outputs from this tasks (i.e. the sensor readings) are used as inputs in subsequent tasks. Artificial olfaction comprises several tasks that aim to provide intelligent systems with capabilities to e.g. detect, identify and localize chemical compounds. When robotic platforms are equipped with gas sensors, information such as the estimated robot's pose [39] and representations of the explored environment [40] are needed in order to associate the acquired measurements with a position in a global reference frame. In addition,

the outputs generated by the artificial olfaction tasks can be used e.g. as inputs to sensor and path planning algorithms that suggest exploration trajectories and identify informative measurement positions [41, 14].

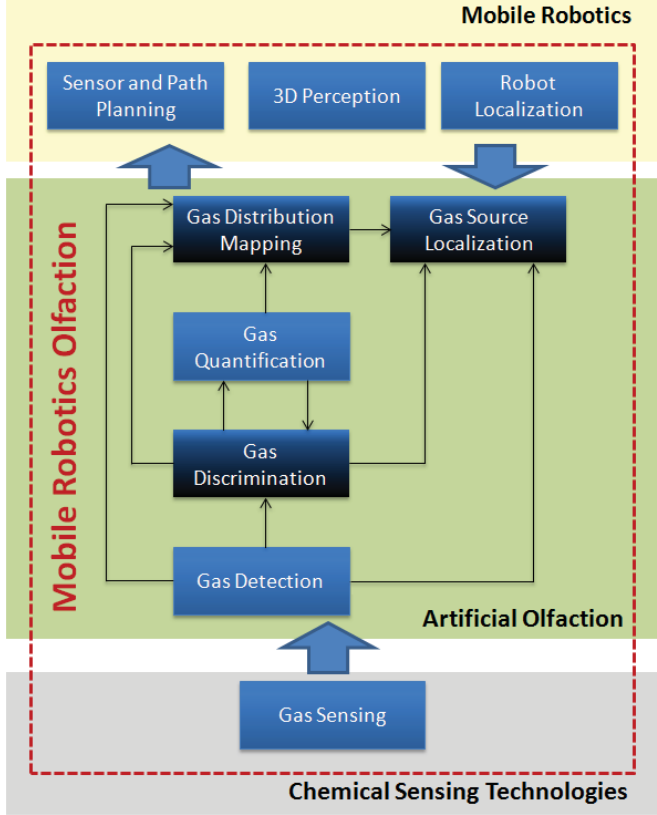


Figure 2.6: Block diagram of Mobile Robotics Olfaction and its related tasks. The blocks coloured in darker tones of blue indicate the tasks that are addressed in this dissertation.

### 2.2.1 Gas Detection

The detection of changes in the emission profile of a gas source is a desirable feature for a robot operating in turbulent environments. For example, the detection of events such as the presence/absence of a gaseous component, sudden changes in the concentration and the chemical composition of a gas plume can be used in subsequent in MRO related tasks (Figure 2.6). Simplistic methods to



detect these changes can include the use of concentration thresholds to declare the presence of a given analyte. However, gas sensing in turbulent environments require more sophisticated approaches to detect these emission profile changes.

In addition to the environmental conditions, the limitations of the sensors are a factor to consider. For example, sensors such as Metal Oxide (MOX) gas sensors, are sensitive to environmental conditions (e.g. temperature, humidity), they are cross sensitive to gas interferents and they have slow response and recovery times. In real world applications, the gas sensors are often directly exposed to the environmental conditions (e.g. humidity, ambient temperature, wind flow patterns) in a configuration that is referred to as an Open Sampling System (OSS).

Figure 2.7 depicts the response time series of a Metal Oxide (MOX) when exposed to a gaseous analyte. The shaded area denotes the time interval when the sensor interacted with a gas patch. As previously mentioned in Section 2.1, a low-pass filter effect is introduced by the long response and recovery times of MOX sensors. Therefore, the use of response thresholds to determine the presence/absence of gas (e.g.  $\geq 90\%$  for detection,  $\leq 10\%$  for absence) would lead to a delay in the detection event and a considerably larger delay to declare the absence of gas. A hardware solution to address this problem was proposed in [42], where a multi chamber sensor array was proposed. The key idea behind this sensing configuration is that, when the sensors are in the recovery phase, the system switches to a sensor (or an array thereof) that has not yet been exposed to the gas concentration. In this way, the delay effect of the sensors can be mitigated.

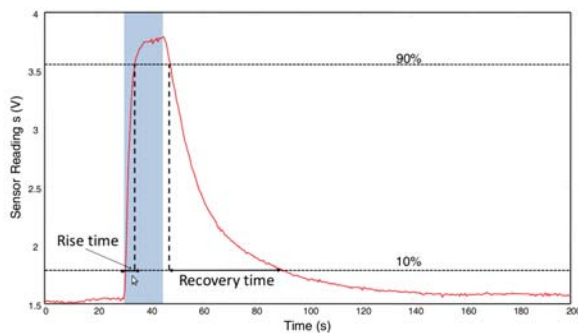


**Figure 2.7:** Low-pass filter effect observed when a MOX sensor is exposed to a sample of acetone. The shaded area denotes the time interval when the sensor interacts with a gas source [42].

Figure 2.8 shows another example where the limitations of the sensing technologies prevent the detection of changes in the composition of a given gas source. The plot was generated with an odour blender [43] emitting intermit-

tent concentration patterns and switching between two different chemicals. A MOX sensor was placed 0.5 m away from the blender's outlet. It can be noticed in the figure that it is hard to detect the transitions between compounds and the absence/presence of gas by simply looking at the sensor response time series.

The work of Pashami and co-authors addresses the problem of change point detection for gas sensing applications [10, 44]. More specifically, the authors proposed a set of algorithms to detect changes in the emission profiles (e.g. sudden exposure, changes in concentration and/or composition) using MOX sensors. By taking into account the low-pass filter effect of a MOX sensor and the asymmetry between the response and recovery times, the authors formulated a non-linear trend filtering approach as a convex optimization problem to detect changes in the sensor response. The sensor response is thus modelled as a piecewise exponential signal where the junctions between consecutive exponentials are considered as change points. Among other advantages, the algorithm proposed by the authors is less computationally expensive than other related approaches and it allows for the automatic learning of parameters.

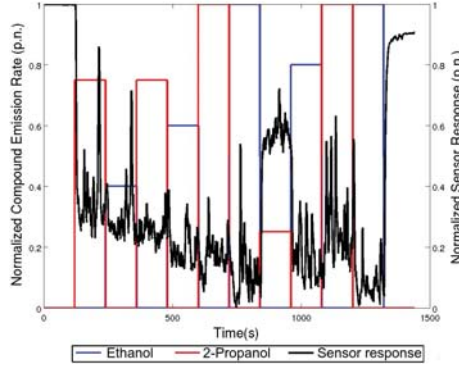


Figure 2.8: Response profile of a MOX sensor exposed to a gas source that changes its emission profile [44].

### 2.2.2 Gas Quantification

For applications such as environmental monitoring or safety related applications, it is required to express the acquired measurements in terms of absolute concentration values. While some gas sensing technologies can measure calibrated concentration values in e.g. parts per million (ppm), technologies based on conductometric principles, such as MOX sensors, report concentration in terms of conductance changes and require a calibration process to associate conductance values to their corresponding concentration levels.

Typically, a calibration procedure is carried out by placing the sensors inside a chamber where the concentration level is kept constant for a period of time and then is gradually increased. The response of the sensor is then measured and the parameters of an exponential model that maps the concentration values against the changes in conductance are estimated [26]. Alternatively, regression techniques such as partial least squares [45, 46], artificial neural networks [47] or support vector regression [48] can be used. The drawback of these approaches is that, when measurements are acquired in open, uncontrolled environments, the sensors are exposed to fluctuating concentration values and environmental conditions, such as temperature and humidity, can affect the sensor response [26].

The work in [49], addresses the problem of gas quantification with a system intended for urban pollution. The calibration of the sensors was performed with data collected outdoors over long periods of time. However, the authors discarded dynamic information by averaging out the acquired measurements. Gonzalez and co-authors presented in [50] a probabilistic approach for gas quantification in open environments. The authors used an array of MOX sensors and an algorithm based on Gaussian processes to estimate, for each acquired measurement a posterior distribution of the concentration from which confidence intervals can be obtained. Having an estimate on the uncertainty of the predictions is of high relevance for MRO, since there are many sources of uncertainty when performing gas sensing in turbulent environments.

### 2.2.3 Gas Discrimination

A drawback of many gas sensing technologies, such as metal oxide sensors, conducting polymers or piezo-electric quartz sensors, is their partial selectivity [51]. An approach to determine the identity of a measurement with partially selective sensors is to construct sensor arrays and use pattern recognition techniques such as support vector machines, artificial neural networks or nearest neighbours classifiers [52] to predict a posterior probability of the measurement identity, given the acquired sensor response profile or *odour print*.

Devices that combine arrays of sensors and pattern recognition algorithms are commonly referred to as electronic noses (e-noses). Gas discrimination can be carried out in tightly controlled scenarios (e.g. inside chambers), where the e-nose is exposed to constant concentration levels for a period of time that allows the sensors in the array to reach a semi-steady response profile [53].

However, when performing gas discrimination with OSS, the sensors in the array are directly exposed to the environment and thus, constant concentration values are not expected. Instead, the gas dispersion patterns in turbulent environments create highly fluctuating and diluted concentration levels. The sensor response is then dominated by noisy transient patterns (see Figure 2.8). An overview of the current state of the art in gas discrimination is given in Chapter 3. In addition, we present in Section 3.3, a gas discrimination algorithm

tailored for uncontrolled environments, which is one of the main contributions of this dissertation.

### 2.2.4 Gas Distribution Modelling

Gas Distribution Modelling (GDM) is the MRO task that creates truthful representations of the observed gas distribution from a set of spatially and temporally distributed measurements of relevant variables such as gas concentration, wind information and temperature [17]. GDM can be performed using *model-based* algorithms, that assume an a priori form for the spatial distribution of the gas concentrations or by using *model-free* approaches, that do not assume underlying models and instead generate statistical representations of the observed gas dispersion.

A key limitation of the *model-based* approaches is that simplifying assumptions have to be made, for example, laminar wind flow patterns [19]. However, when MRO systems operate under turbulent conditions, this assumptions rarely hold. While more sophisticated models can be assumed [54], a key limitation is that, when the boundary conditions are not known, inaccurate gas distribution maps are predicted.

*Model-free* approaches that predict the mean concentration distribution and estimate the gas fluctuations in the form of a variance map [17, 55] have been extensively used in robotics related applications. A variance map is of high importance for related tasks such as gas source localisation [56] or sensor planning [14]. Additionally, algorithms have been developed to integrate wind information [57], robot localisation uncertainty [58], information about physical obstacles [59] and time dependency [60] to the computation of the gas distribution models.

However, an aspect that has been largely overlooked is the presence of multiple heterogeneous chemical compounds in the environment. Multi compound GDM can be challenging since it requires to integrate the task of gas discrimination in the computation of distribution models. In Chapter 4, we present an algorithm for GDM of multiple chemical compounds as well as a comprehensive review of current state of the art in GDM.

## 2.3 Gas Source Localisation

According to Kowadlo and co-authors, gas source localisation (odour localisation), is the task of finding the location of a volatile chemical source in the environment [13]. Due to their exceptional chemical sensing capabilities, insects and other lower order animals have been an important source of inspiration for Gas Source localisation (GSL) algorithms. More specifically, scientists have been trying to emulate odour tracking behaviours, in which a given organism follows a set of chemical cues towards the emitting source [61, 62, 63]. In order to present a general overview of the developments in GSL, we refer to the

taxonomy implemented by Kowadlo and co-authors in [13], where three main development stages are identified according to the complexity of the target environments, as described in the following sections.

### 2.3.1 Early Works and Diffusion Dominated Approaches

These works date back to the early 1990s, and their main characteristic is that no consideration is given to the mechanics of gas dispersion. It is then assumed that gas dispersion is given by smooth gas patches where the concentration decreases following e.g. a Gaussian distribution from the emitting source onwards. In order to localize the source, the movements of the robot were determined only by concentration gradients. This mechanism is referred to as *chemotaxis*. The first pure *chemotactic* robotic platform was implemented by Rozas and co-authors in [64].

While pure *chemotactic* algorithms are not suitable for applications where turbulence and intermittent wind flow patterns are expected, Gaussian-like gradient patterns can be expected at very small scales and in underground environments. Russell and co-authors investigated odour localisation with a buried probe controlled by a robotic manipulator (Figure 2.9(a)). The authors developed a set of algorithms for underground GSL where the movements of the manipulator were determined by the increase of gas concentration levels [65]. The authors successfully tested their algorithms in a small  $0.20\text{ m} \times 0.60\text{ m} \times 0.10\text{ m}$  sandbox where an emitting gas source was placed at a depth of  $0.04\text{ m}$ .

### 2.3.2 Turbulence Dominated Algorithms

As previously stated, at high Reynolds numbers turbulence dominates gas dispersion and thus smooth gas structures are hardly present. In such scenarios, the success rate of pure *chemotactic* algorithms for GSL is rather low. In the taxonomy proposed by Kowadlo, the family of algorithms that address the problem of GSL under turbulent environments are divided in three non exclusive groups namely reactive plume tracking algorithms, long range algorithms and plume modelling algorithms.

#### Reactive Plume Tracking Algorithms

These set of algorithms rely on the assumption that a strong, constant background fluid flow (e.g. water or air) is present in the environment, producing a gas plume that can be traced towards the location of the emitting source.

Plume tracking algorithms commonly operate in three different stages, namely, plume acquisition (finding the plume), plume tracking (moving the robot guided by the gas plume) and gas source declaration (predicting that the source has been found and it is located at a nearby position) [66].

In plume acquisition, the mobile robot acquires odour cues that allows it to enter in contact with the plume. For example, a random walk movement can be performed to detect the presence of the gaseous compound or the robot can stop at a given position and collect measurements until a gas detection event occurs.

Plume tracking algorithms can use different sensing modalities besides chemical sensors. For *anemotactic* approaches, for example, the movement of the robot is determined by the perceived wind flow. Plume tracking algorithms in mobile robotics have been largely inspired by biological behaviours. Among others, the animals that have inspired most of the robotics research in GSL are:

- Moths, which use odour localisation to find mates [67, 68, 69].
- Lobsters, which use odour localisation to locate food [70].
- *Escherichia Coli*, which use odour localisation to locate nutrients [71].
- Dung Beetles, which use odour localisation to find hatching niches, habitation, and food [71].

Gas source declaration is the process of determining the certainty that a source is in the immediate vicinity [72]. Commonly, when plume tracking algorithms are validated, gas source declaration is carried out by a human observer. For example, when the robot is located within a short distance from the gas source, it is determined that the robot has successfully localized the source.

Automatic gas source declaration algorithms have been proposed in different works. Hayes et al. proposed in [73] an algorithm that declares a gas source by searching transitions between high and low concentration levels in upwind directions. Lilienthal et al. [72] proposed a machine learning centred approach. The authors equipped a mobile robot with a set of metal oxide sensors (Figure 2.9(b)) and measurements were acquired by moving the robot in rotating manoeuvres. A classifier was trained using features extracted from the sensor response in negative and positive examples. In this way, the authors successfully determined the presence of a gas source with a maximum success rate of 87%.

Neumann and co-authors [74] developed a probabilist approach, based on a particle filter to declare the location of a gas source. The approach integrates gas and wind measurements, collected with a micro Unmanned Aerial Vehicle (UAV) (Figure 2.9(c)), to reconstruct plausible trajectories followed by gas patches, from the emitting source to the micro UAV's sensors. The algorithm considers the turbulent nature of the environment by modelling the uncertainty in the wind direction and the uncertainty in the measurements is determined by a measurement model.

### Long Range Algorithms

Long range algorithms can combine the use of gas sensors with e.g. cameras to detect gas sources (Figure 2.9(d)), under the assumption that emit-

ting gas sources can be distinguished by their visual appearance. The work in [75, 76, 77] are examples of this family of algorithms were *in-situ* gas sensors are used along with visual information to detect gas sources. This category of algorithms can be expanded by considering the use of remote gas sensing capabilities. Remote gas sensors can measure concentration levels distantly without entering in contact with a gases patch.

The use of remote gas sensors for GSL is one of the aspects investigated in the *RoboGasInspector* project<sup>7</sup>. The general goal of this project is to automate routine inspections in large industrial environments. The robotic platform (Figure 2.9(e)) is equipped with a pan-tilt unit and a *sensor-head* composed of different remote sensors among others, a Tunable Diode Laser Absorption Spectroscopy (TDLAS) sensor and an Infra Red (IR) camera.

In [78], the *RoboGasInspector* platform is used to detect leaks in two industrial plants and at a landfill site. The authors implemented an ad-hoc triangulation algorithm to steer the robot towards the suspected location of a gas leak. While the robot was able to successfully locate the gas source in the experimental scenarios, it was observed that the performance of the algorithm depends on the strong assumption that the detected concentration is located at the end of the beam.

The use of IR imaging for GSL was explored in [79]. It has been well documented that when gas escapes from pressurized equipment (e.g. transport pipes, storage tanks) to the environment, it cools down. The authors of [79] assume that the temperature profile of a leak can be described by a two dimensional Gaussian distribution. Thus, informative features for classification were extracted by cross correlating the acquired IR images with typical temperature profiles of potential leaks. The authors achieved a high success rate when the algorithm was validated in a *mock-up* scenario, where a leak was simulated using pressurized air escaping from a ½ inch iron pipe painted in black to minimize reflections.

### Plume Modelling Algorithms

This family of algorithms diverge from the pure reactive, trail following schemes and instead, they can utilize measurements acquired in an exploration trajectory to estimate the gas dispersion pattern using analytical or stochastic methods. For example, in [80, 19], wind and gas concentration measurements are used to fit a Gaussian plume model to locate an emitting gas source while in [81, 82], Bayesian inference methods are used, along with a Gaussian “random walk” dispersion model, to compute a likelihood lattice in which the location of a gas source is determined by the posterior probabilities, computed for each cell in the grid.

---

<sup>7</sup><http://www.robogasinspector.de/>

While assuming a priori models for the gas plume is a successful strategy under constant, strong fluid flows, these conditions are rarely found in realistic scenarios. In these scenarios, turbulence and the changing direction of the fluid flows can cause irregular gas patches instead of a well defined trail. Thus, a predefined plume shape (e.g. Gaussian-like) cannot generally be assumed.

Lilienthal and co-authors proposed to use the implicit information contained in gas distribution maps as a mean to perform GSL. In [56], the authors propose to use the Concentration Maximum Estimate (CME) as an indicator to localize emitting gas sources. The CME corresponds to the location of the maximum mean concentration value predicted by the gas distribution map. In a later work, the authors compared two different indicators for GSL namely, the CME and the Best Fit Estimate (BFE). The BFE is computed by fitting the functional parameters of a pre-defined plume model, using the predictions of the gas distribution map as inputs. The authors concluded that the CME outperforms the BFE in scenarios where the best fit is not a good approximation of the gas distribution or where only a weak wind flow is present.

In [16], different indicators for GSL were evaluated. It was observed that the fluctuations on the gas concentration are often a more reliable predictor for GSL than mean concentration maps. Gas distribution models that generate maps of the gas fluctuations for example, in the form of a predictive variance map [17] can be used in the task of GSL. In [83] the variance maps are used to estimate the location of an emitting gas source. The Variance Maximum Estimate, which is the location of the maximum variance value predicted by the model, is used as an indicator of the location of the gas source and it was observed that the VME often outperforms the CME.

In a similar way, gas distribution maps generated with remote gas sensors can be used as inputs for GSL. In [84], we presented the Gasbot prototype (Figure 2.9(f)). The robot is equipped with different sensing modalities for perception and environmental monitoring (e.g. a thermal camera and an anemometer). Gas sensing is carried out with a TDLAS remote gas sensor. Using the gas tomography algorithm originally proposed in [85], the prototype was used to create gas distribution models of an underground corridor and a decommissioned landfill where a methane source was placed. Using the location of the Concentration Maximum Estimate (CME) as an indicator, the prototype successfully predicted the location of the methane source with an average error of  $0.60 \text{ m} \pm 0.36 \text{ m}$ .

Similar to the case of gas distribution maps created with *in-situ* sensors, the Variance Maximum Estimate (VME) was observed to be more accurate than the CME as an estimator for GSL. In [86], the maps created with the gas tomography algorithm are evaluated with respect to their capability to predict the location of a gas source in a large outdoor scenario. It was observed that the VME can predict the location of a gas source with a higher degree of accuracy. This is described in more detail in Chapter 5.



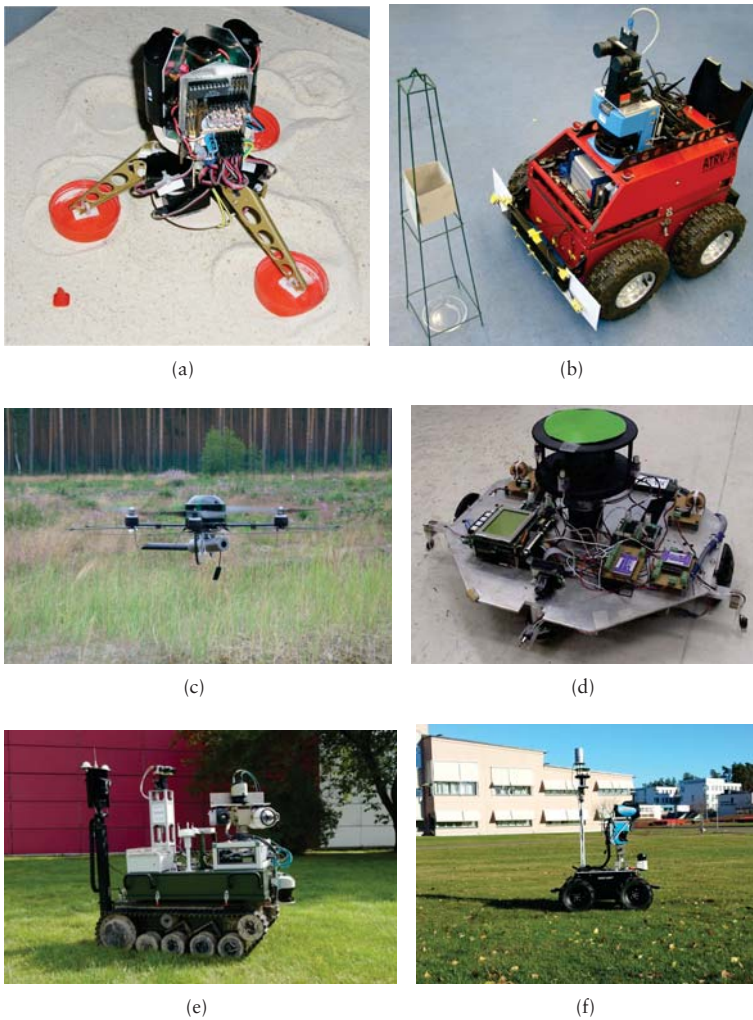


**Figure 2.9:** Examples of robotic platforms for GSL. (a) Underground GSL robotic platform [65]; (b) Wheeled gas sensitive robot [72]; (c) Micro UAV equipped with gas sensing capabilities [74]. (d) Vision-aided gas sensitive robot [76]; (e) The *RoboGasInspector* platform [87]; (f) Gasbot, a *proof of concept* platform for  $\text{CH}_4$  monitoring.

## 2.4 Are Bio-inspired MRO Algorithms Suitable for Realistic Applications?

In this section, we present a set of experiments conducted with wheeled and flying platforms in different environments, ranging from an unventilated, closed room (i.e. a robot arena) to an outdoor open field. The purpose of these experiments is two-fold. First, we present sensor and environmental characterizations in order to illustrate the challenges posed by the limitations of current technologies when performing gas sensing in turbulent environments. Second, using gas source localisation as an example task, we argue that bio-inspired algorithms and/or simplification assumptions (e.g. laminar wind flows) are not the most reliable alternative for MRO systems that operate in realistic environments. Instead, we propose to follow an engineering approach to address GSL. The experiments and the results presented in this section correspond to the contributions originally published in [83] by the author of this thesis.

### 2.4.1 Robotic Platforms

The experiments were performed with two different wheeled robots and one micro UAV (Figures 2.10(a) to 2.10(c)). Compared to flying platforms, wheeled robots have a higher payload, a longer battery life and they can carry more computational resources on-board. In the specific task of gas sensing, a key drawback of using UAVs is that their rotors can influence significantly the air flow, modifying the original gas distribution. On the other hand, flying platforms have less restrictions regarding mobility, compared to wheeled robots. Flying robots for example, are not limited by rough terrain conditions and they can acquire measurements at locations that are not accessible to ground robots (e.g. rooftops, chimneys).

#### Wheeled Robots

Two different ground platforms were used in the data collection process, namely an all terrain robot and a compact, two wheeled platform (Figures 2.10(a) and 2.10(b)). The platforms were originally presented in [88] and in [89] respectively.

The all-terrain platform is an ATRV-JR robot intended for outdoor locations and rough terrains. The two wheeled platform is a Pioneer 3-DX platform from MobileRobotics and, compared to the ATRV-JR, is ideal for experiments indoors in locations with space restrictions. Both platforms are equipped with a laser range scanner (SICK LMS-200) that is used for navigation and localisation purposes. The range measurements from the LMS-200, along with encoder readings from the platform's wheels, are inputs to the AMCL ROS

node<sup>8</sup> module. The AMCL node is an implementation of the adaptive Monte-carlo localisation [39].

In both robotic platforms, gas sensing was performed by using a ppbRAE-3000 PID sensor and an array of MOX sensors in an open sampling configuration. For these experiments, we consider only the TGS2620 from the available sensors in the array. Wind measurements were performed with ultrasonic anemometers. The placement of the anemometer had to be a compromise between the desire to measure the air flow as close to the gas sensors and as undisturbed as possible. It was finally placed above the top of the robot in order to minimize the influence of the fan of the electronic nose and the body of the robot itself. Appendix A provides a comprehensive list of the sensing payload on both platforms.

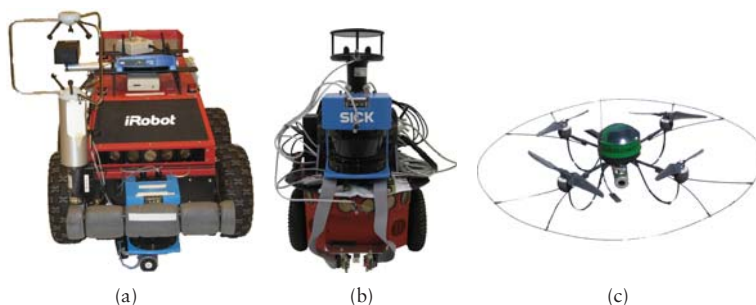


Figure 2.10: Robotic platforms. (a) ATRV-JR. (b) P3-DX. (c) AR-100B.

### Flying Platform

The third platform used is shown in Figure 2.10(c). It is an AR100-B micro UAV developed by AirRobot GmbH & Co. The UAV was modified by the Federal Institute for Materials Research and Testing (BAM, Germany) to incorporate gas-sensitive devices as a payload [66]. The AR100-B is a highly manoeuvrable and compact platform. With a diameter of 1 m and a weight of approx. 1 kg, it supports up to 200 g of payload and its LiPo battery can provide a maximum flight time of about 20 – 30 min. The flight control relies on an on-board Inertial Measurement Unit (IMU) that comprises a three axis accelerometer and a three axis rotation rate sensor. The IMU is also used along with a GPS unit and a compass for localisation purposes. Communication with the ground station is established through a 2.4 GHz RF link in which the data packets sent can include steering instructions or data coming from the payload and the micro UAV's sensors.

---

<sup>8</sup><http://wiki.ros.org/amcl>

Due to payload restrictions, the micro UAV neither carries an anemometer nor a PID. Instead, wind measurements were acquired with the wind triangle approach, as presented in [90] and gas measurements were acquired with a calibrated MOX sensor, specifically, a *Taguchi-type* TGS2611<sup>9</sup>. A calibration curve was obtained by exposing the sensor to known concentrations of the target compound inside a sealed chamber.

## 2.4.2 Experimental Scenarios

In order to have a wide variety of testing environments, experiments were conducted inside a closed room (i.e. a robot arena), an indoor corridor and two different outdoor courtyards. In addition to the description provided in the following paragraphs, a more detailed summary of the experiment conditions can be found in Appendix A.

The robot arena is a  $5\text{ m} \times 5\text{ m} \times 2\text{ m}$  closed room as shown in Figure 2.11(a). Although no artificial air flow was induced, a weak circulating air flow field ( $0.01 - 0.03\text{ m/s}$ ) was formed in the room by natural convection. Ethanol and propanol were released in six separate trials at a constant rate of  $0.2\text{ l/min}$  from a tube placed on the floor. The robot was programmed to move along a predefined spiral path that covered the whole experimental area, stopping at regular intervals to collect measurements. At each measurement point, the sensor data were recorded for 30 seconds and the sensors were sampled at  $4\text{ Hz}$ . The collected datasets were originally presented in [89].

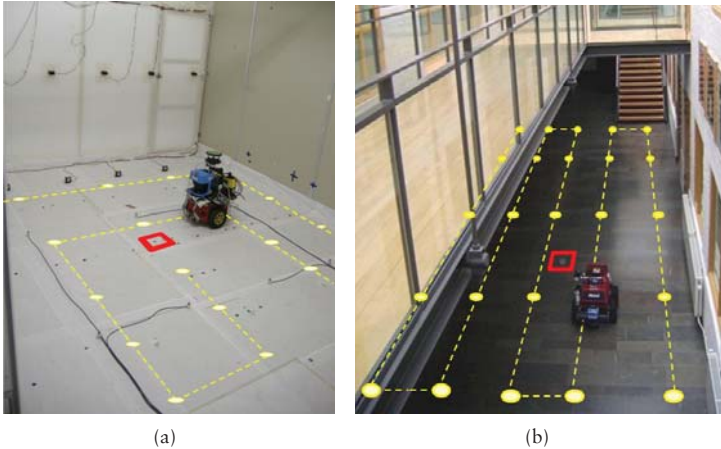


**Figure 2.11:** Indoor experimental scenarios. (a) Robot arena. (b) Indoor corridor.

<sup>9</sup><http://www.figarosensor.com/gaslist.html>

A second set of experiments were conducted in an indoor corridor (Figure 2.11(b)). Compared to the robot arena, the experiments conducted in this scenario were significantly less controlled, since the corridor was not closed during the experimental trials and people were allowed to transit and to open and close nearby doors. The size of the experimental location was  $14\text{ m} \times 2.0\text{ m}$  and a cup filled with ethanol was used as a gas source. The ATRV-JR was commanded to follow a pre-defined exploration path and measurements were recorded at stop points for 30 s, with a sampling frequency of 1 Hz. A total of five experiments were carried out in this scenario as reported in [88].

In order to collect data under conditions of strong wind, experiments were also conducted in two different outdoor scenarios. First, data was collected with the ATRV-JR in an  $8\text{ m} \times 8\text{ m}$  open area with no buildings nearby (Figure 2.12). Ethanol was used as a gas source and the ATRV-JR was commanded to collect measurements at a sampling frequency of 1 Hz, stopping 10 s at pre-defined way-points. Four experimental trials were performed in this scenario, as reported in [88].



**Figure 2.12:** Outdoor experimental scenario. Data was collected with the ATRV-JR platform.

A set of five additional trials were conducted in an open field, as shown in Figure 2.13, using the gas sensitive micro UAV. These experiments were conducted in cooperation with the Federal Institute for Materials, Research and Testing in Berlin, Germany<sup>10</sup>. Methane ( $\text{CH}_4$ ) was released from a cylinder placed in a  $14\text{ m} \times 14\text{ m}$  open area surrounded by nearby trees. In order to spread the analyte away from the cylinder, a fan was placed near the odour outlets. The air current introduced by the fan also prevented the  $\text{CH}_4$  to immediately rise up to the atmosphere when released. The AR-100B was programmed to explore the experimental area following a sweeping trajectory and stopping at way-points for 20 s. Data samples were acquired at 8 Hz and transmitted down to the ground station using the micro UAV's RF link.

<sup>10</sup><http://www.bam.de/en/index.htm>



Figure 2.13: Experiments in the open field with the gas sensitive micro UAV.

### 2.4.3 Environment and Sensor Characterization

As previously presented in Section 2.3, biology is an important source of inspiration in the development of MRO algorithms. More specifically, roboticists have been interested in designing robotic platforms and algorithms that are capable of e.g. detecting and tracking odour cues towards the emitting source. However, as we discussed in [83], the current limitations in the sensing and actuating modalities and the challenges associated with gas dispersion in turbulent environments, prevents the use of biologically inspired algorithms.

Regarding the actuation capabilities of robotic platforms typically used in MRO, ground robots usually operate at linear speeds between  $0.05 - 0.1$  m/s and can perform much less than one turn per second. The limitation in linear speed is mostly chosen to avoid spatial averaging over large areas, which occurs because the gas sensors act as a low-pass filter due to their slow response and recovery time. In comparison, a moth can fly at a linear speed of roughly  $0.5$  m/s and with an average turning rate of roughly  $3.5$  turns/s [91]. Based on these differences it seems possible that current ground robotic platforms are just too slow to perform insect-like reactive steering strategies that allow successful plume tracking in a highly dynamic environment with turbulent air flow. While indeed, UAVs can reach linear and turning speeds comparable to the manoeuvring capabilities of insects, the drawback is their limited payloads that do not allow to equip sophisticated gas sensors on-board and the fact that their rotors can disturb the gas dispersion patterns in the environment.

In order to establish an analogy between the gas sensing capabilities of insects and mobile robots, we can mention the work of Justus and co-authors [92], where it is reported that the filtering applied by moth antennae is a linear, noise-free representation of odourant concentrations in the range of  $1 - 10$  Hz, while the gain is reduced for frequencies below  $1$  Hz. It is argued that the most likely cause for this effect is the adaptation of the receptor cells, a common feature of biological sensory receptors that is most often seen as a slowing or



cessation of response to a constant stimulus. According to the data we collected in the four different scenarios described in this chapter, the bandwidth of the signal collected with MOX gas sensors contains frequencies in the range of 0 – 0.04 Hz while the signal collected with a PID contains frequencies between 0 – 0.15 Hz. It is striking that currently available chemical sensors stop filtering out the signal in the bandwidth that insects actually can perceive and use for tracking an odour plume. On the other hand, chemical sensors capture the signal in a bandwidth that insects filter out through the adaptation process. Therefore, the perception of the chemical stimulus is considerably different for insects, compared to perception with commonly used gas sensors in MRO.

In Figures 2.14 and 2.15 examples of the response profiles of the PID and a MOX sensor are shown. The PID response is linear with respect to the chemical compound concentration and the rise and decay time constants of this sensor are symmetric and much smaller than of the MOX sensors. If located close to a MOX sensor, the PID response can thus provide a good reference of the concentration the MOX gas sensor was exposed to. The plot in Figure 2.14 shows the non-linearity in the response of the MOX gas sensor, and most importantly, the slow dynamics of the MOX gas sensor. The asymmetric low pass filtering performed by the MOX sensor is evident, especially during the long recovery of the MOX sensors.

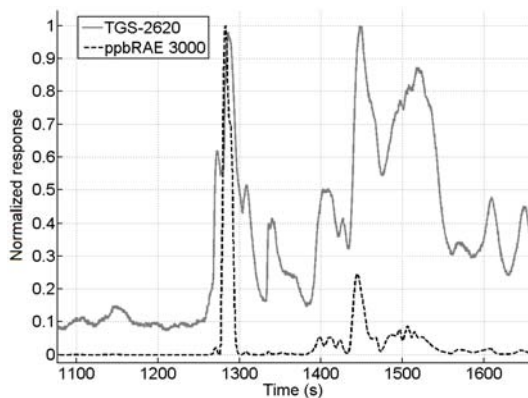


Figure 2.14: Time domain response patterns of the gas sensors in the robot arena.

The spectra of the measurements collected with the MOX sensors and the PID are plotted in Figure 2.15. Due to their slow response time, most of the components of the MOX sensor response are located at low frequencies. For the PID on the other hand, a wider spectrum can be noticed with components located at higher frequencies than for the MOX sensor.

A common simplifying assumption made by different bio-inspired algorithms is that a uniform wind field can be assumed in the exploration areas.

In order to verify the validity of this assumption, we presented in [83] a characterization of the wind flow in the different experimental scenarios. At each experimental location, an air flow map was generated using the data collected in one of the trials and at each way-point, where the robot stopped to collect measurements, a mean wind vector was computed.

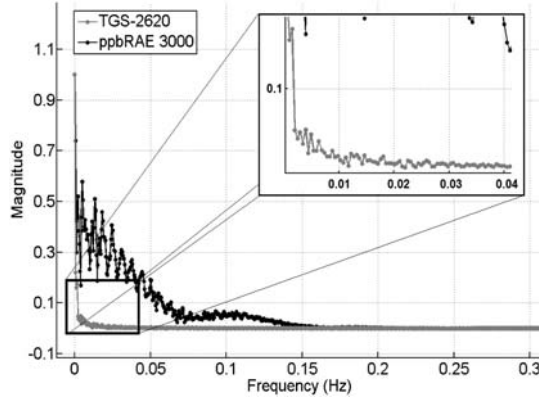


Figure 2.15: Time domain response patterns of the gas sensors in the robot arena.

Figures 2.16(a) to 2.17(b) show the exploration trajectories and the computed air flow maps. The arrow's length represents the average wind speed and the circular mean direction is represented by the arrow's orientation. Although the explored areas are not of considerable size and the measurement points are spatially dense, regularity in the wind flow direction is hardly observed. This clearly indicates that the assumption of a laminar air flow does not hold in any of the four environments. A special case is the air flow map generated with data collected with the micro UAV. Notice that the average air flow direction points to a similar direction in most of the way-points. This is due to the fact that a fan was placed in the experimental scenarios, in order to introduce an advective air flow (See Figure 2.13).

Large directional fluctuations were also observed between measurements taken at single way-points. The polar plots (i.e. wind roses) shown in Figures 2.16(a) to 2.17(b) were computed from a selected way-point (denoted by black squares in the corresponding figures) on the robot's trajectory. Each arrow in the plot corresponds to an individual measurement. The length is proportional to the wind speed and the arrow's direction represents the wind angle. Notice the irregular distribution of the measured wind directions in the rose plots. Accordingly, the circular mean direction (denoted by a dashed grey line) is not a good indicator of the wind conditions present at the way-point, since it does not reflect the observed wind direction fluctuations. To further characterize the observed variability in the wind flow, wind speed histograms



were computed for the selected way-points. Notice that uneven speed distributions were observed, even in the indoor locations, where one might expect less pronounced fluctuations.

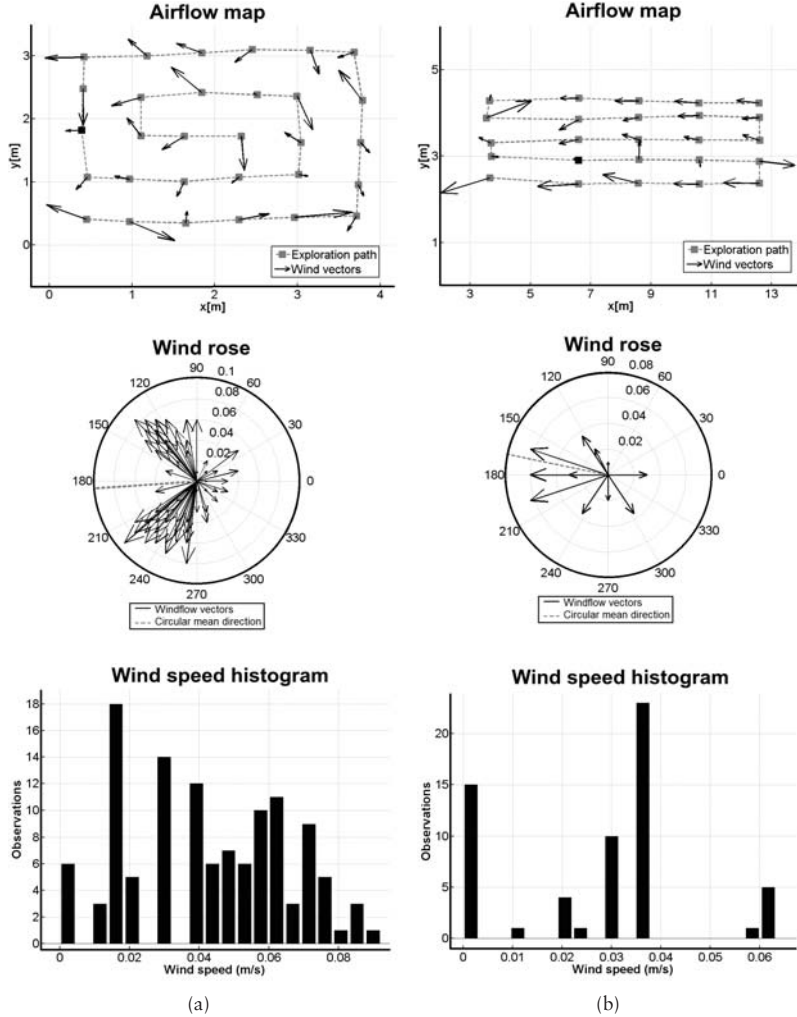


Figure 2.16: Air flow characterization in the indoor environments. (a) Robot arena. (b) Indoor corridor.

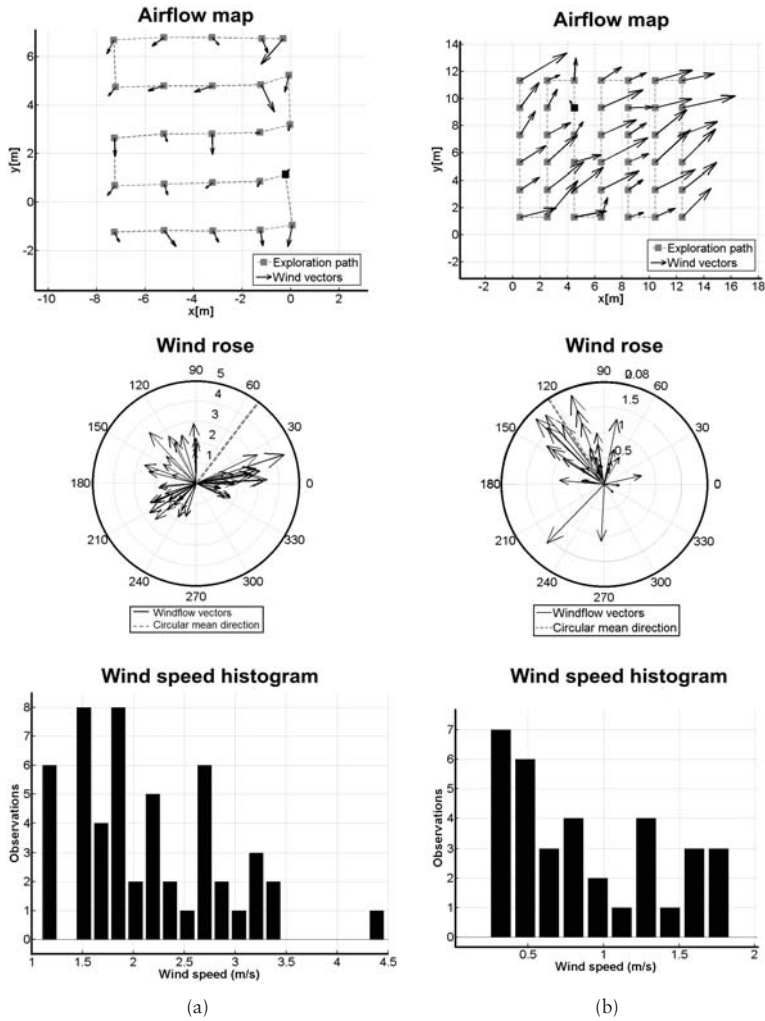


Figure 2.17: Air flow characterization in the indoor environments. (a) Outdoor courtyard. (b) Open field.

### 2.4.4 A Statistical Approach to Detect Gas Leaks

Considering the data, laminar air flows cannot be assumed. This means that gas source localisation algorithms that rely on laminar wind fields, for example the biologically inspired algorithms presented in Section 2.3, are not suitable for these scenarios. In addition, a predefined functional form, such as a Gaussian plume cannot be assumed for the experiments conducted indoors. Refer to the indoor wind speed histograms and the wind roses of Figures 2.16(a) and 2.16(b) where low wind speeds and high directional fluctuations are observed at each measurement point. It can be then assumed that gas dispersion in these environments are dominated by turbulence, which prevents a Gaussian shaped plume to be formed.

As previously stated in Section 2.2, models of the spatial distribution of the gas concentrations can be used to detect emitting sources under turbulent environments with low advective air flows. In order to generate a model of the gas distribution, we use the Kernel DM+V algorithm, proposed by Lilienthal and co-authors in [17]. Kernel DM+V is a non parametric algorithm that does not make strong assumptions about the particular form of the gas dispersion pattern but instead derives a statistical representation of the observed gas dispersion. In addition to a mean concentration map, Kernel DM+V computes a predictive variance map, which allows to predict the gas fluctuations at a given query location. Chapter 5 details on how gas distribution models are generated with Kernel DM+V and provides a review of related state of the art.

According to [56], the Concentration Maximum Estimate (CME) (i.e. the area with the highest concentration value) is a feature that can be used to locate the gas source. Additionally, the Variance Maximum Estimate (VME) (i.e. the area with the highest concentration fluctuation) is another feature correlated with the gas source position [16]. Figures 2.18(a) to 2.19(b) show the mean and variance maps computed using Kernel DM+V, with the acquired concentration measurement at the evaluated experimental scenarios. Notice that in the indoor experiments, where low advective air flows were present, the CME may not be a good estimator of the gas source location since high concentration levels can occur away from the actual gas source (Figures 2.18(a) and 2.18(c)). However, the VME provides a highly reliable estimator for all the experimental scenarios, since areas of high variance are correlated with the actual location of the gas source as previously reported in [16].

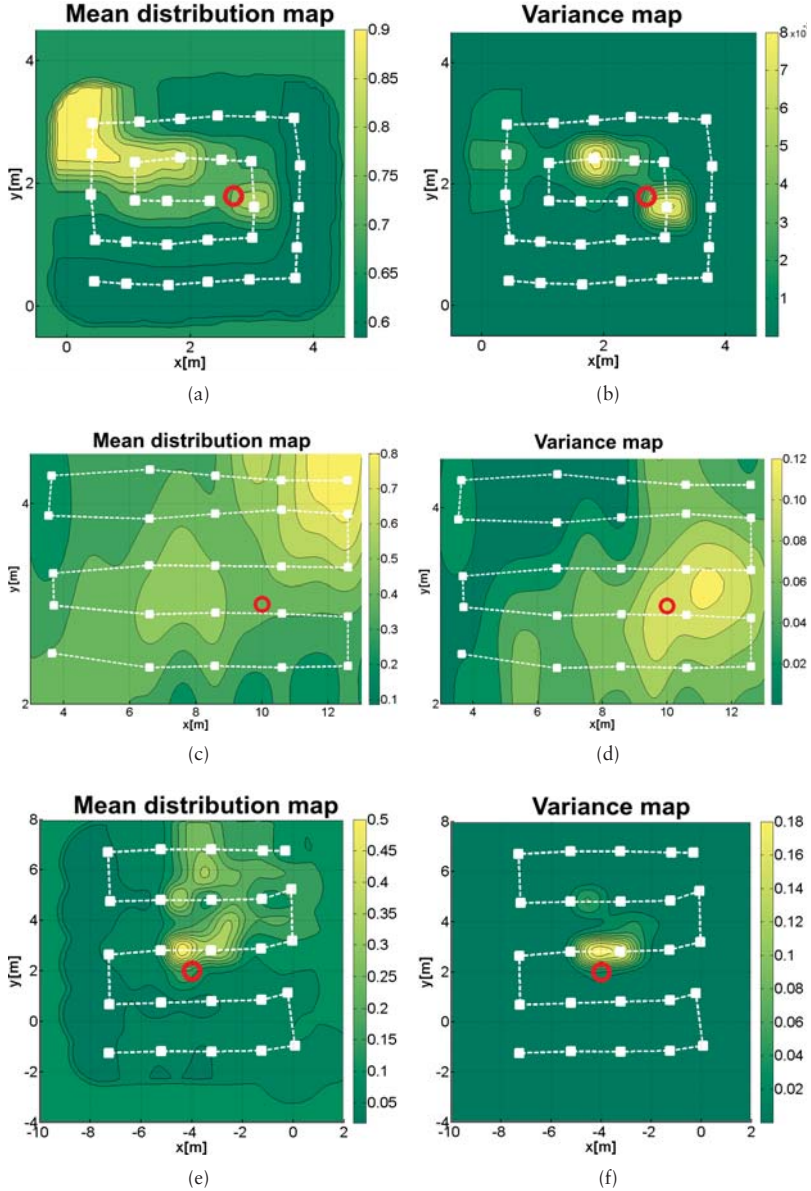
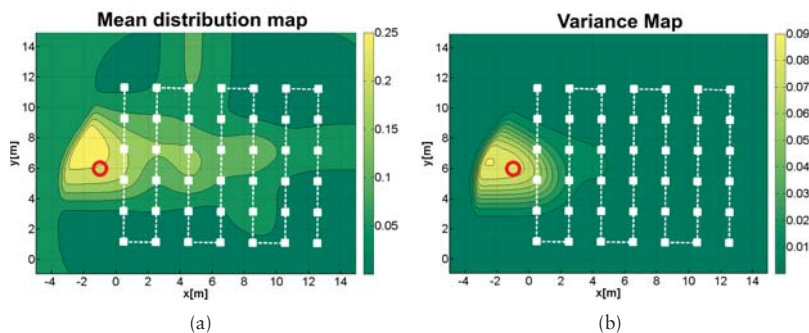


Figure 2.18: Mean and variance maps generated for the evaluated experimental locations. The red marker denotes the actual gas source location while the white dashed lines denote the exploration path followed by the robot. (a), (b) robot arena. (c), (d) indoor corridor. (e), (f) outdoor courtyard.



**Figure 2.19:** Mean and variance maps generated for the evaluated experimental locations. The red marker denotes the actual gas source location while the white dashed lines denote the exploration path followed by the robot. (a), (b) Open field.

## 2.5 Conclusions

This chapter presented a brief overview on the research area of MRO, from its initial developments in the early 1990s, where *toy-like* gas sensitive robots performed reactive plume tracking in tightly controlled scenarios, to current state-of-the-art, in which the first proof of concept prototypes have successfully carried out gas sensing in realistic experimental conditions.

The main contribution of this chapter was originally presented in [83], where the challenges in MRO are identified. The aspects discussed in this chapter are thus the simplifying assumptions made in MRO as well as the current limitations of state of the art gas sensors and actuation mechanisms. In order to characterize the gas sensing mechanism and in order to identify the challenges of gas sensing with MRO, data was collected in a set of prototypical environments, in which different robot platforms collected gas measurements under a variety of experimental conditions. It was shown that, in all of the environments, a constant laminar air flow cannot be assumed. Furthermore, the gas sensing and actuation capabilities of typical MRO systems are not comparable to their biological counterparts and thus, engineering and in particular statistical approaches are preferable to biologically inspired algorithms when performing gas sensing in turbulent environments.

Indeed, the current developments in MRO are promising. However, in order to build MRO systems able to solve practical problems, a number of simplifying assumptions need to be removed. Real world scenarios are dominated by turbulence and thus, unidirectional air flow patterns and an a priori functional form for gas dispersion cannot be assumed. Robust algorithms for gas sensing with mobile robots should consider the limitations of the robotic platforms as well as the challenges implied by gas sensing in turbulent environments. MRO sys-

tem should also address several tasks beyond plume tracking, for example, gas detection, gas quantification, gas discrimination (Chapter 3), gas distribution mapping (Chapters 4 and 5) and gas source localisation. In addition, research in MRO should consider emerging gas sensing technologies, such as remote gas sensors (Chapter 5) or IR cameras that can provide valuable inputs for locations that are meters away from the actual position of the robot.

## Chapter 3

# Gas Discrimination with Mobile Robots

The capability of predicting the identity of acquired gas measurements is of high importance when designing Mobile Robotics Olfaction (MRO) systems. The presence of multiple chemical compounds is expected in most target application scenarios and therefore, MRO systems should be able to discriminate, for example, target compounds from interferent substances. As presented in Chapter 2, gas discrimination can be carried out with laboratory or hand-held equipment based on spectroscopy, optics and analytical chemistry. However, these devices are expensive and often, their bulky size prevents them to be used on-board mobile robots in field inspection routines. An alternative method to carry out gas discrimination is to use arrays of low-cost, partially selective sensors coupled with pattern recognition algorithms. These devices are commonly referred to as *electronic noses* (e-noses).

Early developments in e-nose technology can be traced back to 1920 when Zwaardemaker and Hogewind performed experiments with fine sprayed water to detect the presence of aromatic compounds [93]. The idea that a sensor could be used to discriminate among different gaseous substances was first proposed in [94], where the authors developed a simple device that consisted of a platinum wire and a micro-voltmeter that registered the voltage changes that occurred when the wire was exposed to different compounds. In later research, Moncrieff proposed that an array of six sensors constructed with six different coating materials could be used to discriminate between a large amount of gaseous compounds [95]. It was not until 1982 when independent experiments from Persaud and Dodd [96] and Ikegami and Kaneyasu [97] showed the feasibility of using intelligent sensor arrays for gas discrimination. The term electronic nose was coined in 1988 by Gardner and Bartlett who defined an e-nose as “*an instrument which comprises an array of electronic chemical sensors with partial specificity and appropriate pattern recognition system capable of recognizing simple or complex odours*” [53].

While in its early years e-nose research was heavily inspired by biological principles, this does not necessarily imply that the aim of current e-nose research is to create devices that mimic the capabilities of e.g. the human sense of smell [98]. Instead, e-nose technologies can be considered as complementary devices for the human nose. For example, e-nose systems can be used to identify chemicals that cannot be detected by the human nose (e.g. carbon dioxide) or they can be used to monitor the presence of dangerous substances without risking human lives in the process.

A significant amount of research effort in the e-nose field has been focused on the discrimination of gaseous compounds in laboratory conditions. Under laboratory conditions, humidity and temperature are tightly controlled and gas samples interact with a sensor array in pre-defined exposure cycles. Advances in gas sensing technologies, along with more robust pattern recognition algorithms have allowed to bring e-nose systems outside laboratory conditions to uncontrolled environments. In such scenarios, e-noses can be used as stationary sensing devices or mounted on mobile platforms in an open sampling configuration to address practical tasks related to environmental monitoring [99]. However, gas discrimination becomes significantly more challenging in the absence of laboratory conditions. This is due to the fact that in uncontrolled environments the sensors are under the direct influence of the environment's dynamics and thus, the acquired measurements reflect the unpredictable nature of the turbulence phenomenon.

In the remaining of this chapter we explore the task of gas discrimination using e-nose systems, with the focus on applications of Open Sampling Systems (OSS) in uncontrolled environments. In Section 3.1, the architecture of an e-nose system is presented. In addition, we discuss the differences between gas discrimination under laboratory conditions and gas discrimination with OSS, where the sensors directly interact with the environment without a controlled exposure mechanism. Section 3.2 presents related work in gas discrimination and different application for e-nose technologies. Section 3.3 presents a novel algorithm specifically designed for gas discrimination in uncontrolled environments. This algorithm was originally introduced in [100] and is one of the main contributions of this dissertation. Section 3.4 ends this chapter with conclusions and final remarks.

### 3.1 E-Nose Architecture

Figure 3.1 shows a block diagram of a typical e-nose system. It consists of a sampling and delivery system, an array of non selective sensors and a pattern recognition block. When a gas sample is delivered to the sensor array, a response pattern or a *odour finger print* is generated and in subsequent stages, it is processed in the pattern recognition block. The output of the e-nose system



is then a class estimate or a posterior probability of the sample identity, given the acquired response pattern. The different components of an e-nose system are described below.

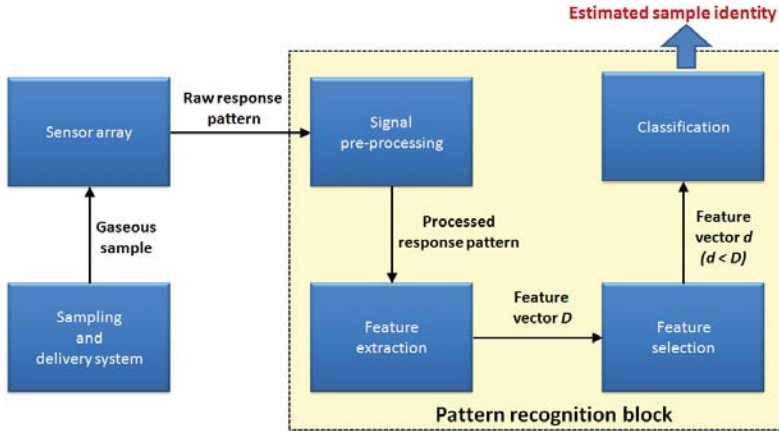


Figure 3.1: Block diagram of an e-nose system.

### 3.1.1 Sampling and Delivery System

In laboratory applications, the sampling process is typically carried out at controlled humidity and temperature levels and gas samples of constant concentration are acquired using for example, vacuum pumps, sampling flow systems or pre-concentrators [101]. The sensors are then exposed to the samples using a controlled exposure cycle commonly referred to as a three phase sampling process (Figure 3.2(a)). In a three phase sampling process, the sensors are first exposed to a reference gas (e.g. clean air) in order drive the sensors to a known state or a *baseline response* level. Then, a gas sample of constant concentration is transported towards the sensor array. When the sensors start interacting with the gas sample a *transient response* pattern is produced. After a few seconds to a few minutes, the sensors reach a *steady response* where typically data analysis is carried out. The sampling process concludes when the gas sample is flushed away and the sensors are allowed to recover their baseline level before injecting a new sample.

However, the three phase sampling process is hardly feasible in MRO applications due to payload restrictions. For example, UAVs or small ground vehicles, cannot carry heavy sensor chambers and they cannot operate vacuum pumps or sampling systems for long periods of time due to energy consumption restrictions. Therefore, the sensors have to be directly exposed to the dynamics

of the environment in a configuration commonly referred to as an Open Sampling System (OSS). Moreover, when performing gas sensing in uncontrolled environments, it is hard to keep constant exposure profiles due to the fluctuating concentration levels produced by the environmental conditions.

Figure 3.2(b) shows the response of a set of MOX sensors mounted on a mobile robot that was commanded to explore an indoor location where a gas source was present. Notice that, compared to Figure 3.2(a), the sensor response does not show a clear three phase profile and that a steady response is never reached. This is due to the lack of a controlled exposure process and due to the chaotic nature of the environment where the gas concentrations fluctuate faster than sensors time constant [98].

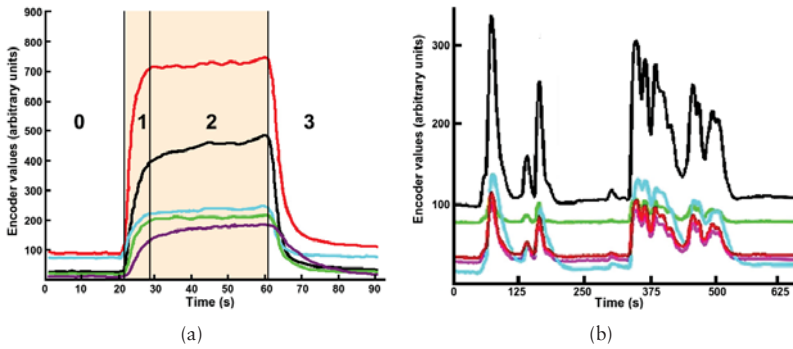


**Figure 3.2:** Response patterns acquired with arrays of MOX sensors using different sampling processes. (a) Three phase sampling process. The numbers on the figure indicate the different stages of the sensor response: 0 - Baseline response, 1 - transient response (rising edge), 2 - steady state, 3 - transient response (recovery edge). The shaded area denotes the time interval during which the sensors were exposed to the gas sample. (b) Response pattern acquired with an OSS mounted on a mobile robot. Both images are adapted from [98].

### 3.1.2 Sensor Array

The sensor array (Figures 3.3(a) and 3.3(b)) is composed of a set of non specific gas sensors. This means that two or more sensors in the array can show sensitivity to the same chemical compound. The different response rates of each sensor in the array produce a characteristic response pattern or a “finger print” when they are exposed to volatiles with a similar chemical composition. Sensor arrays can be constructed using different sensing technologies, for example electrochemical, potentiometric, amperometric, conductometric or optical sensors [27].

Figure 3.3(b) shows a basic measurement circuit for a single MOX sensor (which belongs to the conductometric sensing family). A voltage divider configuration with a load resistor  $R_l$  and an input voltage  $V_s$  are used to measure the sensor's resistance change. The response of a MOX sensor depends on its surface temperature [26] and therefore a heating element ( $R_h$ ), driven by a voltage  $V_h$ , is embedded in the sensor's package. The response pattern is measured at the load resistor  $R_l$ .

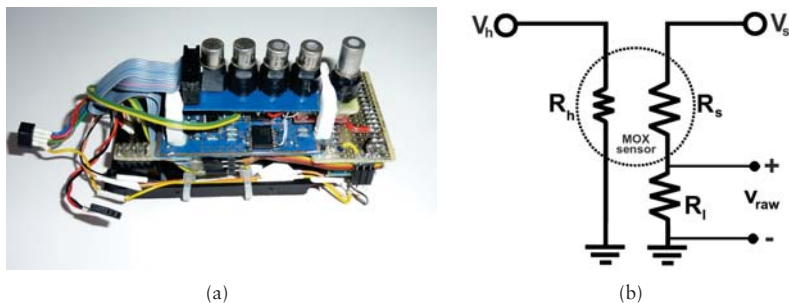


**Figure 3.3:** (a) A sensor array composed by different MOX sensors. (b) Measurement circuit for a MOX gas sensor.

### 3.1.3 Pattern Recognition Block

As previously shown in Figure 3.1, the estimation of the gas identity from the acquired response pattern is carried out in different intermediate computation stages namely signal pre-processing, feature extraction, feature selection and classification as explained below.

#### Signal pre-processing

In this stage, the raw response patterns acquired with the sensor array are conditioned for the further processing carried out in later stages. For example, filters can be applied to suppress unwanted frequency components that are present in the response patterns [101].

As mentioned in the previous chapters, one of the drawbacks of some sensing technologies (such as MOX) is their response drift caused by environmental conditions (e.g. temperature, humidity). Baseline manipulation can be performed in order to limit the effect of the ambient drift and to enhance the contrast of the response patterns. According to [9], baseline manipulation can

be carried out by first recording the baseline response of the array when the sensors are exposed to a reference gas (i.e. clean air). Then, the corrected response is computed by the subtracting the baseline response from the raw response (differential correction), the ratio between the raw response and the baseline response (relative correction) or by a subtracting first and then dividing the raw response by the baseline response (fractional).

### Feature Extraction

The goal of the feature extraction stage is to obtain a set of descriptors from the response patterns that are particularly informative for the classification process. Feature extraction can be seen as a first stage of dimensionality reduction since the aim is to extract a set  $D$  descriptors from a time series of  $N$  samples, where  $N \gg D$ .

Simple feature extraction methods can include for example, the sub sampling of the response pattern at pre-defined intervals or using the average of the sensor response in steady state [98].

In the case of OSS, the lack of a controlled exposure prevents the sensors to reach a steady state response profile. Thus, different authors have proposed to perform feature extraction in the transient (i.e. rise and/or decay) edges of the sensor response.

Feature extraction in the transient edges can be performed by fitting the parameters of an exponential curve [102] or by extracting ad-hoc parameters such as the derivatives of the sensor response or the maximum response value [103]. In addition, feature extraction can be performed by transforming the response transients into a different domain using e.g. the Fourier Transform [104], multi resolution analysis (i.e. wavelet transform) [105] or computing a set of phase space descriptors [106].

### 3.1.4 Feature Selection

In further stages of the gas discrimination process, it is preferable to work with only a subset of features and to remove features that are highly correlated or redundant. In high dimensional spaces, it is difficult to collect enough samples to compute a valid estimate of the discriminant function [107].

Feature selection methods can be grouped in two different categories named filter based methods and wrapper methods [108]. Filter based methods compute a ranking of the features based on an optimality criterion (e.g. linear correlation, information theory ranking) and then, the first  $d$  features in the ranking are selected. Wrapper methods use the success rate of a given classifier to individually evaluate feature subsets. When the search space for the optimal feature subset becomes intractable, search heuristics can be used to ease the computation load. Trincavelli and co-authors proposed in [109] two feature selection

methods (one filter based and one wrapper based) to perform feature selection for the specific task of gas discrimination with mobile robots. The authors evaluated their proposed algorithms with large datasets collected in indoor and outdoor locations with an OSS-equipped mobile robots that followed different exploration trajectories. The results showed that the accuracy in the classification can be improved when applying the proposed feature selection algorithms and that the selection of the optimal feature subset is not intrinsically coupled with the motion of the robot or the particular characteristics of the explored area.

### 3.1.5 Classification

The last stage in gas discrimination is to create a decision rule that partitions the feature space into regions that represent the different classes or gas identities. Instead of computing discrete labels, some applications may require a confidence value as an output from the gas discrimination process. This means that a posterior probability  $p(l|r_i)$  of a sample  $i$  belonging to class  $l$  is computed given a response pattern  $r_i$ . There are several classifiers that have been extensively used in e-nose applications, among others, multi-layer perceptrons [110], K-nearest neighbours [111], Support Vector Machines [112], and Relevance Vector Machines [11]. The interested reader can consult [113] for a thorough review on classification methods commonly used in gas discrimination algorithms.

## 3.2 Applications of E-Nose Technologies

### 3.2.1 Gas Discrimination Under Laboratory Conditions

Under laboratory conditions (e.g. using a three phase sampling process), e-nose systems have been successfully applied to solve practical problems in a variety of application areas. The following examples illustrate how e-nose systems can be a viable solution for different practical problems.

E-nose systems have been applied in the coffee production industry. Among others, tasks such as identification of coffee beans [115] and roasting level [116] have been carried out with high performance levels. E-nose systems have also been brought to the milk and dairy industry. Pais and co-authors [117] used an e-nose system to determine the maturity rates of different cheese brands and Ampuero and co-authors [118] successfully determined the presence of Trimethylamine in milk samples. E-nose systems can be used to determine the ripeness of different fruits and vegetables. For example in [114], a success rate of 100% was achieved when determining the ripeness state of tomatoes using an array of 10 MOX sensors.

In agricultural applications e-nose systems have been successfully applied to determine the presence of different pesticide and bacteria contamination,

as reported in [119]. Campagnoli and co-authors successfully detected animal proteins in livestock food using an array of 10 MOX sensors [120]. Regarding medical applications, e-nose systems have been successfully applied to detect lung cancer from breath samples [121, 122]. Trincavelli and co-authors used an e-nose system to successfully identify 10 different bacteria types from human blood culture samples [123]. Gendron and co-authors reported the use of e-nose systems for the detection of tumour cells in [124]. The authors exposed an e-nose systems to skin and tissue samples and they successfully determined the presence of e.g. melanomas.

### 3.2.2 Gas Discrimination in uncontrolled environments

There are several examples of applications in uncontrolled environments for e-nose systems such as the detection of air pollutants [125] or the identification of explosives [126]. However, a recurring shortcoming when designing e-nose systems intended for uncontrolled environments is that the experimental validation process is carried out using the three phase sampling system, with no interaction with the environment. Such experimental processes do not reflect the actual conditions that can be expected in the target applications. As shown in Figure 3.2(b), when performing experiments in uncontrolled environments with OSS, the response patterns are considerably different compared to the response profiles generated when performing experiments under controlled exposure (e.g. the three phase sampling process).

An early example of an e-nose system for applications outside laboratory conditions was presented by Nicolas and co-authors in [127]. The authors addressed the problem of odour monitoring using an OSS where an array of MOX sensors was directly exposed to the environment. The authors recorded measurements at different locations such as printing houses, paint shops, sewage water treatment plants and sugar cane mills. Data analysis was performed over the recorded data in order to evaluate the feasibility of gas discrimination. While a classification algorithm was not implemented, the authors concluded that, besides the expected variability of the environmental conditions, promising results were observed when applying techniques such as Principal Component Analysis (PCA) [107].

The same authors presented a follow up work in [128], where a network of five OSS nodes was constructed in order to assess the odour annoyance near a compost facility. The e-nose nodes comprised six commercially available MOX sensors. Gas discrimination was framed as a five class problem, in which each class corresponded to a different annoyance source (e.g. exhaust fumes, green composts). This work concluded that an e-nose system can be sufficiently efficient in predicting possible annoyances in the surrounding area, near a compost facility.

A thorough investigation on the challenge of gas discrimination with OSS was presented by Vergara et al. in [129, 130]. The authors constructed a test-

bed that consists of a  $2.5 \text{ m} \times 1.2 \text{ m} \times 0.4 \text{ m}$  wind tunnel and a set of 9 OSS nodes placed at different distances (Figure 3.4(a)) from an emitting gas source. Ten different chemical compounds were used as target analytes under a variety of wind flow regimes and concentrations. The authors concluded that the performance of the system is heavily influenced by parameters such as wind flow and the distance to the gas source. In order to have a robust classification performance, the classifiers would have to be trained using data collected under all possible combinations of environmental conditions. For practical reasons, however, it is not feasible to acquire exhaustive datasets. Thus, classifiers have to be trained using datasets that represent only a small subset of all the possible environmental conditions.

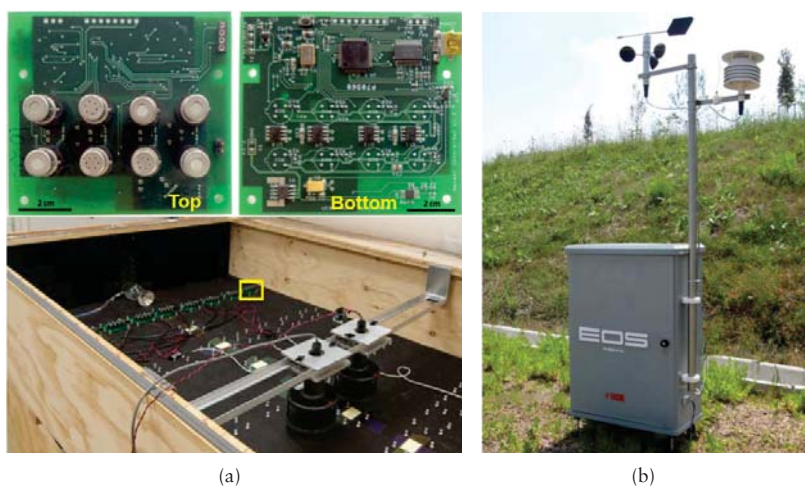


**Figure 3.4:** (a) The wind tunnel and sensor nodes constructed by Vergara et. al. for outdoor gas discrimination [130]. (b) The EOS-507 e-nose developed by Capelli and Dentoni [131, 99].

Capelli and Dentoni presented the development of an e-nose system for odour monitoring in outdoor locations [131, 99]. The authors constructed a sophisticated system (Figure 3.4(b)) composed of an array of MOX sensors enclosed in a chamber where ambient humidity and temperature were kept constant during data collection. Two inlets were connected to the sensor chamber, one for the reference analyte (i.e. neutral air) and a second inlet as an input for the samples. In addition, an anemometers was added to collect wind measurements. The goal of the developed monitoring system was to identify

odour nuisances coming from two water treatment plants and an oil mill. The authors deployed a set of five sensing stations at different locations and data was collected during a period of 10 days. Besides a high classification success rate, the results achieved by the authors are very important in the context of this thesis. First, the authors observed that concentration levels showed strong fluctuations, even when the sensors were placed inside a chamber and sampling systems were used to implement a controlled exposure strategy. Second, the authors concluded that gas discrimination cannot be performed with highly diluted samples (i.e. with low concentration measurements). Therefore, a rejection threshold, analogous to the detection limit of e.g. the human nose, should be set in order to achieve robust classification performances.

### 3.2.3 Gas Discrimination with Mobile Robots

Mobile robots can be equipped with OSS to carry out gas discrimination. Perhaps the earliest prototype of an OSS aimed for robotic applications was presented in [105]. The aim of the proposed system was to construct a module able to provide gas discrimination capabilities for plume tracking robots. The authors in [105] designed an OSS composed of 4 commercial MOX sensors and features were extracted from the rising edges of the sensors response. The authors performed gas discrimination for up to 6 different gas mixtures and found that only 4 seconds of exposure to the gas samples are required to successfully perform gas discrimination. While the authors report a high success rate for some of the target mixtures, the experimental setup is not described in detail and no experiments were carried out with the system mounted on a robotic platform.

Plume tracking and gas discrimination with mobile robots was explored in [132]. The authors developed a mobile platform equipped with an OSS of 10 commercial MOX sensors with the goal of tracking a specific gas plume of either ethanol or butanol (Figure 3.5(a)). Plume tracking was carried out by following concentration gradients measured with two spatially separated OSS placed at either side of the robot and the gas discrimination algorithm uses a spiking neural network [133] as a classification method. The experimental validation carried out by the authors had several limitations that are worth mentioning. First, the exploration area was rather small compared to the size of the robotic platform and more important, gas discrimination and plume tracking were never carried out simultaneously in the same experiment and therefore, the claim of a platform able to track a specific gas plumes was never demonstrated.

A thorough research on mobile robots for gas discrimination was presented by Trincavelli and co-authors in different publications [134, 11, 135, 89]. Among several contributions, Trincavelli evaluated the possibility of performing gas discrimination using different feature extraction techniques such as ad-hoc methods, fast Fourier and wavelet transforms, applied over the transient (rise/decay)



edges of the sensor responses. In addition, different classification algorithms were evaluated. In Trincavelli's work, different arrays of MOX sensors were mounted on ground robotic platforms and the corresponding evaluation experiments were performed in a wide range of experimental scenarios such as a robot arena, different indoor locations (Figure 3.5(b)) and an outdoor courtyard (Figure 3.5(c)), with the goal of discriminating two different gaseous compounds. The authors observed that, when using the rising edges to perform gas discrimination, the robot's movement and the experimental location are factors that influence the performance of the gas discrimination algorithms.

In a subsequent work, Trincavelli and co-authors proposed the use of ensemble classification methods [107] to address the dependency of the discrimination performance on the experimental location [136]. The proposed algorithm followed a two-step process where the experimental location is identified first and in a second stage, gas discrimination is performed. This is, as concluded by the authors, a sub-optimal solution since it imposes the assumption that the robot will be deployed in an already known environment. As an alternative solution, the authors proposed to use only the limited set of features that were found useful for classification across different environments [109].

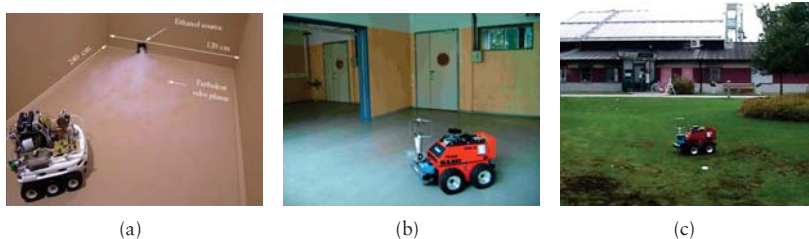


**Figure 3.5:** (a) A toy-like mobile robot aimed at the identification and tracking of specific gas plumes [132]. (b), (c) Examples of experimental scenarios used by Trincavelli and co-authors to validate their gas discrimination algorithms [98].

### 3.3 A Gas Discrimination Algorithm for Uncontrolled Environments

After presenting the different components of an e-nose and reviewing related work, in this section we present a gas discrimination algorithm specifically tailored for OSS. We originally introduced the algorithm in [100]. Compared to the gas discrimination approaches discussed in the previous section, we do not

use a conventional classification algorithm to compute the class posteriors. Instead, the classification process is modelled according to the the particular characteristics of datasets collected with OSS.

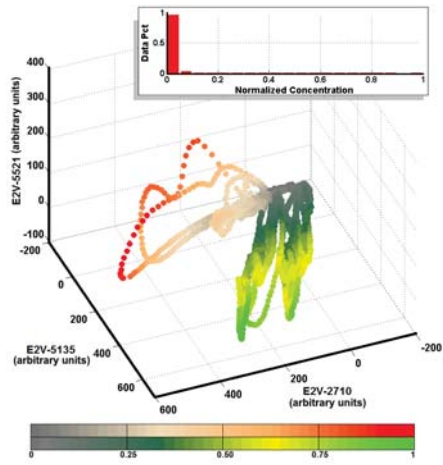
To illustrate the basic principles of the proposed algorithm, refer to figures 3.6(a) and 3.6(b) where two typical OSS datasets are depicted. Both figures represent the feature space plot of a set of measurements collected with a mobile robot equipped with a 3-sensor MOX array. Contrary to the work of Trincavelli and co-authors [109], we do not extract features only at the rising edges of the sensor responses. Instead, the features in the dataset correspond to the recorded instantaneous response of the sensor array. Data collection was performed indoors (Figure 3.6(a)) and outdoors (Figure 3.6(b)), where two sources, namely ethanol and propanol in Figure 3.6(a) and ethanol and acetone in 3.6(b), were placed in separate experiments, one gas source at a time. Brighter color shades are assigned to higher concentration measurements, while low concentrations are plotted in gray tones.

Two key aspects can be noticed in the figures. First, there is a clear correlation between class separability and gas concentration. It can be seen that discrimination at high concentration regions is relatively trivial due to the high separability among the two classes. On the other hand, at lower concentrations, the discrimination problem becomes hard due to the overlapping between the classes.

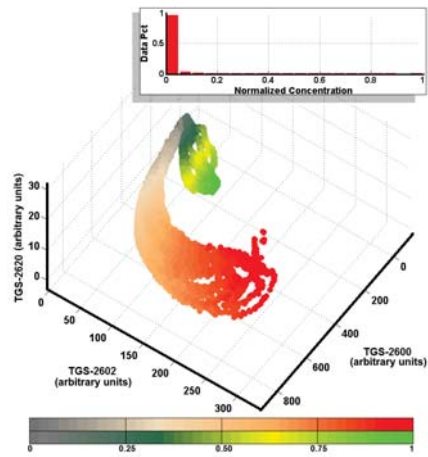
Second, the datasets are unbalanced with respect to the gas concentration. It can be noticed that high concentration measurement are sparse while most of the data lies in the low to mid concentration regions (see the histogram plots at the top right corners on the figures). A density based classification algorithm would tend to assign higher class posterior probabilities to measurement points that lie on densely populated regions, and low posterior probabilities for sparsely represented concentrations. Thus, in order to consider the particular characteristics of the datasets, it is required to incorporate gas concentration information into the algorithm.

From the above observations, we propose a gas discrimination approach for OSS that does not consider the data density to assign class posteriors. Instead, it makes predictions with higher confidence in regions of larger class separability (e.g. at areas of higher concentration), while for areas where the classes overlap, it makes predictions with lower confidence (e.g. areas of low concentration). In addition, by considering class overlap, the posterior of a third implicit class, which denotes the absence of gaseous compounds (i.e. clean air), is learned.

The presented approach assumes that gas sensing is performed only with an array of non calibrated MOX sensors with partially overlapping selectivity and no dedicated sensors for gas quantification (e.g. a PID) are used. While the algorithm is framed as a two class discrimination problem, it can be extended to multi compound applications. The stages of the proposed algorithm are described in the following subsections.



(a)



(b)

**Figure 3.6:** Feature space plots for a two class gas discrimination problem. Each data point is an instantaneous measurement acquired with a 3 sensor array. The color shades denote the normalized response level. (a) Robot arena. Green: ethanol. Red: propanol. (b) Outdoor courtyard. Green: ethanol. Red: Acetone.

### 3.3.1 Signal pre-processing

In the pre-processing stage, differential baseline manipulation is carried out over the raw ADC signals acquired at the load resistor in the measurement circuit (see Figure 3.3(b)). Differential baseline manipulation aims to minimize the effects of temperature, humidity and short term sensor drift [9] by subtracting the baseline response  $\delta_0$  from the raw readings  $\mathbf{v}_{\text{raw}}$  as follows:

$$\mathbf{r} = \mathbf{v}_{\text{raw}} - \delta_0, \quad (3.1)$$

In the previous equation,  $\mathbf{r}$  is an  $n \times D$  response matrix in which  $D$  is the number of sensors in the array and  $n$  is the number of instantaneous sensor measurements. The baseline response  $\delta_0$  is a  $1 \times D$  vector that can be obtained by averaging the individual sensor responses, measured as the voltage drop in the load resistor, when the array is exposed to clean air for a given period of time.

### 3.3.2 Feature Extraction

As shown in Figure 3.2(b), the response pattern in an OSS is given by a set of intermittent transients with no steady state profiles. As proposed by Trincavelli [134], an alternative for the feature extraction process is to segment the sensor responses and extract features only at the rising/decaying edges. Then, a classifier is trained to discriminate between the target compounds. Having in mind that one of the goals of the proposed approach is to learn a class posterior that denotes the absence of gas (i.e. clean air), gas discrimination should not be carried out only at the transient edges but instead, gas discrimination should be performed for each of the  $n$  measurements in the response pattern time series. Therefore, we consider that each measurement in the response pattern is described by a set of  $D$  features given by the instantaneous response of the  $D$  sensors in the array.

### 3.3.3 Feature Selection

As a feature selection stage, we extract a subset of  $\hat{d}$  sensors from the array that improves the gas discrimination success rate. However, feature selection is computationally expensive since, in order to find  $\hat{d}$  by e.g. K-fold cross validation, its required to train and test  $\sum_{d'=1}^D K \times \binom{D}{d'}$  classifiers with  $d'$  subsets of sensors.

By using a class separability metric, it is possible to avoid training and testing multiple models in the sensor selection process. Muezzinoglu and co-authors proposed to use the Mahalabonis distance (MD) as a metric to quantify the separability among classes in gas discrimination problems [137]. The MD is proportional to the distance between-class centres and inversely propor-

tional to the individual covariances. For normally distributed data, MD is the best possible quantification of the class overlap.

In order to use the MD as a separability index, it is required that the distributions under comparison have the same dimensionality, which for the specific case of feature selection, is not always the case since the subsets  $d'$  may have different number of elements. A solution to have a uniform dimensionality over all possible  $d'$  is to compute the MD over the first principal components of the PCA projection of  $d'$ . The number of principal components can be selected according to the percent variance captured by the PCA projection of  $d'$ . Thus, the MD is computed over the first three principal components, which capture at least 90% of the percent variance, and the optimal  $\hat{d}$  is determined as follows:

$$\hat{d} = \underset{d' \subset D}{\operatorname{argmax}} \sqrt{(\mu_1^{(d')} - \mu_2^{(d')})^T S_{12}^{(d')} (\mu_1^{(d')} - \mu_2^{(d')})}, \quad (3.2)$$

where  $\mu_1^{(d')}$  and  $\mu_2^{(d')}$  are the class centres and  $S_{12}^{(d')}$  is the pooled covariance matrix.

### 3.3.4 Classification Algorithm

As previously explained, concentration information is correlated with class separability in gas discrimination problems with OSS. In order to incorporate concentration information in the gas discrimination process, we compute a rough, non calibrated indicator  $I_c$  of the concentration level using the instantaneous measurements acquired with the sensor array. The instantaneous sensor responses can be used as concentration indicators, since over a certain concentration range the logarithm of the change in resistance of a MOX sensor is linearly proportional to the logarithm of the gas concentration [26].

For a given array of  $D$  MOX sensors, the non calibrated concentration indicator  $I_c$  can be computed from the response matrix  $\mathbf{r}_i$  as follows:

$$I_c(\mathbf{r}_i) = \max_{\mathbf{r}_i^{(j)} \in \mathbf{r}_i} \left( \mathbf{r}_i^{(1)}, \mathbf{r}_i^{(2)}, \dots, \mathbf{r}_i^{(D)} \right) \quad (3.3)$$

The above equation considers that the response matrix  $\mathbf{r}_i$  is composed of the conductance readings of the sensor array. The conductance values in  $\mathbf{r}_i$  increases according to the concentration level.

The estimation of the class posterior  $p(l|\mathbf{r})$  is performed by coupling the pairwise probabilities between the target chemical compounds ( $P_{l_1 \vee l_2}$  and  $P_{l_2 \vee l_1}$ ) and the pairwise probabilities between each of the compounds and the rejection class  $l_a$  ( $P_{l_1 \vee l_a}$  and  $P_{l_2 \vee l_a}$ ). The probabilities  $P_{l_1 \vee l_2}$  and  $P_{l_2 \vee l_1}$  are computed with a binary classifier that discriminates only between the compounds  $l_1$  and  $l_2$  and hence,  $P_{l_1 \vee l_2} = 1 - P_{l_2 \vee l_1}$ . The proposed algorithm does not impose a specific requirement on the classification method to compute  $P_{l_1 \vee l_2}$  and  $P_{l_2 \vee l_1}$  and thus, the choosing of the algorithm is implementation free.

The vector of concentration estimations  $I_c$  is integrated in the classification process in the computation of the pairwise posteriors  $P_{l_1 \vee l_a}$  and  $P_{l_2 \vee l_a}$ . To illustrate the process for determining  $P_{l_k \vee l_1}$  (where  $k$  is the gas identity), a plot of  $I_c$  versus  $P_{l_2 \vee l_1}$  is shown in Figure 3.7. It can be noticed that at low concentrations the value of  $P_{l_2 \vee l_1}$  (computed by the binary classifier and denoted by the blue markers) strongly fluctuates. This is an indication of the high uncertainty at low concentration regions in the feature space (e.g. Figures 3.6(a) and 3.6(b)) where class overlapping occurs. It is then desirable to model  $P_{l_k \vee l_a}$  in such a way that the confidence in the predictions gradually increases as a function of the concentration estimator  $I_c$ . Notice in Figure 3.7 that  $P_{l_2 \vee l_a}$  (red line), which discriminates between the substance 2 and air gradually increases as the certainty in  $P_{l_2 \vee l_1}$  stabilizes. The pairwise class probabilities  $P_{l_k \vee l_a}$  can be then modelled as an exponential function with  $I_c$  as the input variable as follows:

$$P_{l_k \vee l_a}(I_c) = 1 - e^{-\beta_k I_c} \Big|_{k=1,2}, \quad (3.4)$$

where the functional parameters  $\beta_k$ , determine the rate of change in the class probability predictions. The functional parameters  $\beta_k$  can be individually learned from the data by dividing the training dataset according to their labels  $l_k$  and using the pairwise probabilities between the compounds (e.g.  $P_{l_2 \vee l_1}$ ) as target variables.

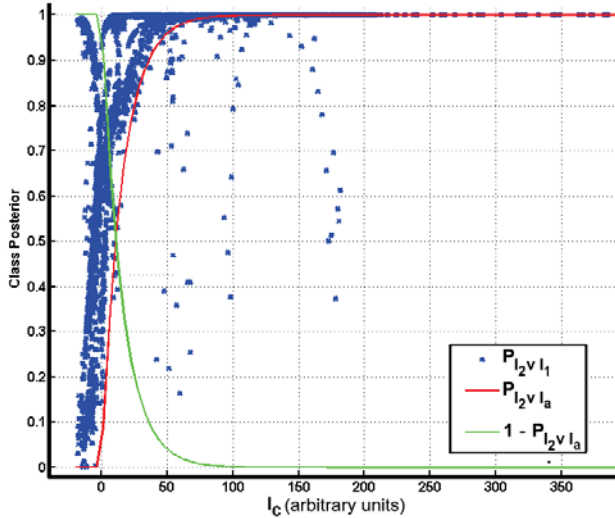


Figure 3.7: Pairwise probability plots. The blue markers denote  $P_{l_2 \vee l_1}$  and the red and green lines are the pairwise probabilities  $P_{l_2 \vee l_a}$  and  $1 - P_{l_2 \vee l_a}$  respectively.

The final computation of the class posteriors  $p(l|r)$  is obtained by coupling the binary class probabilities. In the implementation presented in this work, we used the algorithm proposed by Hastie and Wu in [138, 139], which frames the estimation of the posterior probability as the minimization of the Kullback-Leibler (KL) distance between the pairwise estimates and the true distributions. For a two class discrimination problem,  $p(l|r)$  is computed as follows:

$$p(l_1|r) = 1 - \frac{2 \cdot P_{l_1 \vee l_a} \cdot P_{l_1 \vee l_2} - 2 \cdot P_{l_1 \vee l_a} + 2}{P_{l_1 \vee l_a} \cdot P_{l_1 \vee l_2} - P_{l_2 \vee l_a} \cdot (P_{l_1 \vee l_a} + P_{l_1 \vee l_2} - 1) + 2} \quad (3.5a)$$

$$p(l_2|r) = \frac{2 \cdot P_{l_2 \vee l_a} \cdot P_{l_1 \vee l_2} - 2}{P_{l_2 \vee l_a} - P_{l_1 \vee l_a} \cdot (P_{l_2 \vee l_a} - P_{l_1 \vee l_2}) - P_{l_2 \vee l_a} \cdot P_{l_1 \vee l_2} + 2} + 1 \quad (3.5b)$$

$$p(l_a|r) = 1 - \frac{2 \cdot P_{l_1 \vee l_a} + 2 \cdot P_{l_2 \vee l_a} - 2 \cdot P_{l_1 \vee l_a} \cdot P_{l_2 \vee l_a}}{P_{l_2 \vee l_a} + P_{l_1 \vee l_2} \cdot (P_{l_1 \vee l_a} - P_{l_2 \vee l_a}) - P_{l_1 \vee l_a} \cdot P_{l_2 \vee l_a} + 2} \quad (3.5c)$$

### 3.3.5 Experimental validation

In order to validate the proposed algorithm, we acquired data in two different scenarios namely, the robot arena previously introduced in Section 2.4 and an outdoor courtyard. The experimental conditions allow to evaluate the proposed algorithm under different environmental and wind flow regimes. The robotic platforms and the sensing payloads used in these experiments were introduced in Section 2.4.

In the robot arena, ethanol and propanol were used as target compounds, data collection was performed with the P3-DX mobile robot equipped with an array of six commercial MOX sensors in an open sampling configuration. A total of six single-source experimental trials were conducted in this scenario, with 3 repetitions for each gaseous compound. As described in Section 2.4, the compounds were released using plastic tubes placed on the ground.

A second set of experiments were carried out outdoors in a 9 m  $\times$  7 m outdoor courtyard surrounded by nearby buildings as shown in Figure 3.8. In this scenario, acetone and propanol were released from plastic containers using a *bubbler* that facilitates evaporation and a set of fans were used to spread the gas patches away.

A total of two experiments, one for each compound were carried out in this scenario. At each trial, the ATRV-JR robot (introduced in Section 2.4) was remotely controlled to follow a random exploration trajectory where the robot stopped at way-points for 30 s. Data was recorded during the whole experiment with a 4 Hz sampling rate using an array of 4 commercial MOX sensors in an open sampling configuration. Each experimental trial had a duration of approximately 2400 s. The experimental configurations are detailed in Appendix A.1.1 and A.1.5.



Figure 3.8: The outdoor experimental scenario used for validation.

### Parameter Selection

As previously presented, the proposed approach computes the class posteriors by coupling the pairwise probabilities between the target compounds  $P_{l_1 \vee l_2}$  with the pairwise probabilities between the compounds and air  $P_{l_k \vee l_a}$  (where  $k = 1, 2$ ). As presented in the previous section, the pairwise probabilities  $P_{l_k \vee l_a}$  can be learned from the data. However, the computation of  $P_{l_1 \vee l_2}$  requires to train a classifier which depends on meta-parameters. Therefore, the overall performance of the gas discrimination algorithm depends solely on the parameter selection of the classifier used to compute  $P_{l_1 \vee l_2}$ .

To evaluate the sensitivity of the proposed approach to the selection of parameters, we used two different classifiers to compute  $P_{l_1 \vee l_2}$  namely, a Mixture of Gaussians Classifier (MoGC) and K-Nearest Neighbours classifier (K-NNC). A MoGC is a mixture model [107] that computes the data densities  $p(\mathbf{x}|\gamma)$  by a linear combination of  $\gamma$  Gaussian functions weighted by mixing coefficients. The data densities are used to compute the pairwise probability  $P_{l_1 \vee l_2}$  using Bayes theorem. In a MoGC, the only parameter to optimize is the number of Gaussians  $\gamma$ .

A K-NNC is a non parametric approach that, in order to estimate a prediction on the class label, counts how many members of each class are the set of the  $k$  nearest neighbours [140]. Pairwise probabilities can be given according to the fraction of neighbouring points that belong to each class. In a K-NNC, the number of neighbours  $k$  is the parameter to optimize.

To evaluate the performance of the gas discrimination algorithm with respect to the selection of the classifier's parameters, we considered two metrics namely the classification success rate and the log-likelihood of the predictions. In addition, we compute the percentage of the measurements that are labelled as air (i.e. the measurements that fall in the low concentration rejection class). The success rate and the prediction likelihood are computed using only the data points that do not fall in the rejection class. Notice that ground truth with respect to the target analyte is available since the experiments were carried out



with a single chemical compound placed in the validation scenario. The log-likelihood loss function is then given as follows:

$$\mathcal{L}(\rho|\mathbf{r}) = \sum_{i=1}^n \left[ l_1 \log \left( p(l_1|\rho, \mathbf{r}) \right) + l_2 \log \left( p(l_2|\rho, \mathbf{r}) \right) \right] \quad (3.6)$$

where  $l_1$  and  $l_2$  are the ground truth labels,  $\rho$  is the parameter to optimize ( $\gamma$ , for the MoGC and  $k$  for the K-NNC) and  $p(l_1|\rho, \mathbf{r})$  and  $p(l_2|\rho, \mathbf{r})$  are the estimated class posteriors.

## Results

Figures 3.9(a) to 3.10(d) show the obtained errorbars for the different performance metrics. In both experimental scenarios, the plots were obtained using a search space  $\gamma = [2, 3, \dots, 12]$  for the MoGC and  $k = [5, 10, \dots, 60]$  and 5 fold cross validation.

Regarding the log-likelihood  $\mathcal{L}$  (Figures 3.9(a) and 3.9(b)), it can be seen that the performance of the algorithm improves with larger numbers of neighbours (for K-NNC) or larger numbers of Gaussians (for MoGC). In the case of the MoGC, a larger number of Gaussians implies a more complex model and thus, the risk of overfitting the model increases. In the experiments conducted in the robot arena (Figure, 3.9(b)), it can be noticed that the general tendency is that the selection of the classifier's parameters do not change the classifier's performance drastically.

With respect to the success rate, a similar behaviour can be observed (Figures 3.10(a) and 3.10(b)). While higher success rates can be achieved when increasing the number of Gaussians, the difference between the best and the worst performance of the trained classifiers is not substantially different (2% outdoors and around 1% in the robot arena). As previously mentioned, a complex model implies a higher risk of overfitting. This result is also observed for the K-NNC classifier, in which the success rate of those models trained with a lower number of neighbours (e.g. models with a higher complexity) does not deviate substantially from the models trained with a larger number of neighbours (e.g. models with a lower complexity).

With respect to the samples that cannot be classified due to their low concentrations (i.e. the rejection class), it can be observed in Figures 3.10(c) and 3.10(d) that, for the experiments performed in the robot arena, most of the data was rejected (i.e. labelled as *air*), while in the case of the experiments performed outdoors, only 10% of the data was labelled as air. This can be explained by the fact that the used MOX sensors show a high sensitivity to acetone, which was one of the compounds used in the outdoor experiments. This allowed to perform classification at lower concentration levels. From Figures 3.10(c) and 3.10(d) it can also be observed that the percentage of the rejected measurements

does not vary substantially with respect to the selection of the parameters with either MoGC or K-NNC.

Figures 3.11(a) and 3.11(d) show segments of the  $I_c$  coloured according to their predicted posteriors. Figures 3.11(a) and 3.11(c) are coloured according to the class posteriors computed with a standard classifier (i.e. MoGC) without incorporating concentration information. Figures 3.11(b) and 3.11(d) are computed using the proposed approach. In all figures, the misclassified points are highlighted with a squared marker.

It can be noticed in the figures that with the proposed approach, predictions are made with higher confidence for measurements where the concentration estimator  $I_c$  is higher while at lower values of  $I_c$ , predictions are made with lower confidence. Notice that with the proposed approach classification errors occur close to the baseline response level while with a standard classifier, classification errors can occur at high concentrations and highly confident predictions are made at low concentrations, close to the sensors baseline response. In addition, the proposed approach does not assign high confidences to the erroneous predictions. Misclassified predictions were made with an average confidence of 49% in the robot arena and 59% in the outdoor courtyard. In comparison, erroneous predictions were made with an average confidence of 78% in the robot arena and 88% in the outdoor courtyard using a standard classifier.

It is also interesting to observe the location of the rejected samples (i.e. clean air) with respect to  $I_c$ . It can be seen in Figures 3.11(b) and 3.11(d) that the samples labelled as air are located at low concentration regions at the baseline level. Notice how the confidence for the measurements labelled as *air* decreases as the estimated concentration  $I_c$  increases.

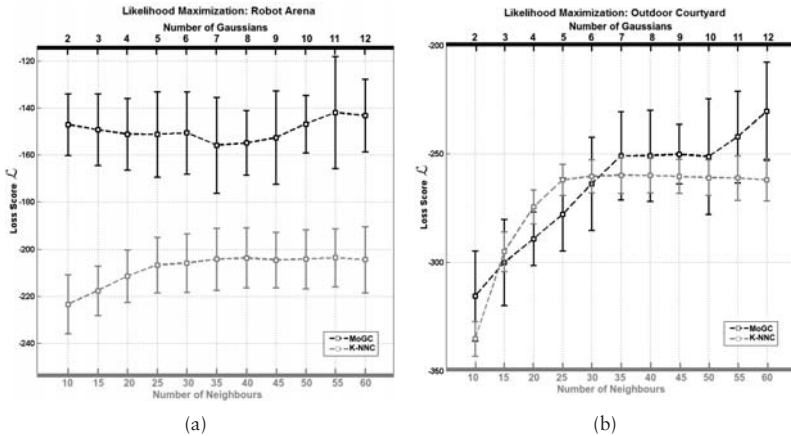


Figure 3.9: Likelihood errorbar plots: (a) Robot arena. (b) Outdoor courtyard.

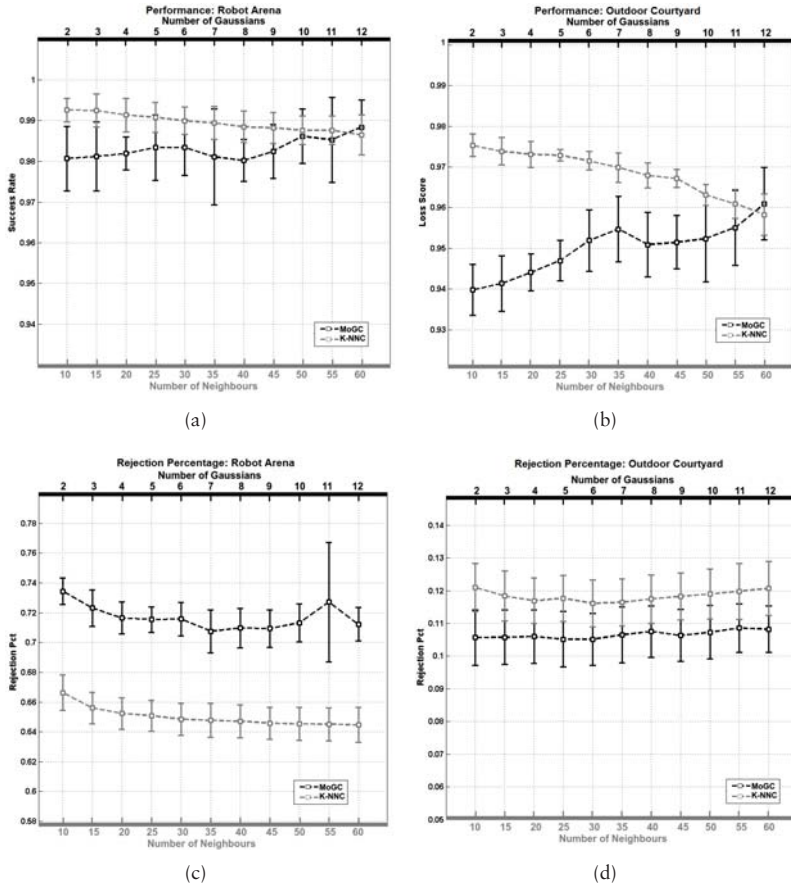
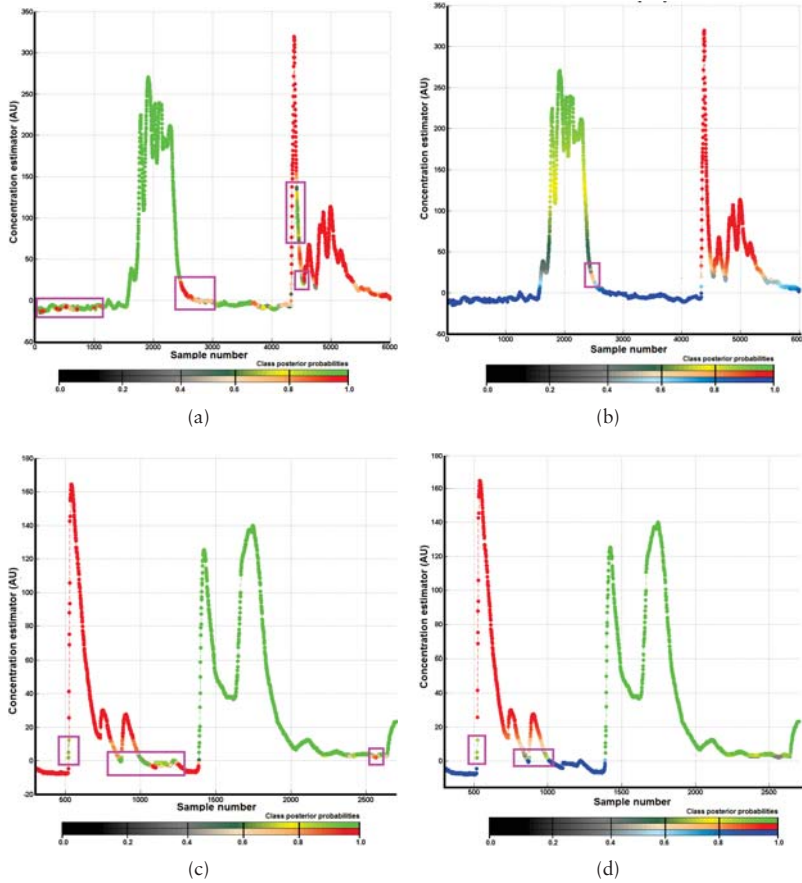


Figure 3.10: Classification performance: (a) Robot arena. (b) Outdoor courtyard. Data rejection percentage: (c) Robot arena. (d) Outdoor courtyard.



**Figure 3.11:** Classification results for a set of testing points using a standard classifier and the proposed approach. The rejected measurements are coloured in shades of blue. Misclassified measurements are highlighted with magenta square markers. (a) Results in the robot arena using a standard MoGC. (b) Results using the proposed approach. For both figures, red shades correspond to propanol and green shades to ethanol. (c) Results in the outdoor courtyard using a standard MoGC. (d) Results using the proposed approach. In both figures, green shades are used for ethanol and red shades are used for acetone.

## 3.4 Conclusions

In this chapter, the task of gas discrimination for mobile robotics applications was explored. Gas discrimination in outdoor environments is not trivial due to environmental factors that influence the phenomenon of gas dispersion. While there are several sensing technologies that can be used to identify chemical compounds on-board mobile robots, we consider e-nose systems due to their low cost, compact size and their relative fast response times compared, for example, with portable analytical chemistry devices such as chromatography devices and ion mobility spectrometers.

The key contribution of this chapter is a novel gas discrimination algorithm that considers the particular characteristics of the datasets collected with e-nose systems in uncontrolled environments using open sampling configurations. As shown in this chapter, the different concentration levels in these datasets are not equally represented, this means that most of the collected data have low concentration values and measurements of high concentration are rather sparse.

In addition, it was observed that class separability increases at higher concentrations while at lower levels, class overlapping occurs. Thus, the proposed algorithm computes the likelihood of the class labels based on the estimation of the concentration level rather than using a data density approach. In this way, concentration information is incorporated in the gas discrimination process so that predictions are made with higher confidence at higher concentrations, while for lower concentration levels, predictions are made with low confidence.

Another key contribution was the introduction of a method to learn a rejection class which is assigned to those samples where discrimination is not feasible due to a low concentration level. Intuitively, the rejection class corresponds to samples of clean air. While in previous works, a rejection class was presented in the form of a threshold [99], in the proposed algorithm a posterior probability is associated to the rejected measurements, which is of high importance for subsequent tasks such as gas distribution mapping, as presented in [100] and discussed in the next chapter.

The presented algorithm was evaluated with data collected with a mobile robot in two different scenarios, namely a robot arena and an outdoor courtyard. High classification success rates were obtained in the validation procedure (in both cases, the success rate was over 97%), and the performance of the algorithm was found not to depend sensitively on the selection of its meta-parameters. Higher success rates can be achieved when more complex models are trained. However, the improvement on the performance is not significant, compared with simpler classification models.



# Chapter 4

## Gas Distribution Modelling With In-Situ Gas Sensors

Gas Distribution Modelling (GDM) is the task of creating truthful representations of the observed gas distribution from a set of spatially and temporally distributed measurements of relevant variables, foremost gas concentration but also wind, pressure and temperature [17].

Maps that show the spatial distribution of gas concentrations are of high interest in different application scenarios. For example, gas distribution maps can be used to identify areas where high concentrations are present (i.e. *hot spots*). The implicit information conveyed by the gas distribution maps can be used to predict the location of gas leaks. Furthermore, gas distribution maps can be used as inputs to create long term emission models of a given facility [141].

The existing GDM algorithms can be broadly divided in *model based* and *model free* approaches. *Model based* algorithms assume that the spatial distribution of gas concentrations can be explained by an underlying mathematical model regulated by a set of functional parameters. This family of algorithms are also often used to simulate gas dispersion in large scale areas, up to hundreds of Kilometres [54].

On the other hand, *model free* algorithms, do not make strong assumptions regarding the underlying functional model that determines the distribution of gases, but rather treat sensor measurements as random variables and derive statistical representations of the observed gas dispersion. A key advantage of these algorithms is that their functional parameters can be learned from the acquired measurements using e.g. cross validation techniques. Due to the computation demands of cross validation, the process of parameter selection is commonly carried out offline. A common assumption made by *model free* algorithms was that only one chemical compound is present in the environment and thus the presence of multiple chemical compounds was not modelled in the computed gas distribution maps. While not being restricted by the size of the target area, *model free* algorithms have been mostly used in small scale applications, for

example to generate distribution maps in indoor and outdoor locations of a few square metres.

GDM can be addressed by using either point measurements, acquired with *in-situ* sensors, or integral concentration measurements, acquired with remote sensors. As explained in Chapter 2, point measurements report the concentration level within a small area around the sensor's surface, typically of a few square millimetres. Integral measurements, on the other hand, report spatially unresolved concentration measurements along an optical beam that can reach up to hundreds of metres [31]. Due to the drastically different nature of remote and *in-situ* sensing, the approaches developed to address GDM with either sensing mechanisms differ substantially.

In this chapter, we focus on the task of creating gas distribution maps with MRO systems equipped with *in-situ* sensors. We present in Section 4.1 and 4.2, the state of the art and related work. For its relevance to this dissertation, we present in Section 4.3 the Kernel DM+V algorithm [17], a *model free* approach for GDM. Then, we present two contributions of this dissertation related to GDM. First, in Section 4.4, we present an algorithm, alternative to cross validation, that can be used to perform parameter selection for GDM in an online fashion, as measurements are being acquired. This algorithm was originally introduced in [142]. Then, in Section 4.5, the Multi Compound (MC) Kernel DM+V algorithm is presented. MC Kernel DM+V removes the assumption of a single chemical compound and thus, individual distribution maps, one for each identified compound, can be produced. MC Kernel DM+V is the main contribution of [143] and [144]. Section 4.6 concludes this chapter with a final discussion and directions for future work in the context of GDM.

## 4.1 Model Based GDM Approaches

Gas distribution models can be created by assuming simple underlying forms for the gas dispersion phenomenon. The use of Gaussian plume models is perhaps the oldest *model based* approach for GDM. This family of algorithms assumes that gas dispersion can be explained by Gaussian shaped plume patterns. Gaussian models have been largely used to solve practical applications such as gas source localization in small scales [80] and large scale release rate prediction of airborne chemicals [19]. However, one of the key disadvantages of this model is that it tends to over simplify the gas dispersion phenomenon, since it does not consider conditions such as terrain distribution and the non uniform wind flow regimes that affect the shape of the gas plume.

More complex approaches can incorporate different meteorological and terrain conditions in their computations. For example, gas dispersion can be modelled as a large number of puffs released in a rapid succession [145] or as point-like particles that represent traces of a given gaseous compound on their path through the atmosphere [146]. While these algorithms can model sophisticated plume shapes, they rely on a large number of parameters such as diffusion



coefficients, that have to be approximated according to the environmental conditions [147].

Computational Fluid Dynamics (CFD) principles can be incorporated in the computation of gas distribution maps. The fundamental basis of CFD models are the Navier-Stokes equations, which describe the motion of fluids. CFD models allow to perform a full three-dimensional analysis where it is possible to infer the wind velocity, ambient temperature distribution and concentration fields [148]. However, tractability becomes an issue since precise knowledge about the boundary conditions is required, which are commonly not known. Simplifications are possible (e.g. unidirectional wind fields) but again lead to unrealistic models and thus, inaccurate predictions.

## 4.2 Model Free GDM Approaches

The earliest example of *model free* GDM is the work developed by Ishida et al. [149]. The authors generated a discrete representation of the gas distribution where the concentration at each measurement point was modelled by the average of the sensor's response measured during five minutes. Hayes and co-workers [73] proposed an algorithm in which two dimensional histograms were used to represent the spatial distribution of water vapour. The bins in the histograms count the number of *odour hits* registered at a given location in the exploration path. An odour hit is counted if the sensor response exceeded a threshold value.

Lilienthal and Duckett [150] introduced the Kernel DM gas distribution modelling algorithm, which performs spatial integration of the sensor measurements with a radially symmetric 2-D Gaussian function. The gas distribution model generated by this algorithm is represented in the form of a grid map, in which a mean concentration value is estimated for each cell. More recently, Lilienthal and co-authors presented in [151] a novel GDM algorithm. Rather than modelling the spatial distribution of average gas concentrations, it models the spatial distribution of *detection* events of a given target chemical compound. The algorithm is based on the Bayesian Inference framework and models the likelihood of *detection* events at a given query location. The advantage of this method is that readings from sensors with different sensing principles can be integrated in the computation of the distribution maps.

A shortcoming of the methods discussed above is that no estimation is given about the fluctuations of the gas concentration. As previously presented in Chapter 2, the estimation of the gas fluctuations, presented in the form of a variance map, can convey useful information. It has been widely demonstrated that areas of high fluctuations are good indicators that can be used for localizing emitting gas sources in environments dominated by turbulence under a weak advective wind flow [16]. The spatial correlation between the gas source and areas of high concentration variability has been pointed out in different works. For example in [152] measurements on turbulent underwater plumes

showed that the magnitude of the concentration fluctuations exhibit a steeper gradient along the downstream direction than the average concentration.

The estimation of the predictive variance provides several advantages for gas distribution modelling, for example, it allows to evaluate the model quality in terms of the data likelihood [153]. In addition, the predictive variance can be used in sensor planning algorithms to suggest new measurement locations [14].

There are several examples of algorithms that provide an estimation of gas fluctuations. Arguably, one of the most commonly used *model free* algorithms in MRO is the Kernel DM+V algorithm, introduced by Lilienthal and co-authors [17]. Kernel DM+V generates mean and variance maps by spatially extrapolating a set of localized concentration measurements using a Gaussian kernel. Due to its relevance in this dissertation, Kernel DM+V is described in detail later in Section 4.3. Stachniss and co-authors [55] presented an approach based on Gaussian Process Mixture (GPM) models. The proposed method allows to represent the rather smooth “background signal” and the areas of high concentration by using different components of the GPM. The components of the mixture model and a gating function, that decides to which component a data point belongs, are learned using Expectation Maximization (EM). Blanco and co-authors presented in [59] a Bayesian approach to generate mean and variance gas distribution models in 2D environments. The authors used a sparse implementation of a Kalman filter that allowed to update the models and make predictions on-line. This algorithm was validated with a dataset collected with a gas sensitive mobile robot inside a sealed room.

The algorithms discussed above implicitly assume that the gas structures are time invariant and therefore, the mean and variance maps are structures that remain constant over time. Recently proposed solutions [60, 59] also consider the time stamps of the acquired concentration measurement in such a way that recent measurements are more significant when computing the gas distribution models.

Another simplifying assumption made by state of the art GDM algorithms is that only one gas compound is present in the environment. In realistic scenarios, where MRO systems are expected to operate, this assumption rarely holds and therefore, the presence of multiple chemicals has to be modelled in the gas distribution maps. To the author’s best knowledge, the work presented in [154] is, besides the contributions we presented in [143, 144], the *only model free* algorithm for multi compound GDM. In [154], the authors used a mobile robot equipped with an e-nose to collect data indoors and outdoors where two different chemical substances were placed, either separated by a physical barrier or separately in independent experimental trials. The authors successfully generated non calibrated mean distribution maps for each of the substances using the algorithm from [150] and a classifier to decide to which map the measurement exclusively contributes. However, gas fluctuations were not modelled. Moreover, in [154], a significant amount of measurements, and thus information, was discarded using a threshold, which rejected low concentration

measurements. However, low concentration measurements can convey useful information for GDM since they can be used to model the absence of gas in the environment.

### 4.3 The Kernel DM+V Algorithm

Kernel DM+V is based on the Nadaraya-Watson estimator [155], which is used to compute, in a sequential way, an average gas concentration map ( $\mu$ ) and a predictive variance map ( $\nu$ ). Kernel DM+V discretizes the exploration area in a grid of cells and concentration measurements are spatially extrapolated using a Radial Basis Function (RBF) Kernel  $\mathcal{N}$ . In the example shown in Figure 4.1(a), the squared marker denotes the location of a single measurement  $c_x$  while the crosses represent the cell centres in the map. At the location of the measurement  $c_x$ , an RBF kernel  $\mathcal{N}$  is placed. The kernel determines the influence of the measurement in the computations of the predictions at neighbouring cells. For illustration purposes,  $\mathcal{N}$  is normalized between 0 and 1. It can be noticed in the example that, due to its proximity to cell  $k_1$ ,  $c_x$  has a higher contribution in the computations for cell  $k_1$  than e.g. for cell  $k_2$ .

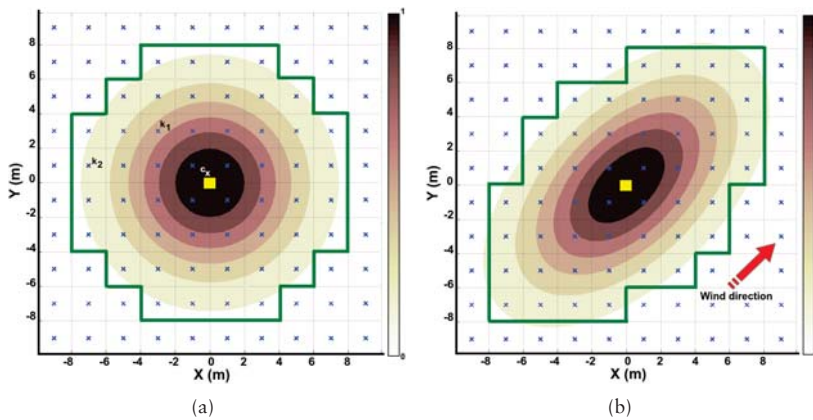


**Figure 4.1:** (a) Spatial extrapolation of measurements using an RBF kernel. (b) Wind information integrated in the spatial extrapolation process with the use of a bi-variate RBF kernel [88]. In both Figures, the squared markers denotes the location of an acquired measurement while the crosses represent the cell centres.

Considering a set of  $n$  localized concentration measurements, the computation of the average concentrations for each cell  $k$  in the mean distribution map  $\mu$  are given as follows:

$$\Omega^{(k)} = \sum_{i=1}^n \mathcal{N}(|\mathbf{x}_i - \mathbf{x}^{(k)}|, \sigma) \quad (4.1a)$$

$$C^{(k)} = \sum_{i=1}^n \mathcal{N}(|\mathbf{x}_i - \mathbf{x}^{(k)}|, \sigma) \cdot c_i \quad (4.1b)$$

$$\alpha^{(k)} = 1 - e^{\frac{-(\Omega^{(k)})^2}{(\sigma \cdot \sqrt{2\pi})^{-2}}} \quad (4.1c)$$

$$\mu^{(k)} = \alpha^{(k)} \cdot \frac{C^{(k)}}{\Omega^{(k)}} + \{1 - \alpha^{(k)}\} \cdot c_0 \quad (4.1d)$$

Equations 4.1a and 4.1b are intermediate computations and correspond to the weight map and the weighted concentration map.  $\mathcal{N}$  is the RBF kernel that models the importance of the measurements acquired at  $\mathbf{x}_i$  to the cell centre  $k$ , as previously shown in Figure 4.1(a). The parameter  $\sigma$  (i.e. the Kernel Bandwidth) controls the smoothing level of  $\mathcal{N}$  and thus a proper selection of  $\sigma$  determines the predictive capabilities of the model.

In order to assign a measurement of confidence in the predictions, Kernel DM+V introduces the concept of a confidence map, computed using Equation 4.1c. The confidence map  $\alpha^{(k)}$  provides an estimate of the confidence in the predictions at a given cell  $k$ . When  $\alpha^{(k)}$  is close to 1, the estimations were computed using a large number of measurements recorded close to the center of cell  $k$ , while a value close to 0 means that only a very few or no measurements were available to compute the posterior estimation at cell  $k$ .

According to Equation 4.1d, the predicted mean concentrations at each cell in the map ( $\mu^{(k)}$ ) are computed by weighting between the extrapolated measurements and a prior assumption using the value of the confidence map at the corresponding cell. This means that, when  $\alpha \simeq 0$ , the output of the model will be close to the prior assumption.

The equations for the computation of the variance maps  $v$  are given below:

$$V^{(k)} = \sum_{i=1}^n \mathcal{N}(|\mathbf{x}_i - \mathbf{x}^{(k)}|, \sigma) \cdot (c_i - \mu^{(k)}(\mathbf{x}_i))^2 \quad (4.2a)$$

$$v^{(k)} = \alpha^{(k)} \cdot \frac{V^{(k)}}{\Omega^{(k)}} + \{1 - \alpha^{(k)}\} \cdot v_0 \quad (4.2b)$$

Similar to the computation of the mean map  $\mu$ , an intermediate computation is performed to extrapolate the squared prediction errors between each of the measurements (acquired at locations  $\mathbf{x}_{i,\dots,n}$ ) and the predictions made by the mean map  $\mu(\mathbf{x}_{i,\dots,n})$  as shown in Equation 4.2a. The confidence map  $\alpha$  is then used to weight between the extrapolated errors and a prior assumption on the variance distribution.

The intuitive implementation of Kernel DM+V allows to extend the original algorithm to different scenarios. For example, by using a multi variate kernel function  $\mathcal{N}$ , three dimensional gas distribution maps can be generated [57]. In addition, wind information can be integrated in the computation of the distribution models by using a bi-variate kernel [88], which can be reshaped according to the wind vector as shown in Figure 4.1(b).

While the computation of the mean map  $\mu$  can be framed as an iterative process, the variance map  $\nu$  cannot be updated iteratively, since it requires the latest update of the mean map  $\mu$  in order to compute the square prediction errors for each acquired measurement measurement and hence, the computation of  $\nu$  has to be carried out from scratch each time a new measurement arrives.

## 4.4 Towards Online Parameter Selection for Gas Distribution Mapping

The performance of a given *model free* GDM algorithm is determined by a proper selection of its meta parameters. Parameter selection is commonly carried out by minimizing a loss function using, for example K-fold Cross Validation (CV). The computational cost of CV is high due to the need for evaluating several gas distribution models, trained with different data folds. Therefore, parameter selection has to be carried out offline.

For critical applications, where parameter selection cannot be performed offline, it is desirable to have a learning algorithm that allows to select optimal parameters online when data is being collected. In [142] we presented an alternative method to perform parameter selection for GDM.

The key idea behind the proposed algorithm is the use of Virtual Leave One Out Cross Validation (VLOOCV), instead of the more traditional CV. In VLOOCV, it is not required to divide the dataset into multiple training/testing folds. Instead, a single model is trained and evaluated using the full dataset and the loss score is adjusted using a set of leverage factors. This opens the possibility of performing bandwidth selection, while measurements are being collected.

### 4.4.1 Parameter Selection for Kernel DM+V

A common method to select an optimal value for  $\sigma$  in GDM with Kernel DM+V is to perform CV over a search space  $\sigma = [\sigma_1, \dots, \sigma_m]$ , with  $m$  being the number

of bandwidths to evaluate. In CV, the training set is randomly partitioned into  $K$  folds, where  $K - 1$  partitions are used to train a model and the remaining fold is used for validation purposes. This process requires to train and test models. The optimal kernel bandwidth can be found in the search space by minimizing a loss function  $E$  that measures the predictive capabilities of the model. While several methods have been proposed in the past to avoid CV by introducing penalizations for complex models (i.e. Akaike, BIC) [156], these methods are not suitable for Kernel DM+V, since they base the selection only on the mean of the estimation, not considering the variance (i.e. the uncertainty in the prediction).

In the specific case of probabilistic predictive models, such as Kernel DM+V, the loss function  $E$  should evaluate not only with respect to its mean concentration predictive capabilities but also, the produced variance model has to be evaluated. The Negative Log Predictive Density (NLPD) is a loss function that considers the likelihood of unseen measurements drawn by the trained model and penalizes overconfident predictions. In this way, the NLPD favours models that tend to be under confident rather than over confident [157]. Under the assumption of a Gaussian posterior  $p(c_i|x_i)$ , where  $c_i$  is the gas concentration measurement at location  $x_i$ , the NLPD of a set of  $D$  unseen measurements  $\{c, x\}$  is given by:

$$E = \frac{1}{2D} \sum_{i=1}^D \left( \log(\nu(x_i)) + \frac{(c_i - \mu(x_i))^2}{\nu(x_i)} \right) + \frac{1}{2} \log(2\pi) \quad (4.3)$$

The computation of a gas distribution model using Kernel DM+V is dominated by the computation of  $\nu(x)$  since it has to be computed from scratch when a new measurement arrives. An update of the maps together with selection of an optimal kernel bandwidth thus requires performing  $K \times m \times N \times N_g$  operations, with  $N$  being the number of measurements and  $N_g$  being the number of cells in the map.

#### 4.4.2 Virtual Leave One Out CV for Bandwidth Selection

Monari and co-authors proposed in [158] the Virtual Leave One Out Cross Validation (VLOOCV) method. VLOOCV relies on the assumption that the withdrawal of a single example from the training set will yield a model that is not substantially different from the model that is obtained by training on the full dataset. The process to justify this assumption is explained in [159]. VLOOCV computes a leverage factor  $h_j$  for each of the training data points, which measures the influence of the training example  $j$  in the computation of the model. If a given data point has a large influence on the model computation,  $h_j$  will be close to 1. On the other hand, when  $h_j$  is close to 0, the data point

has little effect on the model regardless of its presence or absence in the training set. VLOOCV approximates the loss function as follows:

$$E_j^{(-j)} \simeq \frac{E_j}{1 - h_j}, \quad (4.4)$$

where  $E_j^{(-j)}$  is the loss when data sample  $j$  is left out of the training set and  $E_j$  is the loss when data sample  $j$  is included in the computation of the training error. In the specific case of an uncertain regression model,  $E_j$  can be given by the NLPD computed for the data sample  $j$ .

VLOOCV can be used to reduce the computations to select an optimal kernel bandwidth  $\sigma_0$ . Instead of generating  $K$  models, a single model is trained using the whole dataset for each possible  $\sigma$  in the search space  $\sigma$ , and the leverage factors are computed from:

$$\mathbf{H}_{\sigma_i} = \mathbf{Z}_{\sigma_i} \left( \mathbf{Z}_{\sigma_i}^T \mathbf{Z}_{\sigma_i} \right)^{-1} \mathbf{Z}_{\sigma_i} \Big|_{\sigma_i \in \sigma} \quad (4.5)$$

where  $\mathbf{Z}$  is an  $n \times m$  matrix composed by the numerical gradients of the NLPD values w.r.t. the  $m$  elements in the search space  $\sigma$ . Thus, the leverage factor  $h_{\sigma_i}^j$  for a training point  $j$  in the model computed using  $\sigma_i$  is the  $j$ th element in the diagonal of matrix  $\mathbf{H}_{\sigma_i}$ . In this way, the NLPD computation for each data sample is given as follows:

$$E_{\sigma_i}^j = \frac{1}{2(1 - h_{\sigma_i}^j)} \left( \log(v(\mathbf{x}_j)) + \frac{c_j - \mu(\mathbf{x}_j)}{v(\mathbf{x}_j)} \right) + \frac{1}{2} \log(2\pi) \quad (4.6)$$

In this way, the number of operations required to update the distribution maps, and select an optimal kernel bandwidth using VLOOCV is  $m \times N \times N_g$ . Thus, the computational complexity of VLOOCV is still linear in the number of measurements, as in the case of CV, but at a much smaller factor.

### 4.4.3 Evaluation

The proposed approach was evaluated with data collected in two different scenarios, namely the robot arena, described in Appendix A.1.1 and the outdoor courtyard, presented in Appendix A.1.5. In both scenarios, ethanol sources were used as target analytes and gas concentrations were measured using a PID (MiniRAE Lite) mounted on the robot. Inside the experimental areas, the robotic platforms followed exploration trajectories and data was recorded at 4 Hz during the whole experiment.

Figures 4.2(a) and 4.2(b) show the computed NLPD score vs different kernel sizes for the data collected in the robot arena and the outdoor courtyard.

The red curve in both figures was generated using 5 fold CV in the computations of the NLPD. In order to evaluate the effect of the leverage factors, bandwidth selection was performed by using the full dataset to train the model and to compute the NLPD score. This is shown in the figures as the blue curve. The green curve in the figures correspond to the NLPD scores using VLOOCV, including the leverage factors in the computations. Notice that the green curve is hardly visible in the figures since it is almost exactly under the blue curve. This is due to the fact that NLPD scores computed with VLOOCV only and the NLPD scores that include the correction factors are not substantially different. In addition, it can be noticed that there exists a good agreement between the minima obtained with CV, VLOOCV, and VLOOCV without leverage corrections (0.13 m, 0.12 m and 0.12 m respectively for the indoor experiments and 0.13 m, 0.10 m and 0.10 m for the outdoor experiments).

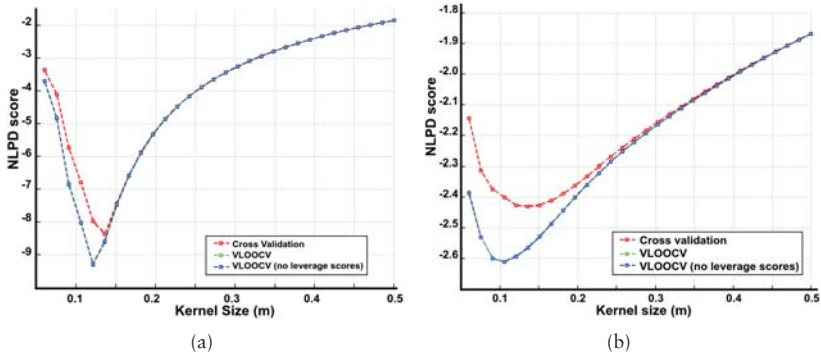


Figure 4.2: NLPD score computed vs kernel sizes. The NLPD was computed using different bandwidth selection methods. (a) Robot Arena. (b) Outdoor Courtyard

In Figure 4.3(a) a plot of the computation time with respect to the number of measurements is shown. The computation times were calculated for CV (red curve), VLOOCV (green curve) and VLOOCV with no leverage scores (blue curve). In the tree cases, the computational complexity is dominated by the update of the variance map and, to a lesser degree, by the computation of the NLPD scores. The generation of different models increases the execution time for CV while, for VLOOCV, the computation of the leverage score increases the computation time linearly, with respect to the number of measurements.

The VLOOCV algorithm is computationally less expensive, while preserving the approximate shape of the objective function. It is worth noting that correcting the negative likelihood with leverage factors does hardly change the VLOOCV result (the green and blue curves in Figure 4.2(a) and 4.2(b) are almost coincident).



The above results suggest that the computation of the leverage factors is not needed for gas distribution mapping data obtained with mobile robots. An explanation is that the models trained with the full dataset and with a fraction of it, as in CV, are very similar and therefore, the leverage scores are close to zero. This can be attributed to the particular structure of the gas sensing data which is highly redundant due to the relatively slow process of gas dispersion, high sampling frequency (4 Hz) and the slow movement of the robot.

VLOOCV relies on the assumption that the withdrawal of a single training data point does not significantly alter the computation of the model. In order to verify this assumption we present in Figure 4.3(b) a comparison between the model computed with the full dataset and a model computed with a fraction of it (i.e K-1 folds). The metric used to compare the models is the overlapping coefficient  $\zeta$ . The overlapping coefficient is a normalized value that measures the overlap between two normal distributions [160]. When  $\zeta \simeq 1$  both distributions are identical, while a value of  $\zeta \simeq 0$  means that the distributions do not overlap.

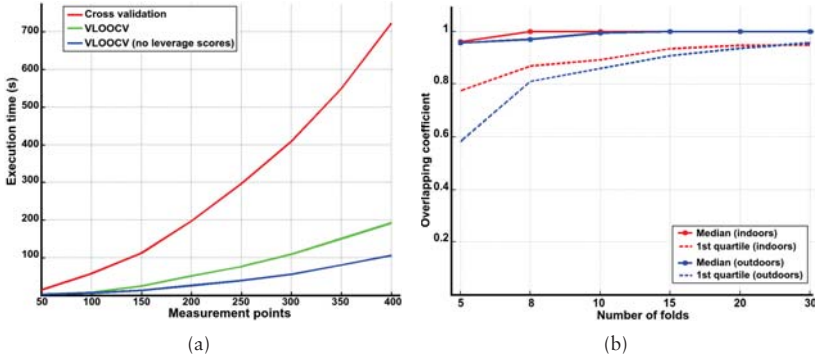


Figure 4.3: (a) Computation time vs number of measurements for different bandwidth selection approaches. (d) Overlapping coefficient of the model calculated on the full dataset and the models calculated on fractions (folds) of the dataset. When the number of folds increases (towards leave one out CV), the similarity between the model obtained with the full dataset and with a fraction of the dataset (computed on K-1 folds) increases as well.

In Figure 4.3(b), the solid line represents the median of the overlapping coefficients while the dashed line represents the first quartile of the data. This means that at least 75% of the data lies above the dashed line. It can be observed that, when the number of folds increases (towards leave one out CV), the similarity between the model obtained with the full dataset and with a fraction of the dataset (computed on K-1 folds) increases as well. This confirms the core

assumption of VLOOCV and demonstrates the high redundancy of the dataset structure.

## 4.5 Gas Distribution Mapping of Multiple Heterogeneous Chemical Compounds

A key desirable feature for a GDM algorithm is the possibility of mapping multiple chemical compounds present at a given area of interest. In order to generate multi compound gas distribution maps, it is necessary to integrate the information regarding the identity of the measured concentration in the computation of the distribution map. In [143, 144], we presented the Multi Compound (MC) Kernel DM+V algorithm. MC Kernel DM+V It is built upon the algorithm developed by Lilienthal et al. in [17] and allows for distribution mapping of multiple chemical compounds by integrating the uncertainty on the gas identification process of each localized concentration measurement.

A block diagram of the MC Kernel DM+V is shown in Figure 4.4. MC Kernel DM+V is a *model free* GDM algorithm that generates a statistical representation of the spatial distribution of multiple chemical compounds. The only assumptions made are that localized gas concentration measurements are acquired with a non selective sensor and that the identity of the measurements is given as a set of posterior probabilities, computed by an external gas discrimination module.

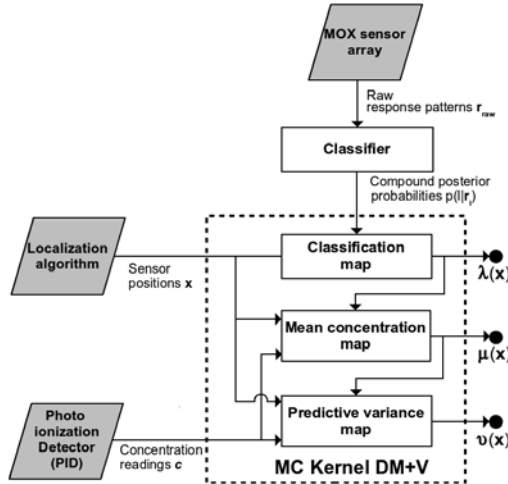


Figure 4.4: Block diagram of the Multi Compound (MC) Kernel DM+V.

As can be seen in Figure 4.4, gas concentration measurements  $c$  are acquired with a PID, and the gas identity of the measurements is provided as posterior probabilities  $p(l|r)$ , computed using the response pattern  $r$  acquired with an array of partially selective sensors. Both  $c$  and  $p(l|r)$  are associated to a measurement location  $x$ . The uncertainty in the computation of the measurement locations  $x$  is not considered in the proposed implementation.

For each identified compound  $l$  ( $l \in L$ ), MC Kernel DM+V computes three maps of the spatial distribution and concentration fluctuation of gas patches at a given exploration area. The mean and variance maps ( $\mu_l(x)$  and  $\nu_l(x)$  respectively) can be seen as a snapshot of the gas distribution in which at each query location  $x$ , predictions of the concentration level and its fluctuations can be drawn. The classification maps ( $\lambda_l(x)$ ) model the likelihood of detecting compound  $l$  at a location  $x$ .

The computation of the maps is carried out in a sequential way from a set of  $n$  measurements. The exploration area is discretised into a grid of cells and the classification maps  $\lambda_l(x)$  are computed first, followed by the predictive mean maps  $\mu_l(x)$  and predictive variance maps  $\nu_l(x)$ . The classification maps  $\lambda_l(x)$  are computed by spatially extrapolating the localized posteriors  $p(l|r_i)$  using the following equations:

$$p_l^{(k)} = \sum_{i=1}^n \mathcal{N}(|x_i - x^{(k)}|, \sigma) \cdot p(l|r_i) \quad (4.7a)$$

$$\lambda_l^{(k)} = \alpha^{(k)} \cdot \frac{p_l^{(k)}}{\Omega^{(k)}} + \{1 - \alpha^{(k)}\} \cdot p_{l,0} \quad (4.7b)$$

where  $\mathcal{N}$  in Equation 4.7a is an RBF Kernel that measures the importance of the measurements, according to their distance to the cell centres  $k$ , as explained in Section 4.3 and the confidence map  $\alpha^{(k)}$  and the weight map  $\Omega^{(k)}$  are computed according to Equations 4.1a and 4.1b respectively. The final computation of  $\lambda_l^{(k)}$  is given by Equation 4.7b, in which  $p_{l,0}$  is a prior assumption on the gas identity. When no other information is available,  $p_{l,0}$  can be set to  $\frac{1}{L}$ .

The predictions of the classification maps  $\mu^{(k)}$  at each cell can be considered as true posterior probabilities since, for a set of  $L$  chemical compounds,  $\sum_{l=1}^L \lambda_l = 1$ . This can be demonstrated by combining equations 4.7a and 4.7b as follows:

$$\begin{aligned} \sum_{l=1}^L \lambda_l^{(k)} &= \alpha^{(k)} \cdot \frac{\sum_{i=1}^n \mathcal{N}(|x_i - x^{(k)}|, \sigma) \cdot p(l|r_i)}{\Omega^{(k)}} + \{1 - \alpha^{(k)}\} \cdot p_{1,0} \\ &+ \dots + \alpha^{(k)} \cdot \frac{\sum_{i=1}^n \mathcal{N}(|x_i - x^{(k)}|, \sigma) \cdot p(L|r_i)}{\Omega^{(k)}} + \{1 - \alpha^{(k)}\} \cdot p_{L,0} \end{aligned} \quad (4.8)$$

Notice that the confidence map  $\alpha$  does not depend on the identity of the compound. Neither does the importance of the measurement computed with the RBF Kernel  $\mathcal{N}$ . Thus, Equation 4.8 can be reorganized as follows:

$$\sum_{l=1}^L \lambda_l^{(k)} = \frac{\alpha^{(k)}}{\Omega^{(k)}} \cdot \left[ \sum_{i=1}^n \mathcal{N}(|\mathbf{x}_i - \mathbf{x}^{(k)}|, \sigma) \cdot (p(1|\mathbf{r}_i) + \dots + p(L|\mathbf{r}_i)) \right] + (1 - \alpha^{(k)}) \cdot [p_{1,0} + \dots + p_{L,0}] \quad (4.9)$$

Considering that  $\sum_{l=1}^L p(l|\mathbf{r}_i) = 1$  and that  $\sum_{l=1}^L p_{l,0} = 1$ , Equation 4.9 can be then simplified as follows:

$$\sum_{l=1}^L \lambda_l^{(k)} = \frac{\alpha^{(k)}}{\Omega^{(k)}} \cdot \sum_{i=1}^n \mathcal{N}(|\mathbf{x}_i - \mathbf{x}^{(k)}|, \sigma) + 1 - \alpha^{(k)} \quad (4.10a)$$

$$\sum_{l=1}^L \lambda_l^{(k)} = \frac{\alpha^{(k)}}{\Omega^{(k)}} \cdot \Omega^{(k)} + 1 - \alpha^{(k)} = 1 \quad (4.10b)$$

The predictions of the classification maps are subsequently integrated in the computation of the mean and variance maps by using the following *maximum a posteriori* function:

$$\psi(\mathbf{x}_i) = \begin{cases} 1 & \lambda_l^{(k)}(\mathbf{x}_i) > \lambda_j^{(k)}(\mathbf{x}_i) \Big|_{l,j \in L} \\ 0 & \text{otherwise} \end{cases} \quad (4.11)$$

$\psi(\mathbf{x}_i)$  evaluates the predictions made by the classification maps  $\lambda_l$  (and not by the gas discrimination algorithm) at each location  $\mathbf{x}_i$ . This implies that, instead of considering individual instantaneous compound posteriors, the identity of neighbouring measurements are as well considered in  $\lambda_l$ . In this way, erroneous predictions in the gas identification are filtered out and they do not contribute to the computation of  $\mu_l$  and  $v_l$ . Equation 4.11 implicitly assumes that  $\lambda_l$  is sufficiently stable over time. The function  $\psi_{li}$  returns an  $L \times 1$  vector in which 1 is assigned to the compound predicted with the highest prior and zero is assigned otherwise. A mean concentration map  $\mu_l$  is then computed for each of the  $L$  target compounds as follows:

$$C_l^{(k)} = \sum_{i=1}^n \mathcal{N}(|\mathbf{x}_i - \mathbf{x}^{(k)}|, \sigma) \cdot c_i \cdot \xi_l \cdot \psi_l(\mathbf{x}_i) \quad (4.12a)$$

$$\mu_l^{(k)} = \alpha^{(k)} \cdot \frac{C_l^{(k)}}{\Omega^{(k)}} + \{1 - \alpha^{(k)}\} \cdot c_{l,0} \quad (4.12b)$$

The parameter  $\xi_l$  in Equation 4.12a corresponds to the *correction factor* for compound  $l$ . This parameter is related to one of the assumptions made by the algorithm, which is that the concentration measurements are given by a non specific gas sensor. In the case of a PID, the device is calibrated with a reference gas (e.g. isobutylene) and the manufacturer provides a table with *correction factors* for different compounds. Thus, once the chemical has been identified, the measurement reported by the device has to be multiplied by the corresponding *correction factor* to obtain calibrated concentration measurements. Similarly to the classification maps,  $\alpha^{(k)}$  in Equation 4.12b balances between the weighted concentration values in Equation 4.12a and a prior assumption on the gas concentration  $c_{l,0}$  for each compound  $l$ . Using a prior assumption on the variance  $v_{l,0}$  for each compound, the variance maps can be computed as follows:

$$V_l^{(k)} = \sum_{i=1}^n \mathcal{N}(|\mathbf{x}_i - \mathbf{x}^{(k)}|, \sigma) \cdot (c_i \cdot \xi_l - \mu_l^{(k)}(\mathbf{x}_i))^2 \cdot \psi_l(\mathbf{x}_i) \quad (4.13a)$$

$$v_l^{(k)} = \alpha^{(k)} \cdot \frac{V_l^{(k)}}{\Omega^{(k)}} + \{1 - \alpha^{(k)}\} \cdot v_{l,0} \quad (4.13b)$$

where Equation 4.13a, computes the weighted square error between the corrected concentration measurements and the predictions made by the mean concentration maps.

In Equations 4.12a and 4.13a, the binary output from  $\psi(\mathbf{x}_i)$  is used to compute  $C_l^{(k)}$  and  $V_l^{(k)}$  instead of directly using the predictions of the classification maps  $\lambda_l(\mathbf{x}_i)$ . The rationality behind this decision is that the predictions made by the external classifier, and thus the predictions from  $\lambda_l(\mathbf{x}_i)$ , do not consider mixtures between target compounds. This means that the predicted class posteriors cannot be considered as mixture percentages. The use of  $\psi(\mathbf{x}_i)$  reflects the assumption of binary gas patches made by the external classifier. A suggested extension is to train a regression function to predict the mixture percentages between the target compounds. Then, the predicted mixture percentage can be directly used in equations Equations 4.12a and 4.13a.

#### 4.5.1 Parameter Selection for Multi Compound Gas Distribution Maps

The kernel bandwidth  $\sigma$  is the only functional parameter that determines the predictive capabilities of MC Kernel DM+V. Compared to algorithms that assume a single chemical compound, the process of learning  $\sigma$  becomes more challenging due to the lack of ground truth to evaluate the gas distribution models for each compound. In order to have ground truth data to evaluate the predicted models, it would be required to acquire measurements with highly selective sensors to measure the concentration levels for each target compound.

In the original Kernel DM+V algorithm,  $\sigma$  is learned by dividing the dataset into training and testing folds and the predictive capabilities of the mean and variance maps are evaluated using the Negative Log Predictive Density (NLPD) loss function. However, this approach is not feasible in the multi compound scenario, since it would require ground truth concentration measurements for each of the identified compounds. This is certainly not feasible to acquire using non specific gas sensors. Therefore, alternative methods have to be developed to learn  $\sigma$ .

In [144], an alternative method was proposed which learns the mapping parameter  $\sigma$  by evaluating the capability of the classification maps  $\lambda_l$  to predict the posterior probabilities  $p(l|r_i)$  of unseen measurements using the Total Variation Distance (TVD) [161] as a metric. The TVD quantifies the distance between two probability distributions, namely the class posteriors drawn by the classifier and the class predictions made by the classification maps  $\lambda$ . The selection of TVD as a metric instead of e.g. the more commonly used Kullback-Leibler (KL) divergence [107] is due to the fact that when the posteriors  $p(l|r)$  are close or equal to zero, the KL divergence is undetermined and thus assumed to be equal to 0. This means that a considerable amount of measurement points would have to be ignored.

The proposed algorithm divides the dataset in training and testing folds and, for each element in the search space  $\sigma = [\sigma_1, \sigma_2, \dots, \sigma_j]$ , the classification maps  $\lambda_{\sigma_j, l}$  are computed. Thus, by using the  $n$  testing data points, the optimal  $\hat{\sigma}$  can be determined as follows:

$$\text{TVD}(\sigma_j) = \sum_{l=1}^L \sum_{i=1}^n |\lambda_{\sigma_j, l}(\mathbf{x}_i) - p(l|r_i)| \quad (4.14a)$$

$$\hat{\sigma} = \underset{\sigma_j \in \sigma}{\text{argmin}} \text{TVD}(\sigma_j) \quad (4.14b)$$

## 4.5.2 Evaluation

The MC Kernel DM+V algorithm was evaluated with data collected in the robot arena and the outdoor courtyard, both introduced in Section 2.4. The robots were equipped with different MOX sensor array configurations for gas discrimination and in both scenarios, true concentration measurements were acquired with a PID. In order to validate the capabilities of the MC Kernel DMV algorithm to map multiple chemical compounds, experiments were carried out with two simultaneously emitting sources of different, in addition to the experiments conducted with single compounds. In the robot arena, ethanol and propanol were used as target compounds and the emitting sources were placed at different distances from each other. A total of 3 experiments were

carried out with the sources separated by 1.5 m, and 3 additional experiments were conducted with the sources separated by 0.5 m. In the outdoor courtyard, ethanol and acetone were used as target compounds. A total of three experiments were carried in which 2 trials were performed with a single gas source (one for each substance), and a third experiment was conducted with the two gas sources present at the same time, separated by 2.0 m.

In both scenarios, the gas discrimination algorithm proposed in Section 3.3 was used to compute the class posteriors. The key advantage of this algorithm is that it provides a class posterior for a class rejection that denotes the absence of chemical compounds. In other words, when used with MC Kernel DM+V it allows to model the presence of clean air inside the exploration area. The experiment trials in the robot arena and in the outdoor courtyard were carried out with different sensor sets and with different combinations of target substances. Therefore, the optimization process for the classifier was run separately for each scenario.

A Mixture of Gaussians (MoG) classifier was used to compute the pairwise probabilities between the target compounds and 5-fold CV was used to select the number of Gaussians  $\hat{\gamma}$  from a search space  $\gamma = [2, 3, \dots, 12]$ . Sensor selection was performed using the Mahalanobis Distance (MD) approach explained in Section 3.3. The data collected in the single source experiments were used to optimize the parameters since for each experiment, the identity of the gas is known and therefore, ground truth is available to compute the classifier's performance. For the robot arena, the classification success rate was  $0.98 \pm 0.07\%$ , with 3 sensors selected (E2V-5135, E2V-2710 and E2V-5521) and  $\hat{\gamma} = 5$ . In the outdoor courtyard, the success rate was  $0.96 \pm 0.01\%$ , with a subset of 3 sensors (TGS-2620, TGS-2602 and TGS-2600) and  $\hat{\gamma} = 12$ .

The obtained gas distribution models can be seen in Figures 4.5(a) to 4.5(c). Only two trials with different spacing between sources for the robot arena are shown. The bandwidth  $\sigma$  for each experiment was learned using the proposed TVD approach. For all experiments, the bandwidth search space was  $\sigma = [0.05, 0.1, 0.15, \dots, 2.00]$  and for the experiments presented in Figures 4.5(a) to 4.5(c), the optimal bandwidths  $\hat{\sigma}$  were 0.15, 0.15 and 0.20 respectively. The classification map is presented in the form of a maximum a posteriori plot. The maps show higher probabilities of detecting the analytes at locations where neighbouring data samples were consistently classified with high confidence. In the case of Figure 4.5(b), it can be noticed in the classification map that the Propanol likelihood drops close to 50% in the neighbouring locations around the gas source, while for locations away from it, the likelihood drastically rises up to 100%. Intuitively, high posteriors would be expected close to the actual gas source. However, due to the low concentration levels recorded by the robot nearby the source, the confidence in the predictions dropped.

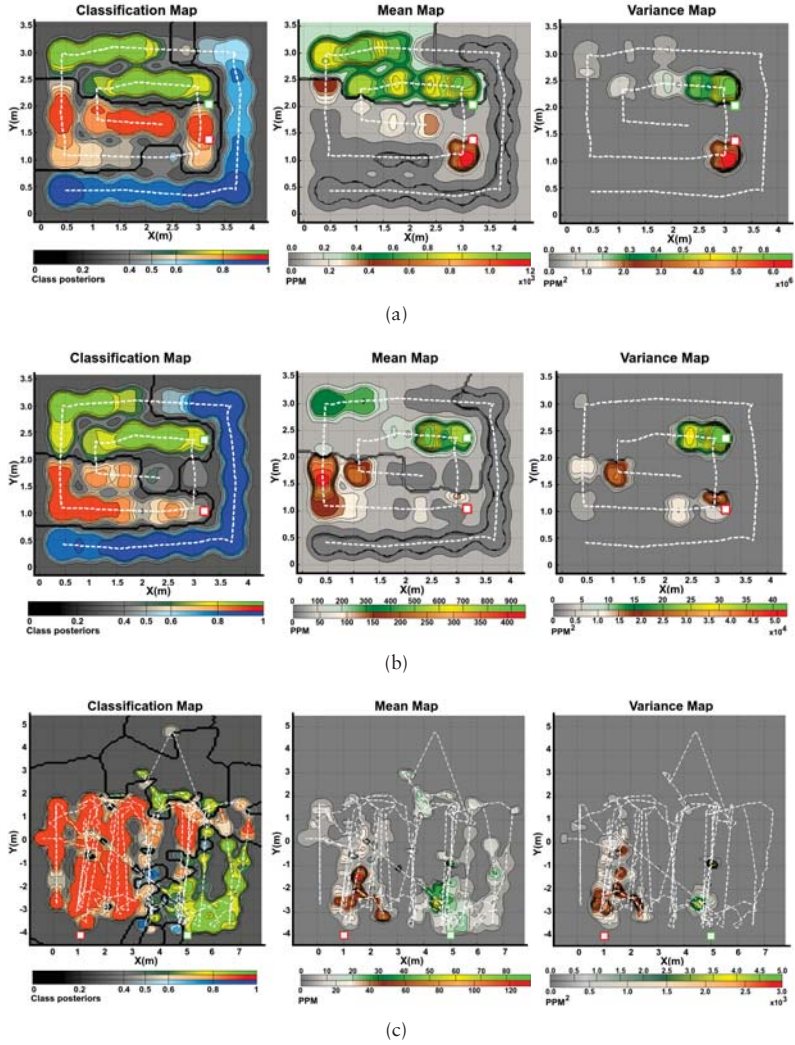


Figure 4.5: Generated gas distribution models in two experiments in the robot arena with ethanol (green) and propanol (Red) gas sources separated by (a) 0.5 m and (b) 1.5 m. (c) Generated models in the outdoor experiment. In all the maps, green shades correspond to ethanol and red shades correspond to acetone. For both experiments, the blue shades in the classification maps denote the likelihood of finding clean air at a given position in the explored area. The dashed lines denote the robot's path and the actual source locations are indicated by squared markers.



The predictive mean concentration maps were generated by combining the individual mean concentration maps for each substance masked with the classification maps. While we do not have ground truth to evaluate the accuracy of the distribution maps, it can be noticed that the computed distribution maps predict well defined plumes at the neighbouring locations of the actual source locations.

In a similar way as with the mean distribution maps, combined variance maps were generated as shown in Figures 4.5(a) to 4.5(c). We can qualitatively evaluate the produced models by considering the implicit information they contain. It can be noticed that, areas with high variance are located in the vicinity of the actual gas source locations, which is an expected result since concentration fluctuations are often found to peak significantly near an emitting gas source [16].

Figure 4.6 shows an additional trial inside the robot arena. Notice that in the classification map, the probability of detecting propanol (red shades) is low (less than 50%) at locations near the emitting source. In a similar way, the mean map predicts concentration values close to 0 ppm near the propanol source, and also the case of the variance maps, do not predict no noticeable gas fluctuations.

The resulting maps computed in this trial can be explained by the concentrations measured during the experiment. In Figure 4.7, the acquired concentration measurements are shown. The measurements are coloured according to their computed class posterior (see the color code at the left). Please notice that low concentrations were measured close to the location of the propanol source and therefore, the gas discrimination algorithm assigned low posteriors due to the uncertainty in the classification process.

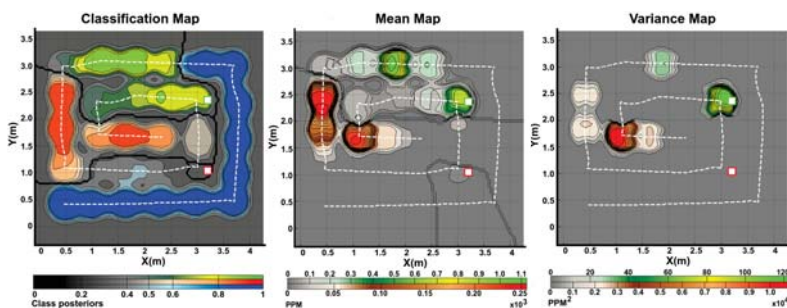


**Figure 4.6:** An additional experiment conducted in the robot arena with ethanol (green) and propanol (Red) gas sources separated by 1.5 m. Notice that the maps do not predict the presence of propanol near the source.

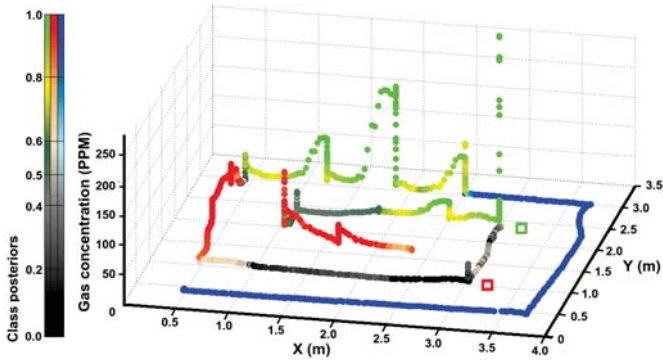


Figure 4.7: Acquired concentration measurements during in experimental trial shown in Figure 4.6. The measurements are coloured according to the computed class posteriors (green - ethanol, red - propanol, blue - air).

## 4.6 Conclusions

Gas Distribution Mapping (GDM) aims to generate truthful representations of the spatial distribution of gas concentrations in a given area of interest. Gas distribution maps are of high importance in different gas monitoring related applications, for example for leak localization, detection of *hot spots* and prediction of release rates.

While a brief review on different GDM approaches is presented in this chapter, the main focus is on a specific subset of algorithms, commonly referred to as *model free* GDM algorithms. *Model free* algorithms do not make strong assumptions regarding the underlying equations that govern the gas dispersion phenomena, but rather derive statistical representations of the acquired sensor measurements. In this context, two related contributions were presented, namely an approach to reduce the computation time for parameter selection and an algorithm to learn gas distribution maps of multiple chemical compounds. While the presented contributions were evaluated with datasets collected with mobile platforms, they are not, in any means limited to mobile robotics and could therefore be applied to applications where data was collected with localized sensing nodes.

The predictive capabilities of *model free* algorithms depends on a set of meta parameters that are commonly selected using computational expensive algorithms such as Cross Validation (CV), which needs to train and evaluate multiple models. In this respect, a parameter selection algorithm that uses Virtual Leave One Out (VLOOCV) was proposed. The advantage of VLOOCV is that it only requires to train and evaluate a single model and to compute a set of leverage factors needed. The evaluation performed with datasets acquired in a

robot arena and in an outdoors courtyard showed that similar parameter selection can be achieved when compared with CV, but at a reduced computational time.

For the specific case of gas sensing, it was demonstrated that the computation of the leverage factors can be obviated due to the particular structure of the gas sensing data, which is highly redundant due to the relatively slow process of gas dispersion and high sampling frequency. Thus, the possibility of performing parameter selection using VLOOCV can be further explored in related applications such as gas discrimination and gas quantification.

One of the assumptions made by state of the art algorithms is that only one chemical species is present at a given time. This assumption rarely holds in realistic scenarios. In addition, it is often required to estimate the distribution of more than one chemical species at a given location in tasks such as emission characterization in industrial facilities [162].

The Multi Compound (MC) Kernel DM+V, presented in this chapter, represents an important step in GDM of multiple chemical compounds. MC Kernel DM+V generates  $L$  gas distribution maps, one for each of the  $L$  identified compounds by integrating the posterior probabilities in the estimation of the gas distribution maps. The assumption made by MC Kernel DM+V is that concentration measurements are acquired with a non selective sensor (such as a PID), and the compound posteriors are estimated by, e.g. an e-nose. A key feature introduced by the algorithm is the computation of classification maps. A classification map is computed by spatially extrapolating the compound posteriors in order to estimate the likelihood of detecting a given compound at a query location. In this way, the posteriors of neighbouring locations are considered when drawing an estimation of the identity of a given measurement.

The gas distribution maps derived with MC Kernel DM+V can be considered as true concentration estimations since the algorithm allows the introduction of *correction factors* that are given by the sensor manufacturer. Considering the assumption that concentration measurements are acquired with a non specific sensor, the *correction factors* are needed in order to adjust the acquired readings according to its corresponding gas identity.

A key issue, not only in the case of multi compound GDM, but in gas sensing in uncontrolled environments is the lack of ground truth. Therefore, the evaluation of the multi compound models computed using MC Kernel DM+V with respect to their predictive capabilities was not possible. However, the obtained results show consistent distribution maps where plume shaped structures predict high concentration areas around near the measurement points where a high average concentration was sensed. In addition, it was observed that the multi compound variance maps provide useful information by highlighting areas near the locations of the chemical sources.

The presented implementation of MC Kernel DM+V allows for several expansions as future work. First, the algorithm can be extended to allow for multiple kernel bandwidths, one for each identified compound. This however,

would increase the computational complexity of the parameter selection process.

Second, gas mixtures can be introduced in the computation of the distribution maps. For the specific case of a set-up where concentration measurements are acquired with a PID, the introduction of gas mixtures would not not require further changes in the algorithm. This is due to the fact that that the *correction factors* for gas mixtures can be computed as a linear combination of the individual *correction factors* for each identified compound. In this context, the key challenge would be to train a regression algorithm that computes the gas mixture percentages with the corresponding uncertainty estimation.

## Chapter 5

# Gas Distribution Modelling With Remote Gas Sensors

One of the main drawbacks of *in-situ* gas sensing technologies is their limited spatial coverage. Each reported measurement is a point concentration that covers only a few square centimetres around the sensor and for some sensing technologies, such as metal oxide sensors, a direct interaction between the sensor surface and the target compound is required. Thus, gas sensitive robots equipped with *in-situ* technologies require to navigate to the target measurement locations in order to acquire measurements. This poses a serious challenge in areas where mobility is restricted or where navigation is not possible at all. In addition, battery life becomes a factor to consider for such systems since the need for physically travelling to each measurement location translates into a higher energy consumption.

An alternative is to equip Mobile Robotics Olfaction (MRO) systems with remote sensors that, as explained in Chapter 2, allow to acquire gas concentration measurements without e.g. chemically interacting with the target compounds. Robots equipped with remote sensors bring clear advantages over *in-situ* equipped MRO systems. For example, larger areas can be covered in shorter periods of time and locations that are not physically accessible (e.g. chimneys, roofs) can be remotely scanned.

However, one of the drawbacks of some remote sensing technologies such as spectroscopy based devices is that they report spatially unresolved integral concentration measurements. This means that the sensor itself does not provide any information regarding the path followed by the emitted beam or the gas distribution along the optical path. While alternative physical principles allow to acquire spatially resolved gas measurements, devices built on such principles are expensive and some of them require extremely bulky arrangements that are mounted only on-board large vehicles such as buses or trucks [31] and thus their use is limited to outdoor field inspection.

In this chapter, we address the task of Gas Distribution Mapping (GDM) using integral concentration measurements. In literature this task is commonly referred to as Computed Tomography of Gases (CTG). CTG is inspired by Computer Assisted Tomography (CAT) where the image of a static object is reconstructed from a set of attenuation measurements. In CTG however, the phenomenon of interest (i.e. gas dispersion) is highly dynamic. CTG is commonly carried out using fixed measurement geometries, where emitters, receivers and reflectors are placed at known positions and they are never changed during the operation of the measurement setup. The tomographic reconstruction of the concentration field is then carried out using the acquired concentration measurements and the optical paths as inputs.

We evaluate in this chapter the incorporation of remote sensors in MRO systems to perform GDM. Thus we introduce the concept of *Robot Assisted Gas Tomography* (RAGT) and we evaluate its use with respect to the practical application of landfill monitoring. Compared to static CTG configurations, in RAGT the estimation of the sensor optical path plays a critical role and is heavily determined by the accuracy of the robot's pose estimation algorithms.

This chapter is structured as follows: In Section 5.1 we introduce basic concepts and related work to gas tomography. Section 5.2, presents the concept of RAGT and in Section 5.3, RAGT is evaluated in a landfill monitoring related application. Conclusions and final remarks are then presented in Section 5.4.

## 5.1 Computed Tomography of Gases

The earliest work related to Computed Tomography of Gases (CTG) can be traced back to 1978, when Byer and Shepp [18] proposed a theoretical system to perform *tomographic reconstruction* of gas patches that could be present at a given area of interest. The authors proposed to build a *fan-beam* measurement system that consisted of an actuated tunable laser source placed at the center of an exploration area and a set of detectors placed at the borders. When the emitter is directed towards one of the detectors, the incident ray is reflected, creating a fan beam of angle  $\gamma$  that hits two different detectors placed at different points in the circumference of the measurement array. When the laser source is rotated and aimed towards the different detectors in the array, the whole area surrounded by the detectors can be inspected. The authors proposed a set of equations to compute the number of detectors and the required transmitted power to cover areas of different sizes but the proposed system was not physically implemented. However, the main contribution of this pioneering article was the concept of a measurement system, analogous to CAT, that could be used to estimate the distribution of gas concentrations inside an area of interest.

A practical realisation of a CTG system can be seen in Figure 5.1(a). In the measurement geometry shown in the figure, a set of sensors are placed at known positions and are aimed towards the inspection area. The optical paths

are shown in different shades of grey and along them, integral concentration measurements can be acquired. Depending on the technology, the sensors can either emit a single beam, such as in the case of Tunable Diode Laser Absorption Spectroscopy (TDLAS) sensors, or multiple beams such as Differential Optical Absorption Spectroscopy (DOAS) sensors. In the case of single beam sensors, actuators can be used to increase the number of optical paths and to improve the coverage of the measurement geometry. For technologies such as DOAS or FTIR, artificial reflectors have to be introduced in the setup. TDLAS sensors on the other hand, can be pointed e.g. towards the ground or walls to reflect the emitted rays.

Different approaches have been proposed to perform tomographic reconstruction. Similarly to GDM with *in-situ* sensors, CTG can be carried out by assuming a priori functional forms for the gas distribution pattern. Perhaps the most widely used *model based* CTG approach is the Smooth Basis Function Minimization (SBFM) algorithm proposed by Drescher et al. in [163]. The authors parametrized the concentration field as a summation of a set of Gaussian functions. The parameters of the Gaussians are then fitted to the acquired integral concentration measurements using e.g. an optimization based approach. While the authors successfully obtained tomographic reconstructions inside indoor locations, one of the main drawbacks of this approach is that a priori assumptions on the gas distribution model rarely hold in turbulent scenarios.

Alternatively, CTG can be carried out using *model free* approaches. This means that no a priori assumption is made regarding the functional form of the gas distribution pattern. CTG is then the task of estimating the concentration field given a set of acquired integral concentrations  $\mathbf{Y}$ . Assuming that the concentration field is known, each acquired integral concentration value  $y_i$  is given by:

$$y_i = \int_{L_i} \mu(L_i) dL_i \quad (5.1)$$

where  $L_i$  corresponds to the optical path of measurement  $i$ . The measurement units of  $y_i$  are then given in  $\text{ppm} \cdot \text{m}$  and they correspond to the integral concentration over the optical path  $L_i$ .

A common approach to model the concentration field is to discretise the exploration area into a finite grid of  $M$  cells. It can then be assumed that at each cell  $k$  there is an uniform concentration  $x_k$  (where  $k = 1 \dots M$ ). Each integral concentration measurement  $y_i$  is then given as the summation of the  $M$  concentrations  $x_k$  multiplied by a basis function  $a_k$ , that models the segment of the optical path travelled inside cell  $k$  [164]. In this way, a set of  $N$  acquired integral concentration measurements can be then described by the following linear system of equations:

$$\mathbf{Y} = \mathbf{A}\mathbf{x}, \quad (5.2)$$

where  $\mathbf{Y}$  is a vector that contains the  $N$  integral measurements,  $\mathbf{x}$  is an  $M$  column vector that contains the concentration values at each cell in the grid. The elements in the  $N \times M$  matrix  $\mathbf{A}$  are computed by a basis function. For example, using a box model basis function [164], each element in  $\mathbf{A}$  corresponds to the intersection between the optical paths  $L_i$  and the cells  $k$ . Thus, each integral measurement  $y_i$  is modelled as follows:

$$a(L_i, k) = \begin{cases} L_i \cap k & L_i \in k \\ 0 & \text{otherwise} \end{cases} \quad (5.3a)$$

$$y_i = \sum_{k=1}^M x_k \cdot a(L_i, k) \quad (5.3b)$$

Figure 5.1(b) illustrates how integral concentration measurements are modelled using box basis function (Equation 5.3b), where  $y_i$  is the summation of the intersections between the optical path  $L_i$  and the traversed cells  $k$ , multiplied by the concentration  $x_k$ .

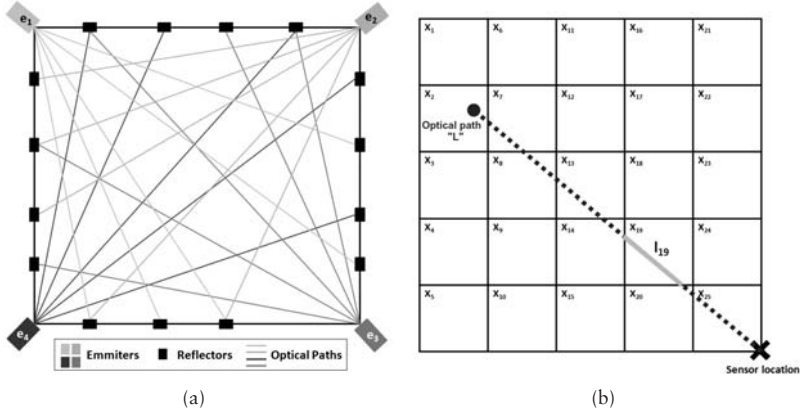


Figure 5.1: (a) A typical CTG setup were four sensors are placed at the corners of an area of interests. (b) Decomposition of a given integral concentration measurement using a set of box basis functions. The measurement in the figure can be thus expressed as  $y = l_2 \cdot x_2 + l_7 \cdot x_7 + l_8 \cdot x_8 + l_{13} \cdot x_{13} + l_{14} \cdot x_{14} + l_{19} \cdot x_{19} + l_{20} \cdot x_{20} + l_{25} \cdot x_{25}$ .

The goal of *model free* CTG algorithms is then to solve the system of equations in 5.2 by finding a vector of concentrations  $\mathbf{x}$  that explains the acquired integral concentration measurements  $\mathbf{y}$  best. The use of conventional Computer



Assisted Tomography (CAT) algorithms has been proposed as a mean to estimate the concentration vector  $\mathbf{x}$  [165]. However, gas tomography poses a different set of challenges than image reconstruction and thus conventional CAT algorithms may not be suitable for CTG. Compared to CAT, where the object under study is a rigid body, the reconstruction process in CTG is focused on a very dynamic process caused by gas dispersion, where concentration levels are not static and they show strong fluctuations. Proposed *model free* CTG approaches can include, for example, the use of least squares to compute the concentration vector  $\mathbf{x}$ , the inclusion of a priori information such as constraints on the concentration values and the use regularization terms that imply the assumption of a smooth concentration field [166, 85].

In common CTG setups, the number of optical paths is scarce. This means that the coverage of the measurement geometry is limited and thus, a number of cells can go unobserved. According to [167], a CAT setup for medical applications can have up to 10,000 paths while in the case of CTG, the number of optical paths rarely exceeds 100. A small amount of optical paths causes several problems in the tomographic reconstruction. For example, high resolution maps (i.e. models with a high number of cells) cannot be estimated using few optical paths since a significant amount of cells would not be traversed. With a limited number of traversed cells, the solution of the system of equations in 5.2 becomes under determined. This means that the problem of estimating the vector of concentrations  $\mathbf{x}$  can have an infinite number of solutions.

In addition, the measurement geometry plays a crucial role in the tomography reconstruction process. According to Hart and co-authors [168], the position and the number of emitters (grey square markers in Figure 5.1(a)) affect the quality of the tomographic reconstruction. In [168] the authors evaluated different measurement geometries that consisted of two, three and four emitters placed in different positions. The authors kept the number of integral measurements and optical paths constant over all the evaluated geometries. Different gas distribution patterns were simulated using Gaussian plumes and tomographic reconstruction was carried out using different algorithms. In order to quantify the quality of the reconstruction, the authors compared the produced models with the simulated gas distribution using e.g. the Nearness index as a metric [165]. The authors concluded that the position and number of emitters affect the quality of the tomographic reconstruction even when the number of optical paths were kept constant for all the evaluated geometries.

Besides the challenges stated above, a key research problem that has yet to be fully addressed is the parameter selection of the tomographic reconstruction algorithm. For *model free* algorithms based on grid maps, the selection of the cell size is crucial [166]. As presented in [166], coarse tomographic reconstructions (i.e. maps with large cells) can lead to substantial errors in the prediction of unseen measurements while tomographic reconstruction with a high granularity (i.e. smaller cell sizes) can become under determined with measurement geometries that provide a scarce coverage.

Several solutions have been proposed to diminish the importance of the cell size selection. In [169], Verkruysse et al. proposed the grid translation method. The authors argued that the location of the cell edges adversely impact the predictions of the produced tomographic reconstruction. The key idea behind the proposed algorithm was to horizontally and vertically shift the centres of the cells in order to produce additional low resolution tomographic reconstructions instead of a single model. These *interim* models are then combined into a higher resolution grid. In a follow up paper [167], the authors proposed to learn the cell size in an iterative way, starting with a model with  $2 \times 2$  cells. The number of cells is then iteratively increased using the original grid translation method presented in [169] and the process is stopped when the projection distance, which is a metric to measure the accuracy of the predictions made with the model, does not significantly decrease or when it increases due to the sparsity of the optical paths.

## 5.2 Towards Robot Assisted Gas Tomography

As discussed in the previous section, the measurement geometry has a high influence on the quality of the tomographic reconstruction process. A straightforward solution to improve the measurement geometry would be to place more sensors at different locations in the area of interest and to increase the number of optical paths by either using sensors that emit more than one beam, or to actuate single beam sensors and point the sensors towards different directions. However, there are different aspects that make this solution impractical. First, remote sensors are expensive and therefore, increasing the number of emitters is not a cost effective solution. Second, there is a correlation between the quality of the reconstruction and the position of the emitters as reported in [168]. Therefore, the position of the emitters has to be carefully determined when constructing the measurement geometry. Third, CTG geometries are static which means that once the measurement system has been installed in an area of interest, the spatial configuration of the emitters, reflectors (if needed) and optical paths remains constant during operation time. It would be, however, interesting to adapt the measurement geometry to the particular characteristics of the observed gas distribution. For example, the density of optical paths and the position of the emitters could be modified to favour areas of high concentration levels while areas where there is no gas present can be coarsely scanned.

We propose a robotic solution to perform CTG. Robot Assisted Gas Tomography (RAGT) combines remote gas sensing capabilities with mobile robotics to produce tomographic reconstructions from a set of spatially unresolved concentration measurements. The concept of a RAGT system can be seen in Figures 5.2(a) and 5.2(b). In a RAGT system, a mobile robot is equipped with a sensing unit that allows to collect integral measurements from multiple optical paths. This means that either a sensor that projects multiple beams (e.g. DOAS) or an actuated beam path sensor (e.g. TDLAS) can be used. As shown in Fig-

ure 5.2(a), the mobile robot is placed at location  $R_1$  inside the exploration area. If the robot is equipped with a single beam sensor, a pan-tilt unit can be used to aim the sensor to the ground in different directions to collect a set of integral measurement ( $y_1, \dots, y_9$ ) across a set of optical paths ( $L_1, \dots, L_9$ ). If the number of optical paths is sufficiently dense, a semi-conic area  $S_1$  can be covered during the scanning process. The robot can then be moved to different locations ( $R_1$  to  $R_3$  in Figure 5.2(b)) and repeat the scanning process.

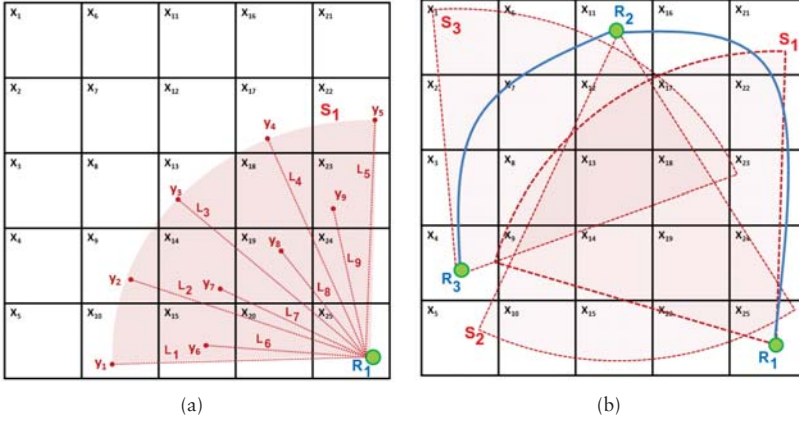


**Figure 5.2:** The concept of a Robot Assisted Tomography of Gases (RATG) system. (a) A single scanning process to cover the semi-conic area  $S_1$  at location  $R_1$  is performed by collecting  $y_1, \dots, y_9$  integral measurements over the optical paths  $L_1, \dots, L_9$ . (b) Multiple scanning processes, where the robot moves to different locations ( $R_1$  to  $R_3$ ) to cover a given area of interest.

RAGT offers a flexible measurement system, compared with the more traditional CTG. This can bring several advantages to the tomographic reconstruction process. For example, large areas can be covered using a single sensor by moving the robot to different measurement positions and adaptive measurement geometries can be realised according to the conditions sensed in the area of interest. While in principle the tomographic reconstruction process is similar to CTG, the implementation of RAGT systems presents additional challenges that have to be addressed. Of particular importance is the estimation of the optical paths. In fixed CTG geometries, this is a trivial problem since the emitters and the reflectors are placed at known locations that do not change during operation. In the case of RAGT, the path travelled by the beams has to be estimated in a process which is commonly referred to as ray tracing. Thus, RAGT is a process in which robot localization and 3D perception play a key role. This

is due to the fact that ray tracing has to be performed from the estimated robot pose and the estimated scene model.

In the next section we evaluate the concept of RAGT in the context of Gasbot, which is a collaborative project that aimed to develop a MRO system for landfill monitoring. The Gasbot robotic prototype is a mobile robot equipped with an actuated TDLAS sensor. Experiments were carried out in realistic scenarios, where the results suggest the feasibility of RAGT and its applicability to solve practical problems related to gas sensing.

### 5.3 Gasbot: Robot Assisted Gas Tomography for Landfill Monitoring

Gasbot was a collaborative project carried out at Örebro University during 2011-2013 in cooperation with Atleverket<sup>1</sup>, which is the waste management agency in the municipality of Örebro, Sweden. The development of the Gasbot system is documented in the publications [85], [84] and [86]. The goal of the project was to develop a proof of concept of a robotic platform able to detect leaks and create maps of the emissions from operational and decommissioned landfills. A landfill monitoring robot should be able to perform two major tasks. (1) Serve as an autonomous and flexible system that can explore large areas in order to measure biogas concentrations for example, carbon dioxide and methane ( $\text{CH}_4$ ). (2) From the acquired measurements, it should be able to provide the landfill operators with useful information such as gas distribution maps and locations of possible gas leaks.

#### 5.3.1 Landfill Site Monitoring

Landfill sites are an important source of Green House Gases (GHG), which are produced by decomposition of organic waste. GHG are mostly composed by  $\text{CH}_4$  and  $\text{CO}_2$  and, to minor extent, mixtures of  $\text{O}_2$ ,  $\text{N}_2$  and  $\text{H}_2$  can be found. The monitoring of gas emissions from landfill sites [6] is gaining interest among the European Union authorities, since they account for roughly 2% of the total Green House Gases (GHG) released by human activity [170].

Landfill leaks are a safety concern for local authorities. Homes built near old, improperly constructed landfills can be at a risk of explosions caused by fugitive  $\text{CH}_4$  emissions. From an economical perspective, emission monitoring is crucial to prevent the waste of valuable resources. Landfill produced  $\text{CH}_4$  is an alternative energy source [6]. According to Atleverket, only in the municipality of Örebro 18000 MWh are produced yearly from two sites, namely an operational landfill (Figure 5.3(a)) and a decommissioned landfill (Figure 5.3(b)), both of them located at the outskirts of the city of Örebro.

---

<sup>1</sup><http://www.orebro.se/3611.html>

In modern landfills, solid waste is encapsulated by several soil and insulating layers. A network of pipes and collection wells are installed in order to capture the by-product gases and to prevent them to escape to the atmosphere [171]. However, leaks are a common problem, even at landfill sites that have been closed for years. Gaseous substances can escape through minor fissures of the insulation layers, leaking collection wells, poorly sealed chambers and faulty pipes [172].



**Figure 5.3:**  $\text{CH}_4$  producing sites in the municipality of Örebro. (a) Operational landfill. (b) Decommissioned landfill.

A landfill operator is required by European regulations to monitor  $\text{CH}_4$  emissions at least once per month [6].  $\text{CH}_4$  monitoring is commonly performed at very specific locations at the landfill, for example collection wells or at the facility's borders and fences. More thorough monitoring methods include *flux box* methods [172]. A *flux box* (Figure 5.4) is a small tent or a box placed on a given location of the landfill, with a sensor placed inside to record the emissions that comes from the enclosed area. Data is collected over a given period of time and several locations can be measured during a single day. The data collected in this way allows to estimate the emissions coming from the landfill as well as the locations of possible leaks.

Once a leak or a *hot-spot* has been detected, the corrective actions that the operator has to enforce range from relatively simple valve and pipe adjustments, patching of insulating layers and wells [171], to more complex corrective actions that would require for example, a major engineering redesign of the gas extraction network [172].

Mobile robotics can make a significant contribution in this area by providing versatile systems for autonomous monitoring of diverse environments. Robotic solutions can adaptively collect sensor measurements, cooperate with other systems, and provide useful indications to landfill operators.

Compared to human operators, mobile robots have the advantage to carry out the required repetitive measurement procedure without suffering from fatigue and therefore, they can perform measurements with a much denser spatio-temporal granularity. Moreover, the use of an automated monitoring platform can minimize the exposure of human operators to hazardous compounds like, for example,  $\text{H}_2\text{S}$ . In addition, the mobile robots that carry the sensors offer the required accurate localization and computational resources to compute for example, on-line gas distribution models.



Figure 5.4: A *fluxbox*, used to characterize emissions from landfill sites<sup>2</sup>.

### 5.3.2 The Robotic Prototype Gasbot

The particular characteristics of the intended application scenarios (e.g. landfill sites) pose a considerable challenge to address from the mobile robotics perspective. First, robot localization has to be performed in large open spaces, where the lack of natural landmarks and uneven terrains, requires the use robust robot localization techniques.

Second, the limited on-board battery life has to be considered in order to maximize the autonomy of the platform. While gas sensing could be performed with *in-situ* sensors, this would require the robot to travel to a considerable amount of sensing positions in order to sufficiently cover the target area. The use of remote gas sensing is an attractive alternative since large areas can be inspected from a single measurement position and therefore, the exploration time and thus the battery consumption can be reduced.

In Figures 5.5(a) and 5.5(b), the two prototypes developed during the project's life cycle are shown. The prototypes were presented in [84] and in [86] respectively. The early prototype, or *Gasbot 1* (Figure 5.5(a)) is an ATRV-JR robotic platform equipped with a remote gas sensing unit, a frontal LiDAR (LMS-200) and a GPS/IMU unit (MTiG).

<sup>2</sup><http://www.golder.com.au/>

The final prototype, or *Gasbot 2* (Figure 5.5(b)), is an all-terrain Husky A-200<sup>3</sup> robot which is also equipped with extra sensing modalities for environmental and gas monitoring, such as an anemometer (Windsonic), a thermal camera (A-645) and a LiDAR (HDL-32E) for 3D perception.

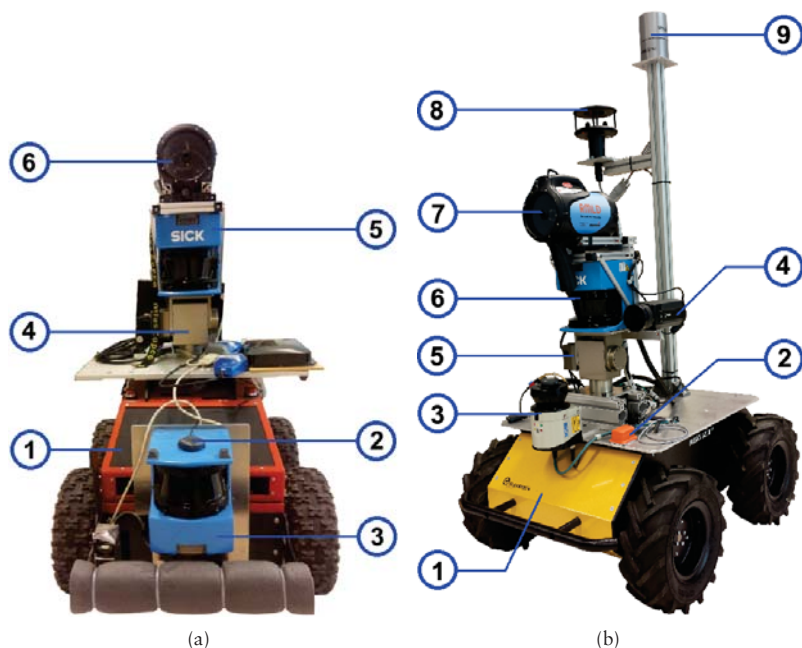


**Figure 5.5:** Gasbot prototypes. (a) The early prototype (*Gasbot 1*). 1-ATRV-JR platform, 2-MTiG IMU/GPS box, 3,5-LMS200 2D LiDAR, 4-PW-70 pan-tilt unit, 6-RMLD remote CH<sub>4</sub> sensor. (b) Final prototype (*Gasbot 2*). 1-Husky A-200 platform, 2-MTiG IMU/GPS, 3-LMS151 2D LiDAR, 4-A645 Thermal camera, 5-PW-70 pan-tilt unit, 6-LMS200 2D LiDAR, 7-RMLD remote CH<sub>4</sub> sensor, 8-Windsonic anemometer, 9-HDL-32E 3D LiDAR.

The gas sensing unit on both prototypes, comprises an RMLD single beam remote gas sensor, an LMS-200 LiDAR and a PW-70 pan-tilt unit. The RMLD is a battery powered, hand-held remote methane sensor based on TDLAS measuring principles<sup>4</sup>. Since the RMLD is an open loop device, no artificial reflectors are needed for its operation. Instead, the device can be pointed towards a

<sup>3</sup>The Husky A-200 platform was provided by Clearpath Robotics as an award for the environmental contributions of the project. See [www.clearpath.com](http://www.clearpath.com) for details.

<sup>4</sup><http://www.sewerin.com/cms/en/products/gas/gas-leak-detection-outdoors/sewerin-rmld.html>



reflective surface (e.g. walls, floor) to get an integral gas concentration reading. According to the manufacturer, the RMLD can measure  $\text{CH}_4$  integral concentrations as low as  $10 \text{ ppm} \cdot \text{m}$  at distances up to 30 m. The pan-tilt unit (PW-70) allows to point the RMLD's beam at different orientations, between  $\pm 120^\circ$  in the tilting axis and  $360^\circ$  in the panning axis.

### Robot Localization

While *off the shelf* IMU units (as in the case of the MTi-G mounted on *Gasbot 1* and *Gasbot 2*) offer built in probabilistic filters that allow to estimate the pose of a moving platform, this feature is oriented towards automotive applications where the velocity has to be above a given threshold that is not comparable to the robot's velocity, in the particular application of landfill monitoring.

Therefore, as a first attempt towards robot localization in large outdoor environments, we presented in [84] an ad-hoc filter to estimate the robot's pose by fusing GPS readings, from the MTi-G module, and odometry, from the robot's wheel encoders. The robot's current location is given by the weighted sum of the position change, reported by the GPS and the position change reported by odometry. The interested reader can consult [84] for implementation details.

Figure 5.6 illustrates the output of the proposed solution. The grey marks represent the raw readings reported by the GPS box, the black marks are the output from the localization filter and the arrows represent the estimated robot orientation. Labels A to D denote the position where the robot stopped.

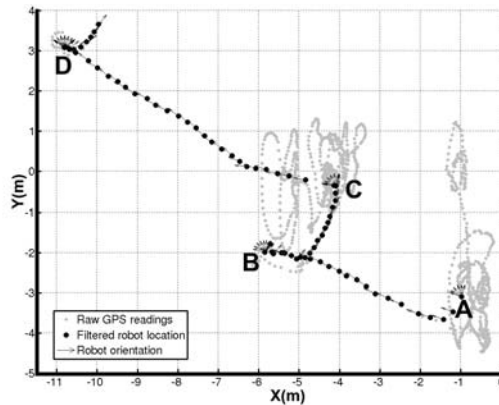


Figure 5.6: Robot localization results obtained with the ad-hoc GPS/IMU approach.

As can be seen in Figure 5.6, the raw GPS readings fluctuate heavily at locations where the robot is stopped. Therefore, the filter output should be predominantly odometry when the robot is moving at a low speed or when it is stopped. When the robot is moving at higher velocities, the filter's output is



predominantly GPS. While this algorithm can be used in open environments, where the GPS signal is stable and when the robot follows a trajectory where abrupt turns are not made, the approach has several limitations. For example, the filter requires the robot to move continuously through a given distance in order to converge to a stable position estimation, as can be seen in Figure 5.6. In addition, the heading estimation computed with odometry information only, is not accurate when the robot performs turns on the spot.

To improve the robot's localization, a 3D Lidar (HDL-32E) was mounted on *Gasbot 2* [86] and robot localization was performed using the NDT fusion algorithm [173] (Figures 5.7(a) and 5.7(b)). The NDT fusion algorithm is based on the Normal Distribution Transforms (NDT) framework and its Occupancy Map extension (NDT-OM [174]). In the NDT framework, the exploration area is discretised and individual Gaussian probability density functions (pdf) are fitted using the measurement points that lie within the voxels in the lattice. Among different localization algorithms, NDT based approaches offer smooth likelihood models, that allow for very accurate localization [175, 176].

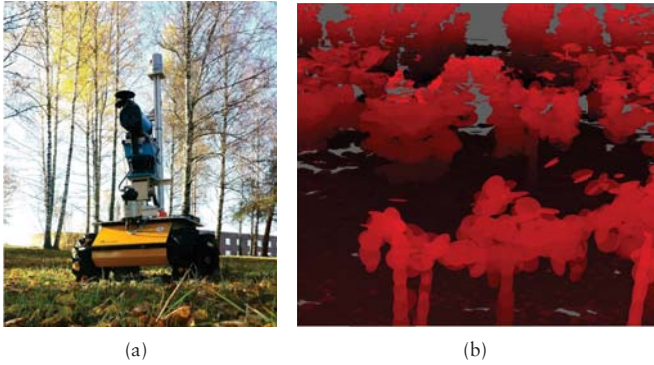


**Figure 5.7:** (a) *Gasbot 2* at an experimental location. (b) Sample NDT fusion model. The ellipsoids represent 0.5 standard deviation of each cell's pdf.

The NDT-OM extension improves the original NDT framework by tracking the probability of occupancy of each cell, and offering efficient incremental update procedures, maintaining numerical stability over an unbounded number of update range points. The NDT-OM approach assumes point clouds collected by a mobile range sensor and provides incremental, viewpoint- and dynamics-aware model updates. The NDT fusion algorithm iterates between two steps. The track step of the algorithm performs an NDT-D2D registration [177] between the acquired range scan and the map. Once the tracking step has converged to a candidate pose, the new point cloud is inserted into the map using an efficient batch-update ray tracing procedure.

The NDT fusion framework is applied directly to obtain consistent vehicle pose estimates and an incrementally constructed environmental map. In Figure 5.7(b), a sample NDT fusion map is shown. The map was generated in an experimental area located at the outskirts of the Örebro University main campus (Figure 5.7(a)).

### Ray tracing

In order to estimate the path travelled by the beam, it is required to have a 3D model of the environment. NDT-OM delivers an environment representation along with the estimated robot's pose, while in alternative localization algorithms, such as the ad-hoc GPS/IMU approach, 3D scene modelling has to be performed independently.

In [84], we addressed 3D modelling using the robot's pose, estimated by the localization algorithm, and the readings of the LMS-200 on the gas sensing unit (Figures 5.5(a) and 5.5(b)) as inputs. A localized point cloud was acquired by performing a vertical sweep of the 2D laser scanner with the pan-tilt unit. The point cloud is used in order to create an *OctoMap* representation of the environment [40]. *OctoMap* generates volumetric 3D models in which occupied, free and unknown areas are represented. At the core of *octoMap*, data is represented using tree like structures where each node represents the space contained in a cubic volume. Ray tracing with *OctoMap* can be thus performed by defining a starting point and a direction vector (e.g. the RMLD's sensor pose) and then, a ray is projected into the model until an occupied voxel is hit.

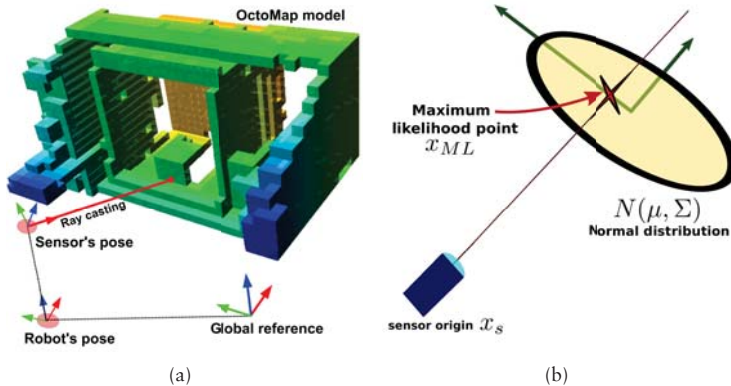


Figure 5.8: Proposed ray tracing approaches. (a) *OctoMap* + GPS/odometry. (b) NDT-OM.

On-board *Gasbot 2*, we perform ray tracing using the NDT-OM approach (Figure 5.8(b)). The beam's starting point is estimated using the position and

orientation of the RMLD sensor relative to the robot's pose in the map. Then, a ray is traced from the start point through the map and the point of intersection is then obtained as the maximum likelihood point  $x_{ML}$  along the ray, given the Gaussian pdf in each traversed cell. If the likelihood is high enough, then the ray is likely to hit the distribution and  $x_{ML}$  is considered as the beam's endpoint.

### Tomography Algorithm

Gas dispersion is a highly dynamic phenomenon where the gas concentrations do not remain static over time. Gas disperses in the environment due to airflow advection and turbulence producing highly dynamic gas distribution patterns. As explained in Section 5.1, previously proposed CTG approaches do not capture the variability of gas concentrations. In comparison, algorithms for gas distribution modelling with *in-situ* sensors can provide models in which the average concentrations and gas fluctuations are given in the form of mean and variance maps respectively [17, 55, 59].

In [86], we presented a CTG algorithm that computes mean and variance maps from integral measurements. The mean and variance maps are discrete representations of the environment in which the exploration area is divided in a uniform grid of cubic cells. The only assumption made by the algorithm is that the mean and variance estimations at each cell remain constant over time. No assumption is made about the functional form of the spatial gas distribution or the number of gas sources present in the environment.

Using the box basis function introduced in Section 5.1, the integral measurements  $y$  are modelled as follows:

$$y = \sum_{i=1}^M l_i x_i + \epsilon = \mathbf{l}^T \mathbf{x} + \epsilon \quad (5.4)$$

where  $M$  is the number of cells,  $x_i$  is the gas concentration in cell  $i$ , and  $\epsilon$  is the measurement noise term. If the beam of the sensor is modelled as a line integral of the gas concentration,  $l_i$  represents the distance travelled by the beam in cell  $i$ . A more realistic approach is to represent the laser beam as a cone and thus, an area integral of gas concentration  $a_i$ , that comes from the intersection of the cone with the grid cell  $i$ , is considered. In this way,  $l_i$  is substituted by  $a_i$  in all the equations. Figure 5.9 shows the measurement models.

The computation of the mean distribution map can be formulated as the estimation of the vector of concentrations  $\mathbf{x}$  that maximizes the likelihood of the acquired integral measurements. Given a set of  $N$  measurements, the vector  $\mathbf{y}[N \times 1]$  that contains all the integral concentrations in the dataset can be defined as follows:

$$\mathbf{y} = \mathbf{L}\mathbf{x} + \epsilon \mathbf{1} \quad (5.5)$$

where matrix  $\mathbf{L}[N \times M]$  contains the line or area integral that each measurement ray tracing produced and  $\mathbf{x}[M \times 1]$  is the mean concentration vector to be estimated.

Assuming Gaussian noise  $\epsilon$  with zero mean and standard deviation  $\sigma$ , the likelihood of the measurements is given as follows:

$$p(\mathbf{y}|\mathbf{x}, \mathbf{L}, \beta) = \prod_{n=1}^N \mathcal{N}(y_n|\mathbf{L}\mathbf{x}, \sigma) \quad (5.6)$$

Maximizing the logarithm of the likelihood (equivalent to maximizing the likelihood itself) boils down to the following non negative least squares problem with the constraint  $\mathbf{x} \succeq 0$ :

$$\begin{aligned} & \underset{\mathbf{x}}{\text{minimize}} && \|\mathbf{L}\mathbf{x} - \mathbf{y}\|_2^2 \\ & \text{subject to} && \mathbf{x} \succeq \mathbf{0} \end{aligned} \quad (5.7)$$

If some cells are never observed or many measurements are highly correlated the problem may become under determined and therefore it is useful to introduce a regularization term, modifying the problem in the following way:

$$\begin{aligned} & \underset{\mathbf{x}}{\text{minimize}} && \|\mathbf{L}\mathbf{x} - \mathbf{y}\|_2^2 + \lambda\|\mathbf{x}\|_2^2 \\ & \text{subject to} && \mathbf{x} \succeq \mathbf{0} \end{aligned} \quad (5.8)$$

which is analogous to choosing a Gaussian prior with zero mean on the average concentration of the cells. The strength of the prior is governed by the hyper-parameter  $\lambda$ . As we presented in [100], we observe in our numerical results that the constraint  $\mathbf{x} \succeq \mathbf{0}$  of Equation 5.9 is never active. This implies that the obtained solution is the ordinary least squares solution ( $\hat{\mathbf{x}} = (\mathbf{L}^T \mathbf{L})^{-1} \mathbf{L}^T \mathbf{y}$ ). The estimator  $\hat{\mathbf{x}}$  is unbiased, which means that  $E[\hat{\mathbf{x}}] = \mathbf{x}_*$ , where  $\mathbf{x}_*$  is the true value of the mean concentration in the cells. The covariance matrix of the estimator is thus:

$$\text{cov}(\hat{\mathbf{x}}) = E[(\hat{\mathbf{x}} - \mathbf{x}_*)(\hat{\mathbf{x}} - \mathbf{x}_*)^T] = \quad (5.9)$$

$$= (\mathbf{L}^T \mathbf{L})^{-1} \mathbf{L}^T E[\epsilon \epsilon^T] \mathbf{L} (\mathbf{L}^T \mathbf{L})^{-1} = \quad (5.10)$$

$$= (\mathbf{L}^T \mathbf{L})^{-1} \mathbf{L}^T (\sigma^2 \mathbf{I}) \mathbf{L} (\mathbf{L}^T \mathbf{L})^{-1} = \sigma^2 (\mathbf{L}^T \mathbf{L})^{-1} \quad (5.11)$$

The diagonal elements of the covariance matrix are the variance of the estimators of the individual parameters, i.e. the variance of the gas concentration in each cell. The process noise  $\sigma^2$  can be computed by using the following unbiased estimator:

$$s^2 = \frac{\mathbf{r}^T \mathbf{r}}{N - M} \quad (5.12)$$

where  $N$  corresponds to the number of measurements,  $M$  is the number of cells in the lattice and  $\mathbf{r}$  is the the vector of residuals  $\mathbf{r} = \mathbf{y} - \mathbf{L}\hat{\mathbf{x}}$ .

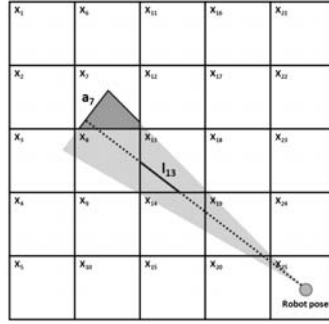


**Figure 5.9:** Example scenario in which a measurement has been taken in an area described by a  $5 \times 5$  lattice, with the sensor being placed in cell 25 and the laser being reflected on the ground in cell 7. The two different measurement models are shown in the figure. The dashed line represents the idealized beam model while the grey coloured area represents the cone model.  $l_{13}$  is the line intersection between the optical path and cell 13 (line model).  $a_7$  is the area intersection between the optical path and cell 7 (cone model).

### 5.3.3 Evaluation

The applicability of RAGT was evaluated in three different scenarios, namely one indoor location and two large outdoor areas. These scenarios were selected due to their resemblance to actual locations where gas inspection platforms could be deployed. An underground corridor (Figure 5.10) located in Örebro University main campus was used as the indoor testing scenario. Due to safety regulations, gas leaks were simulated by placing transparent flasks filled with natural gas (90%  $\text{CH}_4$ ) at two different locations.

In the above mentioned scenario, *Gasbot 1* was commanded to monitor an area of  $20 \text{ m}^2$  by following a pre-defined path in which measurements were collected at three different way-points. At each way-point, the robot performed a scan as explained in Section 5.2. Each scan consisted of 144 optical paths, where the pan-tilt unit stopped for 0.5 s to collect integral concentration measurements. In this scenario, a total of 432 optical paths were generated were approx. 2000 integral measurements were collected. The measurement geometry of this experiment can be seen in Figure 5.14(a) and a summary of the experimental configuration can be consulted in Appendix A.2.1. Tomographic reconstruction was carried out using the collected integral measurements and the algorithm's parameters (cell size and  $\lambda$  in Equation 5.9) were set to 1 m and

$10^{-5}$  respectively. Line integrals were used as a beam model and an example of a produced tomographic reconstruction is shown in Figure 5.11.



Figure 5.10: Indoor evaluation scenario for *Gasbot 1*.

This experimental configuration does not capture the complexities of gas dispersion since the leaks are simulated with static  $\text{CH}_4$  concentrations that are kept isolated from the environment. However, this set-up is ideal for evaluating the leak localization capabilities in terms of the correlation between the actual flask location and the mean concentration maxima predicted by the gas distribution model.

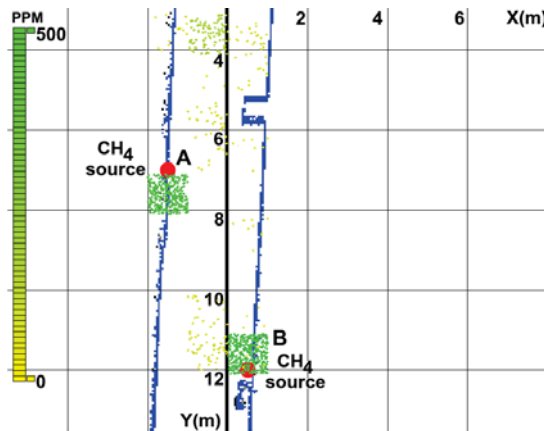


Figure 5.11: An example of a gas distribution maps generated in the indoor scenario.

A total of 8 trials were performed with the  $\text{CH}_4$  flasks at positions A and B as shown in Figure 5.11. The gas distribution maps successfully localized the flask at position A in 7 out of 8 trials with a mean distance of  $0.60 \text{ m} \pm 0.36 \text{ m}$  from the actual location. The second flask (B) was successfully localized in 6 out of 8 trials where the predicted location always agreed with the actual position of the flask.

Additional experiments were carried out with *Gasbot 1* at a decommissioned landfill site as shown in Figure 5.12. The experimental location comprised an area of 140 m<sup>2</sup> and, in order to simulate a leak, natural gas was released from a cylinder connected to a plastic tube ring punctured in multiple places. The robot was commanded to follow an exploration trajectory where the robot stopped at three way-points to perform measurement sweeps. Approximately 3000 integral concentrations were collected, with the pan-tilt unit stopping for 0.5 s at each of the 720 optical paths. The measurement geometry for this experiment can be seen in Figure 5.14(b).



Figure 5.12: Experimental scenario at the decommissioned landfill.

In Figure 5.13, the resulting gas distribution map is shown. The interaction between the released gas and the environment creates complex structures where turbulent airflow moves the gas patches away from the source. This is reflected in the generated gas distribution map, where it can be noticed that high concentration cubes are spread in locations nearby the actual gas source.

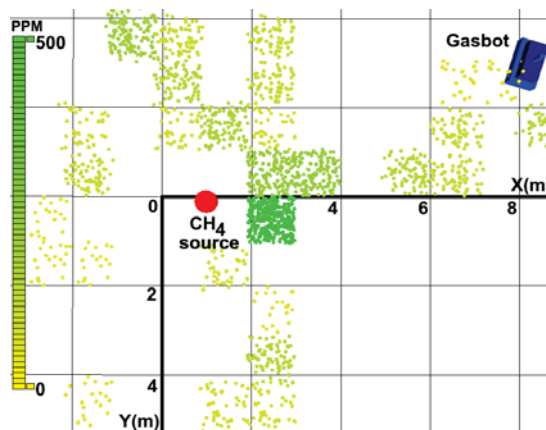
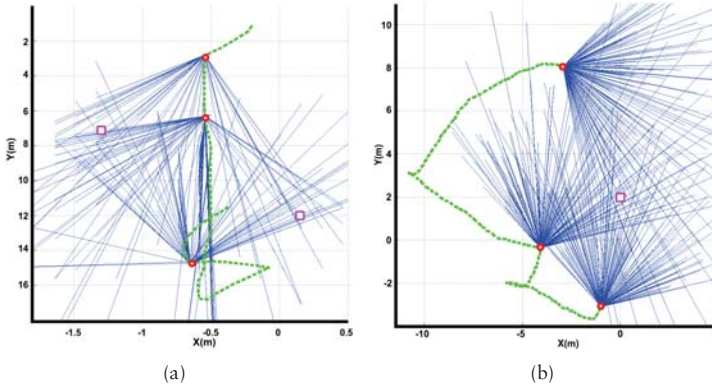


Figure 5.13: Generated gas distribution maps at the decommissioned landfill.





**Figure 5.14:** Measurement geometries generated using *Gasbot 1*. (a) Indoor scenario. (b) Decommissioned landfill. In both images, the dashed line denotes the exploration path, the circular markers denote the robot's position, the solid lines represent the optical paths and the actual position of the gas sources are shown as square markers.

In [86], we presented a numerical evaluation of the gas source localization capabilities using *Gasbot 2*. Two experiments were conducted in a large outdoor location near Örebro University's main campus (Figure 5.15). In the first *Gasbot 2* was commanded to follow an exploration trajectory of 6 way-points inside an area of  $154 \text{ m}^2$ . At each way-point, the robot performed a continuous measurement sweep and a total of 5066 integral measurements were collected over a set of 2450 optical paths.



**Figure 5.15:** Large outdoor experimental scenario near the Örebro University main campus. The experiments were conducted using *Gasbot 2*.

In the second experiment, *Gasbot 2* followed a 12 way-point trajectory inside a  $432 \text{ m}^2$  area. At each way-point, the robot performed a continuous measurement sweep and a total of 9300 integral measurements were collected along 4513 optical paths. A summary of the experiments conducted in this



scenario can be found in Appendix A.2.3. The measurement geometries for this set of experiments can be seen in Figures 5.16(a) and 5.16(b) respectively.

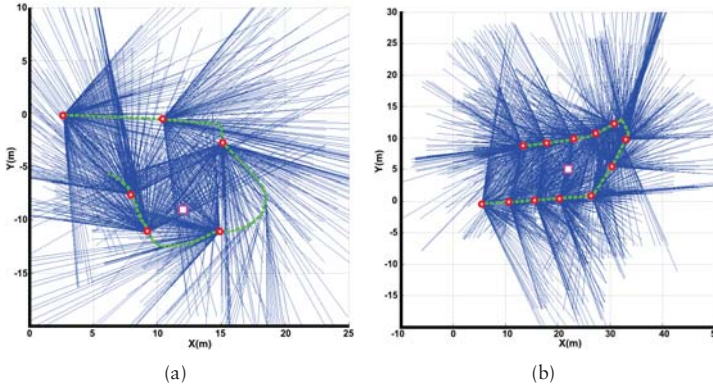
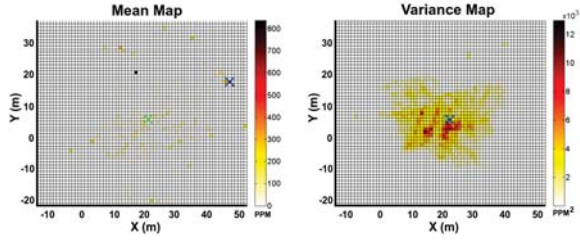


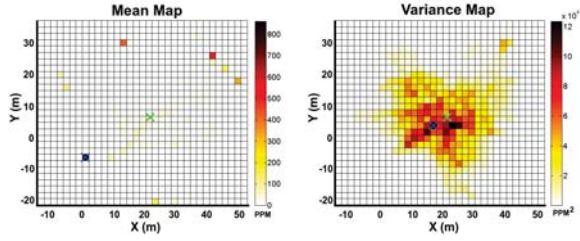
**Figure 5.16:** Measurement geometries generated using *Gasbot 2* in two different experiments conducted at Örebro University. In (a), the robot moved inside a 154 m<sup>2</sup> exploration area while in (b), the robot's path was inside a 432 m<sup>2</sup> area. In both images, green dashed line denote the exploration path, the circular markers denote the robot's position, the solid lines represent the optical paths and the actual position of the gas sources are shown as square markers.

In Figures 5.17(a) to 5.17(d), maps generated with cell sizes  $c = 1$  m to  $c = 4$  m and with a cone measurement model are shown. An area of 432 m<sup>2</sup> was explored with *Gasbot 2*. To evaluate the produced maps, we use their accuracy on the prediction of the gas source location as a metric. Similarly to the case of gas distribution maps produced with *in-situ* sensors, we use the Concentration Maximum Estimate (CME) and the Variance Maximum Estimate (VME) as indicators of the gas source proximity. As explained in Chapter 2, the CME denotes the location where the highest average concentration is predicted while the VME is the location with the highest predicted variance.

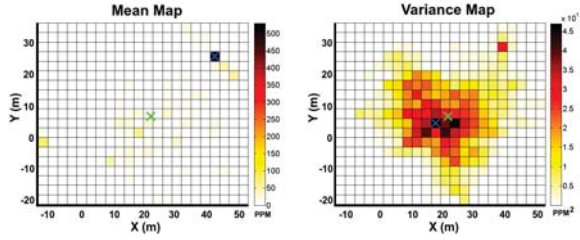
Notice that the CME is not a good indicator of the gas source location, since isolated high concentration cells are predicted at distant locations from the gas source for all the tested cell sizes. In the models with small cell sizes, the gas distribution is given as a set of high concentrations spread all over the exploration area. As the model becomes coarse, high concentrations tend to cluster around the actual gas source location. It can be argued from the produced maps that the selection of the cell size is critical for RAGT systems. This is a similar conclusion observed with static CTG configurations, where the cell size selection has been reported as a factor that determines the quality of the reconstruction process [166].



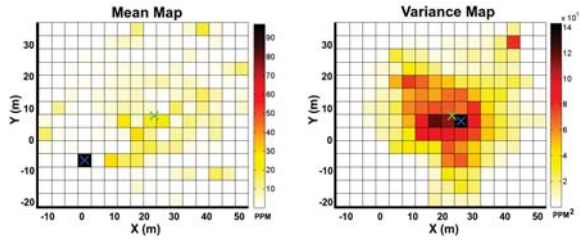
(a)



(b)



(c)



(d)

Figure 5.17: Gas distribution maps generated with different cell sizes ( $c$ ) in the  $432 \text{ m}^2$  exploration area. The blue and green markers denote the predicted and the actual source location respectively. (a)  $c=1 \text{ m}$ . (b)  $c=2 \text{ m}$ . (c)  $c=3 \text{ m}$ . (d)  $c=4 \text{ m}$ .

Regarding the variance maps in Figures 5.17(a) to 5.17(d), notice that high fluctuations are predicted in close proximity to the actual gas source for all the tested cell sizes. With the VME as an indicator for gas source location, the predictions are less sensitive to the cell size compared with the CME. For all the produced maps, the predicted gas source location is one cell away from the actual gas source position.

Figures 5.18 and 5.19 condense the results of both experiments conducted with *Gasbot 2* at the Örebro University campus. The data collected in each of the two experiments was randomly divided in 5 folds each and errorbars were calculated for the accuracy of the gas source position estimation (using both the CME and the VME) with respect to the map's cell size and the beam's model. The parameter  $\lambda$  in Equation 5.9 was set constant to  $10^{-5}$ . Considering the difference between the predicted and actual gas source position, it is clear that the VME (errors consistently below 10m) provide a better indicator of the gas source position than the CME (errors between 25m and 35m).

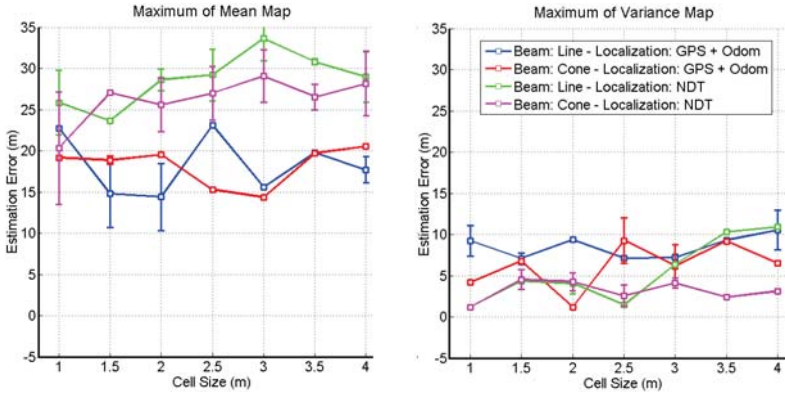


**Figure 5.18:** Gas source localization accuracy evaluation using the data collected inside the 154 m<sup>2</sup> exploration area.

Focusing the attention on the predictions obtained by using the VME as source indicator, it can be seen how in general the positioning and ray tracing obtained with the NDT based localization and ray tracing (errors in the order of 2m – 4m) outperform the positioning based on filtered GPS and odometry (errors around 10m).

Regarding the comparison of the beam models, it can be noticed how the models obtained with the conical beam model (errors between 1m and 4m) clearly outperform the models based on the line beam model in the second experimental run, while in the first experimental run, a clear difference is visible only for cell sizes  $\geq 3$ m.

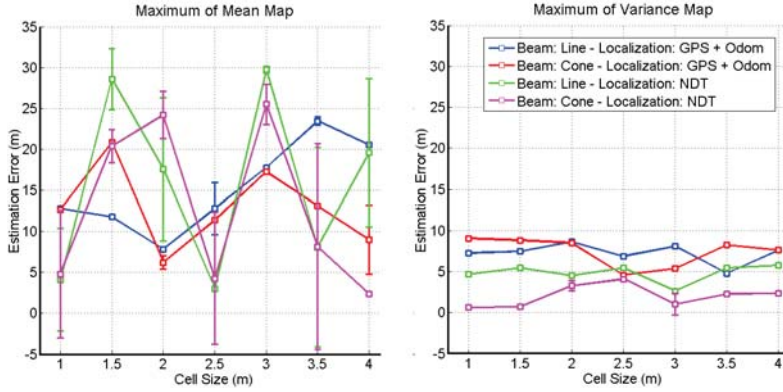


Figure 5.19: Gas source localization accuracy evaluation using the data collected inside the 432 m<sup>2</sup> exploration area.

## 5.4 Conclusions

The use of remote gas sensors in MRO systems brings several advantages towards fully autonomous platforms intended for real world applications. The ability to sense target gases at a distance boosts the detection capabilities of a robot, compared to a platform equipped with *in-situ* chemical sensors that needs to enter in direct contact with the gaseous compounds. With the advantage of remote gas detection, mobile robots can explore larger areas and locations of difficult access can be reached.

The concept of Robot Assisted Gas Tomography (RAGT) was first introduced in the development of the project Gasbot. Contrary to fixed tomography configurations where the sensor location and the optical paths remain constant during data collection, RAGT is carried out with an inspecting mobile robot equipped with remote sensing capabilities. The mobile robot can be thus moved to different locations inside an area of interest. A mobile system brings several advantages compared to a fixed RTG setup. First, the use of a mobile platform allows to place the sensor at different locations. This translates into rich measurement geometries, that allow to acquire integral concentration measurements with a high number of optical paths. Second, as reported in [168], the measurement geometry in a tomographic system is critical for the quality of the reconstruction process. The use of a mobile platform allows to modify the measurement geometry according to the particular characteristics of the intended exploration area. However, an algorithm that selects measurement positions which allow for a better reconstruction process has yet to be developed.

In RAGT robot localization and thus ray tracing are of high importance. Inaccurate robot pose estimation can affect the gas source localization capabil-

ities of the models. As we presented in [86], the use of state of the art robot localization algorithms (such as NDT-OM), along with more accurate models for the remote gas sensor, result in maps that allow to localize gas sources more accurately when the variance maps are considered.

A highly relevant contribution made during Gasbot's project life was the development of a gas tomography algorithm that not only estimates the mean concentrations, but also models the fluctuation of gases in the form of a variance map. This is a remarkable landmark in the context of gas tomography since state of the art algorithms do not allow for the estimation of the gas fluctuations in the explored areas. A variance map brings several advantages in the context of leak localization since it has been shown by different authors and with *in-situ* sensing modalities that areas of high gas fluctuation are correlated with the location of a gas leak. This result is supported as well by plume characterization works where measurements on turbulent underwater plumes show that the magnitude of the concentration fluctuations exhibit a steeper gradient along the downstream direction, compared with the average concentration level [152].

There are open issues that should be addressed towards fully fledged RAGT systems. First, the predictive capabilities of the mean maps have to be improved since isolated, high concentration cells are predicted away from the actual gas source as shown in Figures 5.17(a) to 5.17(d). Second, a more consistent approach to evaluate the gas distribution models has to be implemented. This is an issue that is not exclusive to remote gas sensing systems but also is an issue when using *in-situ* measurement systems. In order to have a better evaluation procedure for gas distribution maps generated with RAGT systems, the acquisition of ground truth information can be highly useful. For example, a network of *in-situ* sensors could be placed in the experimental location and then, the generated tomographic reconstructions can be used to make predictions at the sensors locations. In this way performance indexes such as the NLPD, can be used to evaluate the models.

Third, it is yet to be explored how aspects such as the choice of the measurement locations and the uncertainty in the estimation of the robot's pose can be incorporated in the computation of the gas distribution models. An environment that combines gas dispersion and robot simulation can be developed for the purpose of developing RATG algorithms. The simulation environment would allow to select different parameters such as localization error, sensor models, the position and pattern of gas gas plumes as well as measurement positions.

Fourth, the fusion of different sensing capabilities, along with remote sensing, have to be explored. It is still an open question how to efficiently use wind information in gas distribution mapping and in the case of remote sensing systems, this aspect has not been explored at all. In addition, the fusion of remote and *in-situ* gas measurement is an aspect that has yet to be explored. Thermal imaging is perhaps a promising direction to explore in the context of gas leak

localization. The correlation between soil temperature and gas leaks [178] can be used for example, by planning algorithms that would prioritize the collection of measurements at areas where soil temperature is consistent with a leak pattern.

# Chapter 6

## Conclusions

Mobile Robotics Olfaction (MRO) is the multidisciplinary line of research that studies the problem of integrating gas sensing modalities on mobile robotics platforms. Building MRO systems for real world applications requires to solve a set of related tasks in order to address the challenges imposed by the gas dispersion phenomenon. In this thesis work, we present a set of contributions focused on the tasks of gas discrimination and gas distribution modelling which are critical for MRO intended for practical applications. The approach assumed in all the presented contributions is that, in order to build robust MRO systems, simplifying assumptions have to be removed. The contributions presented in this work were developed in the scope of the regional project Gasbot<sup>1</sup>, which aimed to develop a robotic emission monitoring system for landfill sites.

### 6.1 Contributions

In this section, we highlight the most significant contributions presented in this thesis. The complete list of contributions can be consulted in Section 1.3. First, gas sensors cannot be considered as *black boxes*. This means that MRO algorithms should consider the particular characteristics of a given sensing technology. This aspect is addressed in this dissertation with the design of the gas discrimination algorithm presented in Section 3.3. Rather than using an *out of the box* approach, the proposed algorithm tailors the discrimination process to exploit the advantages and cope with the shortcomings of gas sensing using Open Sampling Systems (OSS). The achieved results showed that, gas discrimination can be carried out with a high success rate in open environments, where environmental aspects such as intermittent wind flow conditions disrupt the gas sensing process.

In a similar way, we demonstrated that the particular characteristics of datasets collected with gas sensors can be exploited when optimizing the meta parameters of an MRO algorithm. More specifically, we showed that the high

---

<sup>1</sup>The project Gasbot was financed by Robotdalen (<http://www.robotdalen.se/>).

redundancy of datasets collected with OSS, composed of metal oxide sensors, can be used to reduce the computational demands when performing parameter selection. We applied the proposed solution in the problem of bandwidth selection for the Kernel DM+V [17] algorithm, which is a widely used approach for Gas Distribution Modelling (GDM). Parameter selection for GDM is a computationally demanding and thus typically carried out offline. With the proposed solution we showed that parameter selection can be carried out at a fraction of the computational cost without significantly deviating from the optimal solutions computed with conventional K-fold validation processes.

Second, a GDM algorithm that considers the presence of multiple heterogeneous substances was proposed. A common assumption made by different GDM algorithms is that a single chemical compound is present in an environment. The presence of multiple target compounds and interferent substances is to be expected in realistic scenarios and thus, it has to be considered by the GDM algorithm. As a contribution in this aspect, we proposed the Multi Compound (MC) Kernel DM+V (presented in Section 4.5), which combines concentration measurements, collected with a non selective gas sensor (such as a PID) and the uncertainty in the predictions of a given classifier to create gas distribution models for each of the target compounds. In this way, gas discrimination and gas distribution modelling is fully integrated when deriving compound-specific distribution models.

Third, we explored alternative gas sensing modalities for the task of MRO. In this work, the concept of Robot Assisted Gas Tomography (RAGT) was introduced. RAGT systems use remote sensors (e.g. spectroscopy based sensors) mounted on mobile robots to produce gas distribution models (i.e. tomographic reconstructions). While the concept of gas tomography, which models the spatial distribution of gases using remote sensors, dates back from the late 70's [18], the key contributions are the use of robotic platforms in the gas tomography process bringing in this way, advantages such as mobility and adaptability.

Fourth, we demonstrated that practical gas sensing applications can be addressed using MRO systems. More specifically, an important part of this dissertation work is dedicated to the design and construction of a proof of concept mobile robotic platform for the task of methane emission monitoring and leak detection at landfill sites. The prototype developed in the Gasbot project is an RAGT system that generates maps of the distribution of gases in an area of interest. Experiments conducted in large outdoor environment showed that by using the gas distribution maps computed with the proposed RAGT system, the actual location of gas leaks can be predicted with a high degree of accuracy.

It is worth mentioning that an indirect contribution of this thesis work was the attention raised towards the area of MRO by the results achieved in the Gasbot project. As a relatively young research field, MRO has received little attention in public and scientific media. The results achieved in Gasbot generated considerable attention from national and international media. Gasbot



was showcased in different international media outlets such as *The Washington Post* [179], *IEEE Spectrum* [8, 180] and *Phys.org* [181].

In addition, the project was the recipient of different awards. Gasbot's research team received the "Award of distinction for environmental contributions" from Clearpath Robotics<sup>2</sup>. Clearpath offers a state-of-the art robotic platform to research teams from all over the world through its PartnerBot Grant Program. More than 150 universities submitted proposals for the grant and Gasbot was selected as one of the 10 recipients. The article "Towards Real-World Gas Distribution Mapping and Leak Localization Using a Mobile Robot with 3D and Remote Gas Sensing Capabilities", presented in this thesis work in Chapter 5, won the "Best Service Robotics Paper Award"<sup>3</sup> at ICRA 2013, the largest and arguably the most prestigious conference in robotics. The award promotes cooperation between robotics science research and industry R&D advancement in the area of service robotics applications (both professional and domestic).

## 6.2 Limitations

This thesis work presents a set of solutions for MRO tasks such as gas discrimination and gas distribution mapping with *in-situ* sensors and remote sensors. However, it is worth noticing that the presented algorithms have limitations that have yet to be studied in order to be implemented as part of a more complex fully autonomous MRO system.

The case of the evaluation of the MC Kernel DM+V algorithm, presented in Section 4.5, did not consider the mixing between the target substances. A more realistic approach would require to train regression functions to predict the mixing percentage between the target compounds. However, the proposed MC Kernel DM+V can be used to generate non binary models once a regression function for the mixture percentage is trained.

Regarding the gas discrimination approach proposed in Section 3.3, the only assumption made is that class overlapping only occurs at low concentrations, while at higher concentration levels the problem of gas discrimination is rather trivial. This assumption holds for the different experimental validation scenarios and the different chemical substances and sensor arrays used in this thesis work. For a different gas discrimination problem, the applicability of the proposed solution would have to be evaluated first. This means that the interested reader that aims to implement the algorithm have to evaluate the collected data, in order to determine whether or not the correlation between gas concentration and class separability holds for the intended gas discrimination problem.

---

<sup>2</sup><http://www.clearpathrobotics.com/>

<sup>3</sup>[http://www.icra2013.org/?page\\_id=153](http://www.icra2013.org/?page_id=153)

The computation of the mean distribution maps in the RAGT approach presented in Section 5.3 have to be evaluated further. As discussed in the experimental validation, the computed mean maps tend to predict isolated cells of high concentrations away from the actual gas source. Rather than presenting isolated *point-like* structures of high concentration, gas dispersion is given by smooth transitions between areas of low and high concentration. In addition, the proposed RAGT solution depends on one free parameter (e.g. cell size) that determines the complexity of the predicted models. An algorithm for parameter selection for RAGT algorithms is still an open problem that has to be investigated.

### 6.3 Future Research Directions

In recent years, significant progress has been achieved in the MRO research community. However, there are several research directions that can be addressed. For example, in the context of GDM with either *in-situ* or remote sensors, the fusion of different sensing modalities has not yet been fully exploited. To the author's best knowledge the fusion of e.g. remote gas sensors and environmental sensors such as anemometers have not yet been explored.

Sensor planning for gas sensitive robots is an open research direction. For example, algorithms that guarantee full coverage of a given exploration area with e.g. remote sensors have not yet being developed. In addition, specific algorithms that suggest measurement locations for the tasks of gas discrimination, gas distribution mapping and gas source localization can be another interesting line of research. Among other advantages, sensor planning algorithms will allow for more efficient exploration trajectories, which in turn translates into lower energy consumption demands and improved robot autonomy.

Another key aspect to be addressed is the lack of ground truth. As in the case of the GDM algorithms presented in this work, a common approach is to evaluate the predicted gas distribution models with respect to their capability to predict the location of a gas source. However, more consistent evaluation procedures must consider the model's capability to predict the gas concentrations at unseen locations. A suggested approach to address the problem of lack of ground truth would be to collect data with calibrated low cost sensors placed at different locations in the exploration area.

Additionally, larger datasets that reflect real world conditions have to be collected in scenarios where MRO systems are expected to be deployed. For example, experimental trials should be conducted in open spaces with uneven terrain, urban locations where buildings and other obstacles disrupt the gas plumes and closed locations that resemble underground tunnels or mines.

Non dedicated platforms can also be used for the task of gas sensing [182]. For example, robots that are not specifically built to collect gas measurements can be equipped with gas sensors and collect measurements as they traverse a given area or when they perform an unrelated task.

The fusion of heterogeneous sensing systems and MRO platforms is another line of research that is worth addressing. One example is the use of low cost sensor nodes along with MRO systems. Sensing nodes built with non calibrated/low cost sensors can be placed at different locations in a given area of interest while robots can be equipped with expensive gas sensors that allows to acquire calibrated measurements and to discriminate between different chemical compounds. In this way, the sensor network can provide a high temporal granularity of measurements, while the mobile robotic platforms can be used to measure specific locations and thus, can provide high spatial granularity in a given area of interest. An example of this line of research is the regional project RAISE<sup>4</sup>, which aims to develop an heterogeneous sensing system to monitor particles and gases that are the by-product of industrial iron casting.

To conclude, it is worth mentioning that a significant amount of the challenges faced in MRO are related to the limitations of current gas sensing technologies. In the author's opinion, there is currently a too loose connection between the gas sensing and the robotics research communities. In order to develop fully fledged MRO systems, a closer collaboration between the robotics and the gas sensing communities has to be established. In this way, sensors that are tailored to the particular demands of gas sensing with mobile platforms (e.g. faster response/recovery times, robustness with respect to climate conditions and portability) can be constructed.

---

<sup>4</sup><http://aass.oru.se/Research/Learning/raise/>




# Appendix A

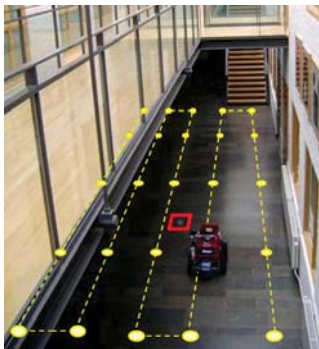
## Experimental Scenarios

### A.1 Experiments with In-Situ Sensors



#### A.1.1 Robot Arena

	Description	Small, unventilated room. No artificial advective windflow. Gas analytes released from tubes placed on the floor.		
	Comments	Dataset originally presented in [89].		
	Total area	5 m × 5 m		
	Robotic platform	P3-DX		
	Robot speed	0.05 m/s		
	PID	MiniRAE Lite		
	MOX sensor array	(1) MICS 2610 (1) MICS 2710 (2) MICS 5521 (1) MICS 5121 (1) MICS 5135		
	Other Sensors	Windsonic Anemometer		
	Sampling frequency	4 Hz		
Trials		Trial duration	Compounds	Separation between gas sources
3		1800 s	Ethanol	—
3		1800 s	Propanol	—
3		1800 s	Ethanol - Propanol	1.5 m
3		1800 s	Ethanol - Propanol	0.5 m

### A.1.2 Indoor Corridor


	Description		Indoor location, ventilated corridor. Disruptions caused by people, opening and closing doors and windows. Open plastic container filled with Ethanol as a gas source.	
	Comments		Dataset originally presented in [88]	
	Total area		14 m × 2 m	
	Robotic platform		ATRV-JR	
	Robot speed		0.05 m/s	
	PID		MiniRAE Lite	
	MOX sensor array		(2) TGS 2600 (1) TGS 2602 (2) TGS 2611 (2) TGS 2620	
	Other Sensors		Young 81000 Anemometer	
	Sampling frequency		4 Hz	
	Trials	Trial duration	Compounds	Separation between gas sources
5	1750 s	Ethanol	— —	

### A.1.3 Outdoor Courtyard I





Description		Outdoor location. No buildings nearby the experimental area. Open plastic container filled with Ethanol as a gas source.	
Comments		Dataset originally presented in [88]	
Total area		8 m × 8 m	
Robotic platform		ATRV-JR	
Robot speed		0.05 m/s	
PID		MiniRAE Lite	
MOX sensor array		(2) TGS 2600 (1) TGS 2602 (2) TGS 2611 (2) TGS 2620	
Other Sensors		Young 81000 Anemometer	
Sampling frequency		4 Hz	
Trials	Trial duration	Compounds	Separation between gas sources
5	1750 s	Ethanol	—

### A.1.4 Open Field

	<b>Description</b>		Open field with no buildings around the experimental area. CH <sub>4</sub> was released from a container. A fan was used to spread the gas plumes away.	
	<b>Comments</b>		Experiments in cooperation with the Federal Institute for Materials Research and Testing (BAM).	
	<b>Total area</b>		14 m × 14 m	
	<b>Platform</b>		AR-100B	
	<b>Robot speed</b>		1 m/s	
	<b>MOX sensor array</b>		(1) TGS 2600 (1) TGS 2602 (2) TGS 2611 (2) TGS 2620	
	<b>Other Sensors</b>		Wind sensing fusing different modalities [90].	
	<b>Samp. freq.</b>		8 Hz	
	<b>Trials</b>	<b>Trial duration</b>	<b>Compounds</b>	<b>Separation between gas sources</b>
	5	1033 s	Methane	—

### A.1.5 Outdoor Courtyard II

	<b>Description</b>		Garden surrounded by nearby buildings. A bubbler was used to evaporate the analytes from open containers.	
	<b>Comments</b>		Datasets acquired as part of this dissertation.	
	<b>Total area</b>		9 m × 7 m	
	<b>Platform</b>		ATRV-JR	
	<b>Robot speed</b>		0.12 m/s	
	<b>PID</b>		MiniRAE Lite	
	<b>MOX sensor array</b>		(1) TGS 2600 (1) TGS 2602 (2) TGS 2611 (2) TGS 2620	
	<b>Other Sensors</b>		Windsonic anemometer	
	<b>Samp. Freq.</b>		4 Hz	
	<b>Trials</b>	<b>Trial duration</b>	<b>Compounds</b>	<b>Separation between gas sources</b>
	1	3400 s	Acetone	—
	1	3400 s	Ethanol	—
	1	3400 s	Acetone - Ethanol	1 m

## A.2 Experiments with Remote Sensors

### A.2.1 Underground Corridor



Description	Underground corridor. Methane concentrations kept inside transparent flasks due safety reasons.		
Comments	Datasets acquired as part of this dissertation.		
Total area	20 m <sup>2</sup>		
Platform	<i>Gasbot 1</i>		
Robot speed	0.12 m/s		
Ray tracing algorithm	Montecarlo localization [39] and OctoMap 3D modelling [40]		
Other Sensors	SICK LMS-200 LiDAR and a PW-70 pan-tilt unit for 3D Scene modelling.		
Samp. Freq.	10 Hz		
Trials	Trial duration	Meas. positions	Optical paths
8	216 s	3	432


### A.2.2 Decommissioned Landfill Site



Description	Open, flat outdoor area. No nearby buildings. A methane leak was produced using a punctured Tube ring connected to a natural gas cylinder.		
Comments	Datasets acquired as part of this dissertation.		
Total area	140 m <sup>2</sup>		
Platform	<i>Gasbot 1</i>		
Robot speed	0.12 m/s		
Ray tracing algorithm	Montecarlo localization [39] and OctoMap 3D modelling [40]		
Other Sensors	SICK LMS-200 LiDAR and a PW-70 pan-tilt unit for 3D Scene modelling.		
Samp. Freq.	10 Hz		
Trials	Trial duration	Meas. positions	Optical paths
1	360 s	3	720



A.2.3 Large Open Field

		Description		Open, flat outdoor area. No nearby buildings. A methane leak was produced using a punctured Tube ring connected to a natural gas cylinder.		
		Comments		Datasets acquired as part of this dissertation.		
		Platform		Gasbot 2		
		Robot speed		0.12 m/s		
		Ray tracing algorithm		NDT-OM [173].		
		Other sensors		HDL-32E 3D LiDAR, Windsonic anemometer, A-645 Thermal camera.		
		Samp. Freq.		10 Hz		
		Trials	Trial duration	Area	Meas. positions	Optical paths
		1	1500 s	432 m <sup>2</sup>	12	4514
		1	960 s	154 m <sup>2</sup>	6	2450



# References

- [1] Martin Magnusson, Tom Duckett, and Achim J. Lilienthal. Scan registration for autonomous mining vehicles using 3D-NDT. *Journal of Field Robotics*, 24(10):803–827, Oct 24 2007. (Cited on page 1.)
- [2] Martin Magnusson and Håkan Almqvist. Consistent pile-shape quantification for autonomous wheel loaders. In *Proc. IEEE/RSJ Int. Conf. on Intelligent Robots and Systems*, pages 4078–4083, 2011. (Cited on page 1.)
- [3] Todor Stoyanov, Rasoul Mojtahedzadeh, Henrik Andreasson, and Achim J. Lilienthal. Comparative evaluation of range sensor accuracy for indoor mobile robotics and automated logistics applications. *Robotics and Autonomous Systems*, 2012. (Cited on page 1.)
- [4] H. Ishida, Y. Wada, and H. Matsukura. Chemical sensing in robotic applications: A review. *Sensors Journal, IEEE*, 12(11):3163–3173, Nov 2012. (Cited on pages 1 and 11.)
- [5] Thomas Barz, Gero Bonow, Jens Hegenberg, Karim Habib, Liubov Cramar, Jochen Welle, Dirk Schulz, Andreas Kroll, and Ludger Schmidt. Unmanned inspection of large industrial environments: Insights into research project robogasinspector. In *Future Security*, volume 318 of *Communications in Computer and Information Science*, pages 216–219. Springer, Berlin Heidelberg, 2012. (Cited on pages 1 and 12.)
- [6] Heijo Scharff. Achieving adequate control of landfill gas in Europe. *Waste Management World*, 2008. (Cited on pages 2, 96, and 97.)
- [7] A. R. Brandt, G. A. Heath, E. A. Kort, F. O’Sullivan, G. Pétron, S. M. Jordaan, P. Tans, J. Wilcox, A. M. Gopstein, D. Arent, S. Wofsy, N. J. Brown, R. Bradley, G. D. Stucky, D. Eardley, and R. Harriss. Methane Leaks from North American Natural Gas Systems. *Science*, 343(6172):733–735, February 2014. (Cited on page 2.)

- [8] White house taps arpa-e to boost methane detection. In <http://spectrum.ieee.org/energywise/energy/environment/white-house-methane-strategy-to-beef-up-methane-detection>. (Cited on pages 3 and 117.)
- [9] J.W. Gardner and P.N. Bartlett. *Electronic noses: principles and applications*. Oxford science publications. Oxford University Press, 1999. (Cited on pages 3, 47, and 56.)
- [10] Sepideh Pashami, Achim J. Lilienthal, and Marco Trincavelli. Detecting changes of a distant gas source with an array of mox gas sensors. *Sensors*, 12(12):16404–16419, 2012. (Cited on pages 4 and 22.)
- [11] Marco Trincavelli, Silvia Coradeschi, and Amy Loutfi. Odour classification system for continuous monitoring applications. *Sensors and Actuators B: Chemical*, 58:265 – 273, 2009. (Cited on pages 4, 49, and 52.)
- [12] Javier Gonzalez Monroy, Achim Lilienthal, Jose Luis Blanco, Javier Gonzalez Jimenez, and Marco Trincavelli. Probabilistic gas quantification with {MOX} sensors in open sampling systems - a gaussian process approach. *Sensors and Actuators B: Chemical*, 188:298 – 312, 2013. (Cited on page 4.)
- [13] G. Kowadlo and R. A. Russell. Robot Odor Localization: A Taxonomy and Survey. *The International Journal of Robotics Research*, 27(8):869 – 894, 2008. (Cited on pages 4, 11, 24, and 25.)
- [14] Patrick Neumann, Sahar Asadi, Jochen H Schiller, Achim Lilienthal, and Matthias Bartholmai. An Artificial Potential Field based Sampling Strategy for a Gas-Sensitive Micro-Drone. In *IROS Workshop on Environmental Monitoring*, 2011. (Cited on pages 4, 20, 24, and 70.)
- [15] Sahar Asadi, Matteo Reggente, Cyrill Stachniss, Christian Plagemann, and Achim J. Lilienthal. *Intelligent Systems for Machine Olfaction: Tools and Methodologies*. IGI Global, 2011. (Cited on page 4.)
- [16] Achim J. Lilienthal, Tom Duckett, Felix Werner, and Hiroshi Ishida. Indicators of gas source proximity using metal oxide sensors in a turbulent environment. In *Proceedings of the IEEE / RAS-EMBS International Conference on Biomedical Robotics and Biomechatronics (Biorob)*, February 20 – 22 2006. (Cited on pages 4, 28, 39, 69, and 85.)
- [17] Achim J. Lilienthal, Matteo Reggente, Marco Trincavelli, Jose Luis Blanco, and Javier Gonzalez. A statistical approach to gas distribution modelling with mobile robots - the Kernel DM+V algorithm. In *Proceedings of the IEEE/RSJ International Conference on Intelligent Robots and Systems (IROS)*, pages 570–576, October 11 – October 15 2009. (Cited on pages 5, 24, 28, 39, 67, 68, 70, 78, 103, and 116.)

- [18] Robert Byer and Lawrence Shepp. Two-dimensional remote air-pollution monitoring via tomography. *Optics Letters*, 4(3):75–77, 1979. (Cited on pages 6, 90, and 116.)
- [19] William R. Hogan, G. F. Cooper, M. M. Wagner, and G. L. Wallson. An inverted gaussian plume model for estimating the location and amount of release of airborne agents from downwind atmospheric concentrations. *ROD technical report, Raltime Outbreak and Disease Surveillance Laboratory, University of Pittsburgh, PA.*, 2005. (Cited on pages 11, 24, 27, and 68.)
- [20] I.L. Mostinsky. Diffusion. In *Thermopedia: A guide to thermodynamic head and mass transfer and fluids engineering*. 2011. (Cited on page 11.)
- [21] P. Roberts and D. Webster. *Turbulent diffusion. Environmental Fluid Mechanics Theories and Application*. ASCE Press, Reston, VA., 2002. (Cited on pages 11 and 12.)
- [22] P.P. Neumann, S. Asadi, V. Hernandez Bennetts, A.J. Lilienthal, and M. Bartholmai. Monitoring of CCS areas using micro unmanned aerial vehicles (muavs). *Energy Procedia*, 37(0):4182–4190, 2013. (Cited on page 12.)
- [23] Jacob Fraden. *Handbook of Modern Sensors: Physics, Designs, and Applications (Handbook of Modern Sensors)*. SpringerVerlag, 2003. (Cited on page 13.)
- [24] R.A. Russell. Survey of robotic applications for odor-sensing technology. *International Journal of Robotics Research*, 20(2):144–162, 2001. (Cited on page 13.)
- [25] Xiao Liu, Sitian Cheng, Hong Liu, Sha Hu, Daqiang Zhang, and Huan-sheng Ning. A survey on gas sensing technology. *Sensors*, 12(7):9635–9665, 2012. (Cited on page 13.)
- [26] K. Ihokura and J. Watson. *The Stannic Oxide Gas Sensor Principles and Applications*. Taylor & Francis, 1994. (Cited on pages 13, 14, 23, 47, and 57.)
- [27] J. Janata. *Principles of Chemical Sensors*. Springer, 2009. (Cited on pages 13 and 46.)
- [28] *The PID Handbook: Theory and Applications of Direct-Reading Photoionization Detectors (PIDs)*, 2013. (Cited on page 15.)
- [29] Judd C. Posner. Portable gas chromatography. In Peter M. Eller, editor, *Manual of Analytic Methods*. US Department of Health and Human Services, Cincinnati, US., 1994. (Cited on page 15.)

- [30] Robert A. Schowengerdt. *Remote sensing: models and methods for image processing*. Academic Press, San Diego, 3 edition, 2007. (Cited on page 16.)
- [31] U.S. Environmental Protection Agency (EPA). *Optical Remote Sensing for Measurement and Monitoring of Emissions Flux*, 2011. (Cited on pages 16, 18, 68, and 89.)
- [32] M.B. Frish, R.T. Wainner, M.C. Laderer, B.D. Green, and M.G. Allen. Standoff and miniature chemical vapor detectors based on tunable diode laser absorption spectroscopy. *Sensors Journal, IEEE*, 10(3):639–646, March 2010. (Cited on page 17.)
- [33] M. Druy, B. Frish, and W. J. Kessler. From laboratory technique to process gas sensor - the maturation of tunable diode laser absorption spectroscopy. *Spectroscopy*, 21:14–18, 2006. (Cited on page 17.)
- [34] U.S. Environmental Protection Agency (EPA). *Measurement and Monitoring Technologies for the 21st Century. Open Path Technologies: Measurement at a Distance UV-DOAS*, 2009. (Cited on pages 17 and 18.)
- [35] Hans Edner, Kent Fredriksson, Anders Sunesson, Sune Svanberg, Leif Uéus, and Wilhelm Wendt. Mobile remote sensing system for atmospheric monitoring. *Appl. Opt.*, 26(19):4330–4338, Oct 1987. (Cited on page 17.)
- [36] M. Kastek, T. Piatkowski, R. Dulski, M. Chamberland, P. Lagueux, and V. Farley. Hyperspectral imaging infrared sensor used for chemical agent detection and identification. In *Photonics and Optoelectronics (SOPO), 2012 Symposium on*, pages 1–4, May 2012. (Cited on page 18.)
- [37] *Environ Sci Technol.*, (44). (Cited on page 18.)
- [38] T. Trefiak. Pilot study: Optical leak detection and measurement. Technical report, October 2006. (Cited on page 19.)
- [39] Dieter Fox, Wolfram Burgard, Frank Dellaert, and Sebastian Thrun. Monte carlo localization: efficient position estimation for mobile robots. pages 343–349, 1999. (Cited on pages 19, 31, and 124.)
- [40] Armin Hornung, Kai M. Wurm, Maren Bennewitz, Cyrill Stachniss, and Wolfram Burgard. Octomap: an efficient probabilistic 3d mapping framework based on octrees. *Autonomous Robots*, 34(3):189–206, 2013. (Cited on pages 19, 102, and 124.)
- [41] M. Vergassola, E. Villermanx, and B. I. Shraiman. ‘Infotaxis’ as a strategy for searching without gradients. *Nature*, 445:406–409, January 2007. (Cited on page 20.)

- [42] Javier Gonzalez-Jimenez, Javier G. Monroy, and Jose Luis Blanco. The multi-chamber electronic nose-an improved olfaction sensor for mobile robotics. *Sensors*, 11(6):6145–6164, 2011. (Cited on page 21.)
- [43] Takamichi Nakamoto and Kenjiro Yoshikawa. Movie with scents generated by olfactory display using solenoid valves. *2014 IEEE Virtual Reality (VR)*, 0:291–292, 2006. (Cited on page 21.)
- [44] Sepideh Pashami, Achim J. Lilienthal, Erik Schaffernicht, and Marco Trincavelli. Trefex: Trend estimation and change detection in the response of mox gas sensors. *Sensors*, 13(6):7323–8220, 2013. (Cited on page 22.)
- [45] Paul J. Gemperline, James R. Long, and Vasilis G. Gregoriou. Nonlinear multivariate calibration using principal components regression and artificial neural networks. *Analytical Chemistry*, 63(20):2313–2323, 1991. (Cited on page 23.)
- [46] H Sundgren, F Winqvist, I Lukkari, and I Lundstrom. Artificial neural networks and gas sensor arrays: quantification of individual components in a gas mixture. *Measurement Science and Technology*, 2(5):464, 1991. (Cited on page 23.)
- [47] Lubomir Hadjiiski, Paul Geladi, and Philip Hopke. A comparison of modeling nonlinear systems with artificial neural networks and partial least squares. *Chemometrics and Intelligent Laboratory Systems*, 49(1):91 – 103, 1999. (Cited on page 23.)
- [48] R.P. Cogdill and P. Dardenne. Least-squares support vector machines for chemometrics: An introduction and evaluation. *Journal of Near Infrared Spectroscopy*, 12(2):93–100, 2004. (Cited on page 23.)
- [49] S. De Vito, E. Massera, M. Piga, L. Martinotto, and G. Di Francia. On field calibration of an electronic nose for benzene estimation in an urban pollution monitoring scenario. *Sensors and Actuators, B: Chemical*, 129(2):750–757, 2008. (Cited on page 23.)
- [50] Javier Gonzalez Monroy, Achim Lilienthal, Jose Luis Blanco, Javier Gonzalez Jimenez, and Marco Trincavelli. Probabilistic gas quantification with {MOX} sensors in open sampling systems - a gaussian process approach. *Sensors and Actuators B: Chemical*, 188:298 – 312, 2013. (Cited on page 23.)
- [51] F. Röck, N. Barsan, and U. Weimar. Electronic nose: Current status and future trends. *Chemical Reviews*, 108(2):705–725, 2008. (Cited on page 23.)

- [52] R.E. Shaffer, S.L. Rose-Pehrsson, and R.A. McGill. A comparison study of chemical sensor array pattern recognition algorithms. *Analytica Chimica Acta*, 384(3):305–317, 1999. (Cited on page 23.)
- [53] J. W. Gardner and P. N. Bartlett. A brief history of electronic noses. *Sensors and Actuators B*, 18(19):211–220, 1994. (Cited on pages 23 and 43.)
- [54] H. R. Oelsen, P. Løfstrøm, R. Berkowicz, and M. Ketzel. Odour model development: Survey of modelling tools and datasets with focus on building effects. *Technical Report 541, NERI, Denmark*, 2005. (Cited on pages 24 and 67.)
- [55] C. Stachniss, C. Plagemann, and Achim J. Lilienthal. Gas distribution modeling using sparse gaussian process mixtures. *Autonomous Robots*, 26(2-3):187–202, April 2009. (Cited on pages 24, 70, and 103.)
- [56] Achim J. Lilienthal, Felix Streichert, and Andreas Zell. Model-based shape analysis of gas concentration gridmaps for improved gas source localisation. In *Proceedings of the IEEE International Conference on Robotics and Automation (ICRA)*, pages 3575–3580, April 18 – 22 2005. (Cited on pages 24, 28, and 39.)
- [57] Matteo Reggente and Achim J. Lilienthal. The 3d-kernel dm+v/w algorithm: Using wind information in three dimensional gas distribution modelling with a mobile robot. In *Proceedings of IEEE Sensors*, pages 999–1004, 2010. (Cited on pages 24 and 73.)
- [58] Achim J. Lilienthal, Amy Loutfi, Jose Luis Blanco, Cipriano Galindo, and Javier Gonzalez. Integrating slam into gas distribution mapping. In *Proceedings of ICRA Workshop on Robotic Olfaction - Towards Real Applications*, pages 21–28, April 10 – 14 2007. (Cited on page 24.)
- [59] Jose Luis Blanco, Javier G. Monroy, Achim Lilienthal, and Javier Gonzalez-Jimenez. A kalman filter based approach to probabilistic gas distribution mapping. In *Proceedings of the 28th Annual ACM Symposium on Applied Computing*, SAC 13, pages 217–222, New York, NY, USA, 2013. ACM. (Cited on pages 24, 70, and 103.)
- [60] Sahar Asadi, Sepideh Pashami, Amy Loutfi, and Achim J. Lilienthal. TD Kernel DM+V: Time-dependent statistical gas distribution modelling on simulated measurements. In *AIP Conference Proceedings Volume 1362: Olfaction and Electronic Nose - Proceedings of the 14th International Symposium on Olfaction and Electronic Nose (ISOEN)*, pages 281–283, 2011. (Cited on pages 24 and 70.)



- [61] A. J. Lilienthal, A. Loutfi, and T. Duckett. Airborne Chemical Sensing with Mobile Robots. *Sensors*, 6:1616–1678, October 2006. (Cited on page 24.)
- [62] Achim J. Lilienthal, Denis Reiman, and Andreas Zell. Gas source tracing with a mobile robot using an adapted moth strategy. In *Autonome Mobile Systeme (AMS)*, 18. *Fachgespräch*, pages 150–160. GDI, December 4 – 5 2003. (Cited on page 24.)
- [63] Achim J. Lilienthal and Tom Duckett. Experimental analysis of smelling braintenberg vehicles. In *Proceedings of the IEEE International Conference on Advanced Robotics (ICAR)*, pages 375–380, June 30 – July 3 2003. (Cited on page 24.)
- [64] R. Rozas, J. Morales, and D. Vega. Artificial smell detection for robotic navigation. In *Advanced Robotics, 1991. 'Robots in Unstructured Environments', 91 ICAR., Fifth International Conference on*, pages 1730–1733 vol.2, June 1991. (Cited on page 25.)
- [65] R. Andrew Russell. A ground-penetrating robot for underground chemical source location. In *Intelligent Robots and Systems, 2005. (IROS 2005). 2005 IEEE/RSJ International Conference on*, pages 175–180, Aug 2005. (Cited on pages 25 and 29.)
- [66] Patrick Neumann. *Gas Source Localization and Gas Distribution Mapping with a Micro-Drone*. PhD thesis, der Freien Universität Berlin, March 2013. (Cited on pages 25 and 31.)
- [67] Yoshihiko Kuwana, Sumito Nagasawa, Isao Shimoyama, and Ryohei Kanzaki. Synthesis of the pheromone-oriented behaviour of silkworm moths by a mobile robot with moth antennae as pheromone sensors. *Biosensors and Bioelectronics*, 14(2):195 – 202, 1999. (Cited on page 26.)
- [68] Pawel Pyk, Sergi Bermudez i Badia, Ulysses Bernardet, Philipp Knüsel, Mikael Carlsson, Jing Gu, Eric Chanie, Bill Hansson, Tim Pearce, and Paul J. Verschure. An artificial moth: Chemical source localization using a robot based neuronal model of moth optomotor anemotactic search. *Autonomous Robots*, 20:197–213, 2006. 10.1007/s10514-006-7101-4. (Cited on page 26.)
- [69] H Ishida, T Nakamoto, T Moriizumi, T Kikas, and J Janata. Plume-tracking robots: a new application of chemical sensors. *The Biological Bulletin*, 200(2):222–226, 2001. (Cited on page 26.)
- [70] F.W. Grasso, J.A. Basil, and J. Atema. Toward the convergence: robot and lobster perspectives of tracking odors to their source in the turbulent

- marine environment. In *Intelligent Control (ISIC)*, 1998. *Held jointly with IEEE International Symposium on Computational Intelligence in Robotics and Automation (CIRA), Intelligent Systems and Semiotics (ISAS), Proceedings*, pages 259–264, sep 1998. (Cited on page 26.)
- [71] R.Andrew Russell, Alireza Bab-Hadiashar, Rod L. Shepherd, and Gordon G. Wallace. A comparison of reactive robot chemotaxis algorithms. *Robotics and Autonomous Systems*, 45(2):83 – 97, 2003. (Cited on page 26.)
- [72] Achim J. Lilienthal, Holger Ulmer, Holger Fröhlich, Andreas Stützle, Felix Werner, and Andreas Zell. Gas source declaration with a mobile robot. In *Proceedings of the IEEE International Conference on Robotics and Automation (ICRA)*, pages 1430–1435, April 26 – May 1 2004. (Cited on pages 26 and 29.)
- [73] A.T. Hayes, A. Martinoli, and R.M. Goodman. Distributed odor source localization. *Sensors Journal, IEEE*, 2(3):260–271, jun 2002. (Cited on pages 26 and 69.)
- [74] Patrick P. Neumann, Victor Hernandez Bennetts, Achim J. Lilienthal, Matthias Bartholmai, and Jochen H. Schiller. Gas source localization with a micro-drone using bio-inspired and particle filter-based algorithms. *Advanced Robotics*, 27(9):725–738, 2013. (Cited on pages 26 and 29.)
- [75] D. Martinez and L. Perrinet. Cooperation between vision and olfaction in a koala robot. *Report on the 2002 Workshop on Neuromorphic Engineering*, pages 51–53, 2002. (Cited on page 27.)
- [76] H. Ishida, T. Ushiku, S. Toyama, H. Taniguchi, and T. Moriizumi. Mobile robot path planning using vision and olfaction to search for a gas source. In *Sensors, 2005 IEEE*, pages 4 pp.–, Oct 2005. (Cited on pages 27 and 29.)
- [77] A Loutfi, S. Coradeschi, L. Karlsson, and M. Broxvall. Putting olfaction into action: using an electronic nose on a multi-sensing mobile robot. In *Intelligent Robots and Systems, 2004. (IROS 2004). Proceedings. 2004 IEEE/RSJ International Conference on*, volume 1, pages 337–342 vol.1, Sept 2004. (Cited on page 27.)
- [78] G. Bonow and A. Kroll. Gas leak localization in industrial environments using a tdlas-based remote gas sensor and autonomous mobile robot with the tri-max method. In *Robotics and Automation (ICRA), 2013 IEEE International Conference on*, pages 987–992, May 2013. (Cited on page 27.)

- [79] Andreas Kroll, Werner Baetz, and Daniel Peretzki. On autonomous detection of pressured air and gas leaks using passive ir-thermography for mobile robot application. In *IEEE International Conference on Robotics and Automation (ICRA 2009)*, pages 921–926, Kobe, Japan, 2009. (Cited on page 27.)
- [80] Yuichiro Fukazawa and Hiroshi Ishida. Estimating gas-source location in outdoor environment using mobile robot equipped with gas sensors and anemometer. *2009 IEEE Sensors*, pages 1721–1724, October 2009. (Cited on pages 27 and 68.)
- [81] Shuo Pang and J.A. Farrell. Chemical plume source localization. *Systems, Man, and Cybernetics, Part B: Cybernetics, IEEE Transactions on*, 36(5):1068–1080, Oct 2006. (Cited on page 27.)
- [82] Victor Pomareda, Victor Hernandez Bennetts, Ali Abdul Khaliq, Marco Trincavelli, Achim Lilienthal, and Santiago Marco. Chemical source localization in real environments integrating chemical concentrations in a probabilistic plume mapping approach. In *Proceedings of the 15th International Symposium on Olfaction and Electronic Nose (ISOEN 2013)*, 2013. (Cited on page 27.)
- [83] Victor Hernandez Bennetts, Achim Josef Lilienthal, Patrick Neumann, and Marco Trincavelli. Mobile robots for localizing gas emission sources on landfill sites: Is bio-inspiration the way to go? *Frontiers in Neuroengineering*, 4(20), 2012. (Cited on pages 28, 30, 34, 36, and 41.)
- [84] Victor Hernandez Bennetts, Achim Lilienthal, Ali Abdul Khaliq, Victor Pomareda Sese, and Marco Trincavelli. Towards real-world gas distribution mapping and leak localization using a mobile robot with 3d and remote gas sensing capabilities. In *Proceedings of the IEEE International Conference on Robotics and Automation (ICRA)*, pages 2327–2332, 2013. (Cited on pages 28, 96, 98, 100, and 102.)
- [85] Marco Trincavelli, Victor Hernandez Bennetts, and Achim Lilienthal. A least squares approach for learning gas distribution maps from a set of integral gas concentration measurements obtained with a tdlas sensor. In *Sensors, 2012 IEEE*, pages 1–4, 2012. (Cited on pages 28, 93, and 96.)
- [86] Victor Hernandez Bennetts, Erik Schaffernicht, Todor Soyanov, Achim Lilienthal, and Marco Trincavelli. Robot assisted gas tomography - localizing methane leaks in outdoor environments. In *Proceedings of the IEEE International Conference on Robotics and Automation (ICRA)*, 2014. (Cited on pages 28, 96, 98, 101, 103, 108, and 113.)

- [87] S. Soldan, G. Bonow, and A. Kroll. Robogasinspector - a mobile robotic system for remote leak sensing and localization in large industrial environments: Overview and first results. In *Automatic Control in Offshore Oil and Gas Production*, pages 33–38, 2012. (Cited on page 29.)
- [88] Matteo Reggente and Achim J. Lilienthal. Three-dimensional statistical gas distribution mapping in an uncontrolled indoor environment. In *AIP Conference Proceedings Volume 1137: Olfaction and Electronic Nose - Proceedings of the 13th International Symposium on Olfaction and Electronic Nose (ISOEN)*, pages 109–112, 2009. (Cited on pages 30, 33, 71, 73, and 122.)
- [89] Yuta Wada, Marco Trincavelli, Yuichiro Fukazawa, and Hiroshi Ishida. Collecting a database for studying gas distribution mapping and gas source localization with mobile robots. In *Proceedings of the 5th International Conference on Advanced Mechatronic (ICAM)*, pages 183–188, 2010. (Cited on pages 30, 32, 52, and 121.)
- [90] Patrick Neumann, Mathias Bartholmai, Jochem H. Schiller, Manol Manolov, and Burkhard Wiggerich. Self optimizing search and characterization of gaseous hazardous substance sources using a micro-drone: A new approach to determine wind speed and direction. In *IEEE International Workshop on Robotic and Sensors Environments (ROSE)*, 2010. (Cited on pages 32 and 123.)
- [91] L. P. S. Kuenen and Ring T. Cardé. Effects of moth size on velocity and steering during upwind flight toward a sex pheromone source by *Lymantria dispar*; (lepidoptera lymantriidae). *Journal of Insect Behavior*, 6:177–193, 1993. 10.1007/BF01051503. (Cited on page 34.)
- [92] Kristine a Justus, Ring T Cardé, and Andrew S French. Dynamic properties of antennal responses to pheromone in two moth species. *Journal of neurophysiology*, 93(4):2233–9, April 2005. (Cited on page 34.)
- [93] H. Zwaardemaker and F. Hogewind. On spray electricity for an waterfall-electricity. *Proc. Acad. Sci. Amst.*, 22:429–437, 1920. (Cited on page 43.)
- [94] J.D. Hartman. A possible objective method for the rapid estimation of flavors in vegetables. *Proc. Am. Soc. Hort. Sci.*, 64:335, 1954. (Cited on page 43.)
- [95] R.W. Moncrieff. An instrument for measuring and classifying odors. *Journal of applied physiology*, 16:742–749, 1961. (Cited on page 43.)
- [96] K. Persaud and G. H. Dodd. Analysis of discrimination mechanisms of the mammalian olfactory system using a model nose. *Nature*, 299:352–355, 1982. (Cited on page 43.)

- [97] A. Ikegami and M. Kaneyasu. Olfactory detection using integrated sensors. In *3rd Int. Conf. Solid.State Sensors and Actuators*, volume 11 of 7, pages 136–139. Transducers, June 1985. (Cited on page 43.)
- [98] Marco Trincavelli. *Data-Driven Batch Scheduling*. PhD thesis, Örebro University, December 2010. (Cited on pages 44, 46, 48, and 53.)
- [99] L. Dentoni, L. Capelli, S. Sironi, R. Del Rosso, S. Zanetti, and M.D. Torre. Development of an electronic nose for environmental odour monitoring. *Sensors (Switzerland)*, 12(11):14363–14381, 2012. (Cited on pages 44, 51, and 65.)
- [100] Victor Hernandez Bennetts, Erik Schaffernicht, Achim Lilienthal, and Marco Trincavelli. A novel approach for gas discrimination in natural environments with open sampling systems. In *IEEE Sensors 2014 (To appear)*, 2014. (Cited on pages 44, 53, 65, and 104.)
- [101] T.C. Pearce, S.S. Schiffman, H.T. Nagle, and J.W. Gardner. *Handbook of machine olfaction*. Wiley, Germany, 2003. (Cited on pages 45 and 47.)
- [102] R. Gutierrez-Osuna, H. Troy Nagle, and S.S. Schiffman. Transient response analysis of an electronic nose using multi-exponential models, sens. actuators b. *Sensors and actuators B*, 61:170–182, 1999. (Cited on page 48.)
- [103] T. Eklöv, P. Mårtensson, and J. Lundström. Enhanced selectivity of mosfet gas sensors by systematical analysis of transient parameters. *Anal. Chim. Acta*, 353:291–300, 1997. (Cited on page 48.)
- [104] N. Nimsuk and T. Nakamoto. Improvement of capability for classifying odors in dynamically changing concentration using qcm sensor array and short-time fourier transform. *Sensors and Actuators, B: Chemical*, 127(2):491–496, 2007. (Cited on page 48.)
- [105] L. Marques, N. Almeida, and A.T. De Almeida. Olfactory sensory system for odour-plume tracking and localization. *Proceedings of IEEE Sensors*, 2(1):418–423, 2003. (Cited on pages 48 and 52.)
- [106] A. Vergara, E. Llobet, E. Martinelli, C. Di Natale, A. D’Amico, and X. Correig. Feature extraction of metal oxide gas sensors using dynamic moments. *Sensors and actuators B*, 122:219–226, 2007. (Cited on page 48.)
- [107] C. M. Bishop. *Pattern Recognition and Machine Learning (Information Science and Statistics)*. Springer, 2006. (Cited on pages 48, 50, 53, 60, and 82.)

- [108] Isabelle Guyon. An introduction to variable and feature selection. *Journal of Machine Learning Research*, 3:1157–1182, 2003. (Cited on page 48.)
- [109] Marco Trincavelli and Amy Loutfi. Feature selection for gas identification with a mobile robot. In *Proceedings of the IEEE International Conference on Robotics and Automation (ICRA)*, pages 2852 – 2857, 2010. (Cited on pages 48, 53, and 54.)
- [110] M. Jamal, M. R. Khan, S.A Imam, and A Jamal. Artificial neural network based e-nose and their analytical applications in various field. In *Control Automation Robotics Vision (ICARCV), 2010 11th International Conference on*, pages 691–698, Dec 2010. (Cited on page 49.)
- [111] K.-T. Tang, S.-W. Chiu, C.-H. Pan, H.-Y. Hsieh, Y.-S. Liang, and S.-C. Liu. Development of a portable electronic nose system for the detection and classification of fruity odors. *Sensors (Switzerland)*, 10(10):9179–9193, 2010. (Cited on page 49.)
- [112] M. Pardo and G. Sverveglieri. Classification of electronic nose data with support vector machines. *Sensors and Actuators B: Chemical*, 107(2):730 – 737, 2005. (Cited on page 49.)
- [113] Amine Bermak, S. Belhouari, M. Shi, and Dominique Martinez. Pattern Recognition Techniques for Odor Discrimination in Gas Sensor Array. In Elizabeth C. Dickey Craig A. Grimes and Michael V. Pishko, editors, *The Encyclopedia of Sensors*. American Scientific Publishers, 2005. (Cited on page 49.)
- [114] A.H. Gomez, G. Hu, J. Wang, and A.G. Pereira. Evaluation of tomato maturity by electronic nose. *Computers and Electronics in Agriculture*, 54(1):44–52, 2006. (Cited on page 49.)
- [115] T. Aishima. Discrimination of liquor aromas by pattern recognition analysis of responses from a gas sensor array. *Analytica Chimica Acta*, 243(2):293–300, 1991. (Cited on page 49.)
- [116] J.W. Gardner, H.V. Shurmer, and T.T. Tan. Application of an electronic nose to the discrimination of coffees. *Sensors and Actuators: B. Chemical*, 6(1-3):71–75, 1992. (Cited on page 49.)
- [117] V.F. Pais, J.A.B.P. Oliveira, and M.T.S.R. Gomes. An electronic nose based on coated piezoelectric quartz crystals to certify ewes' cheese and to discriminate between cheese varieties. *Sensors*, 12(2):1422–1436, 2012. (Cited on page 49.)

- [118] S. Ampuero, T. Zesiger, V. Gustafsson, A. Lundén, and J.O. Bosset. Determination of trimethylamine in milk using an ms based electronic nose. *European Food Research and Technology*, 214(2):163–167, 2002. (Cited on page 49.)
- [119] A. Jonsson, F. Winquist, J. Schnurer, H. Sundgren, and I. Lundstrom. Electronic nose for microbial quality classification of grains. *International Journal of Food Microbiology*, 35(2):187–193, 1997. (Cited on page 50.)
- [120] A. Campagnoli and V. Dell’Orto. Potential application of electronic olfaction systems in feedstuffs analysis and animal nutrition. *Sensors (Switzerland)*, 13(11):14611–14632, 2013. (Cited on page 50.)
- [121] C. Di Natale, A. Macagnano, E. Martinelli, R. Paolesse, G. D’Arcangelo, C. Roscioni, A. Finazzi-Agro, and A. D’Amico. Lung cancer identification by the analysis of breath by means of an array of non-selective gas sensors. *Biosensors and Bioelectronics*, 18(10):1209–1218, 2003. (Cited on page 50.)
- [122] X. Chen, M. Cao, Y. Li, W. Hu, P. Wang, K. Ying, and H. Pan. A study of an electronic nose for detection of lung cancer based on a virtual saw gas sensors array and imaging recognition method. *Measurement Science and Technology*, 16(8):1535–1546, 2005. (Cited on page 50.)
- [123] Marco Trincavelli, Silvia Coradeschi, Amy Loutfi, Bo Soederquist, and Per Thunberg. Direct identification of bacteria in blood culture samples using an electronic nose. *Biomedical Engineering, IEEE Transactions on*, 57(12):2884 – 2890, 2010. (Cited on page 50.)
- [124] K.B. Gendron, N.G. Hockstein, E.R. Thaler, A. Vachani, and C.W. Hanson. In vitro discrimination of tumor cell lines with an electronic nose. *Otolaryngology - Head and Neck Surgery*, 137(2):269–273, 2007. (Cited on page 50.)
- [125] Hanying Zhou, Margie L. Homer, Abhijit V. Shevade, and Margaret A. Ryan. Nonlinear least-squares based method for identifying and quantifying single and mixed contaminants in air with an electronic nose. *Sensors*, 6(1):1–18, 2005. (Cited on page 50.)
- [126] W.J. Peveler, R. Binions, S.M.V. Hailes, and I.P. Parkin. Detection of explosive markers using zeolite modified gas sensors. *Journal of Materials Chemistry A*, 1(7):2613–2620, 2013. (Cited on page 50.)
- [127] J. Nicolas, A. C. Romain, V. Wiertz, J. Maternova, and P. André. Using the classification model of an electronic nose to assign unknown malodours to environmental sources and to monitor them continuously.

- Sensors and Actuators, B: Chemical*, 69(3):366–371, 2000. (Cited on page 50.)
- [128] J. Nicolas, C. Cerisier, J. Delva, and A.C. Romain. Potential of a network of electronic noses to assess in real time the odour annoyance in the environment of a compost facility. *Chemical Engineering Transactions*, 30:133–138, 2012. (Cited on page 50.)
- [129] Alexander Vergara, Jordi Fonollosa, Jonas Mahiques, Marco Trincavelli, Nikolai Rulkov, and Ramon Huerta. On the performance of gas sensor arrays in open sampling systems using inhibitory support vector machines. *Sensors and Actuators B: Chemical*, 185(0):462–477, 2013. (Cited on page 50.)
- [130] Marco Trincavelli, Alexander Vergara, Nikolai Rulkov, Jose S. Murguia, Achim Lilienthal, and Ramon Huerta. Optimizing the operating temperature for an array of mox sensors on an open sampling system. *AIP Conference Proceedings*, 1362:225–227, 2011. (Cited on pages 50 and 51.)
- [131] L. Capelli, L. Dentoni, S. Sironi, and R. Del Rosso. The need for electronic noses for environmental odour exposure assessment. *Water Science and Technology*, 69(1):135–141, 2014. (Cited on page 51.)
- [132] Dominique Martinez, Oliver Rochel, and Etienne Hugues. A biomimetic robot for tracking specific odors in turbulent plumes. *Autonomous Robots*, 20(3):185–195, 2006. (Cited on pages 52 and 53.)
- [133] Wolfgang Maass and Christopher M. Bishop, editors. *Pulsed Neural Networks*. MIT Press, Cambridge, MA, USA, 1999. (Cited on page 52.)
- [134] Marco Trincavelli, Silvia Coradeschi, and Amy Loutfi. Classification of odours with mobile robots based on transient response. In *Proceedings of the IEEE/RSJ International Conference on Intelligent Robots and Systems (IROS)*, pages 4110 – 4115, 2008. (Cited on pages 52 and 56.)
- [135] Marco Trincavelli. Gas discrimination for mobile robots. *Künstliche Intelligenz*, 25(4):351 – 354, 2011. (Cited on page 52.)
- [136] Marco Trincavelli, Silvia Coradeschi, and Amy Loutfi. Classification of odours for mobile robots using an ensemble of linear classifiers. In *Proceedings of the 13th International Symposium on Olfaction and Electronic Nose (ISOEN)*, pages 475 – 478, 2009. (Cited on page 53.)
- [137] Mehmet K. Muezzinoglu, Alexander Vergara, Ramon Huerta, and Mikhail I. Rabinovich. A sensor conditioning principle for odor identification. *Sensors and Actuators B: Chemical*, 146(2):472 – 476, 2010. (Cited on page 56.)



- [138] Trevor Hastie and Robert Tibshirani. Classification by pairwise coupling. *The Annals of Statistics*, 26(2):451–471, 04 1998. (Cited on page 59.)
- [139] Ting Fan Wu, Chih Jen Lin, and Ruby C. Weng. Probability estimates for multi-class classification by pairwise coupling. *J. Mach. Learn. Res.*, 5:975–1005, December 2004. (Cited on page 59.)
- [140] Kevin P. Murphy. *Machine Learning: A Probabilistic Perspective (Adaptive Computation and Machine Learning series)*. The MIT Press, 2012. (Cited on page 60.)
- [141] E. Thoma, R. Green, G. Hater, C. Goldsmith, N. Swan, M. Chase, and R. Hashmonay. Development of epa otm 10 for landfill applications. *Journal of Environmental Engineering*, 136(8):769–776, 2010. (Cited on page 67.)
- [142] Victor Hernandez Bennetts, Marco Trincavelli, Erik Schaffernicht, and Achim Lilienthal. Online parameter selection for gas distribution mapping. *Sensor Letters*, 2014. (Cited on pages 68 and 73.)
- [143] Victor Hernandez Bennetts, Achim Lilienthal, and Marco Trincavelli. Creating true gas concentration maps in presence of multiple heterogeneous gas sources. pages 1–4, 2012. (Cited on pages 68, 70, and 78.)
- [144] Victor Hernandez Bennetts, Erik Schaffernicht, Victor Pomareda, Achim Lilienthal, and Marco Trincavelli. Combining non selective gas sensors on a mobile robot for identification and mapping of multiple chemical compounds. *Sensors MDPI (to appear)*, 2014. (Cited on pages 68, 70, 78, and 82.)
- [145] S. Thykier-Nielsen, S. Deme, and T. Mikkelsen. Description of the atmospheric dispersion module rimpuff. *Technical report RODOS(WG2)-TN(98)-02, Risø National Laboratory, Roskilde, Denmark*, 1999. (Cited on page 68.)
- [146] A. Graff. The new german regulatory model - a lagrangian particle dispersion model. In *8th international conference on Harmonisation within Atmospheric Dispersion Modelling for Regulatory Purposes.*, 2006. (Cited on page 68.)
- [147] F. Pasquill. The Estimation of the Dispersion of Wind borne Material. *Meteorol. Mag.*, 90:33–49, 1961. (Cited on page 69.)
- [148] M. Pontiggia, M. Derudi, V. Busini, and R. Rota. Hazardous gas dispersion: A cfd model accounting for atmospheric stability classes. *Journal of Hazardous Materials*, 171(1?3):739 – 747, 2009. (Cited on page 69.)

- [149] Hiroshi Ishida, Takamichi Nakamoto, and Toyosaka Moriizumi. Remote sensing of gas/odor source location and concentration distribution using mobile system. *Sensors and Actuators B: Chemical*, 49(1-2):52 – 57, 1998. (Cited on page 69.)
- [150] Achim J. Lilienthal and Tom Duckett. Building gas concentration gridmaps with a mobile robot. *Robotics and Autonomous Systems*, 48(1):3–16, August 31 2004. (Cited on pages 69 and 70.)
- [151] Achim Lilienthal, Marco Trincavelli, and Erik Schaffernicht. It’s always smelly around here! modeling the spatial distribution of gas detection events with based grid maps. In *Proceedings of the 15th International Symposium on Olfaction and Electronic Nose (ISOEN 2013)*, 2013. (Cited on page 69.)
- [152] D. Webster, S. Rahman, and L. Dasi. Laser-induced fluorescence measurements of a turbulent plume. *Journal of Engineering Mechanics*, 129(10):1130–1137, 2003. (Cited on pages 69 and 113.)
- [153] Achim J. Lilienthal, Sahar Asadi, and Matteo Reggente. Estimating predictive variance for statistical gas distribution modelling. In *AIP Conference Proceedings Volume 1137: Olfaction and Electronic Nose - Proceedings of the 13th International Symposium on Olfaction and Electronic Nose (ISOEN)*, pages 65–68, 2009. (Cited on page 70.)
- [154] Amy Loutfi, Silvia Coradeschi, Achim J. Lilienthal, and Javier Gonzalez. Gas distribution mapping of multiple odour sources using a mobile robot. *Robotica*, 27(2):311–319, June 4 2009. (Cited on page 70.)
- [155] E. Nadaraya. On estimating regression. *Theory of Probability and Its Applications*, 9(1):141–142, 1964. (Cited on page 71.)
- [156] Max Köhler, Anja Schindler, and Stefan Sperlich. A review and comparison of bandwidth selection methods for kernel regression. Courant Research Centre: Poverty, Equity and Growth - Discussion Papers 95, Courant Research Centre PEG, 2011. (Cited on page 74.)
- [157] J. Quinonero-Candela, C. E. Rasmussen, F. Sinz, and B. Schoelkopf. *Evaluating Predictive Uncertainty Challenge*, pages 1–27. Springer, 2006. (Cited on page 74.)
- [158] G. Monari and G. Dreyfus. Local overfitting control via leverages. *Neural Computation*, 14(6):1481–1506, 2002. (Cited on page 74.)
- [159] Gaétan Monari and Gérard Dreyfus. Withdrawing an example from the training set: An analytic estimation of its effect on a non-linear parameterised model. *Neurocomputing*, 35(1-4):195–201, 2000. (Cited on page 74.)

- [160] Henry F. Inman and Edwin L. Bradley. The overlapping coefficient as a measure of agreement between probability distributions and point estimation of the overlap of two normal densities. *Communications in Statistics - Theory and Methods*, 18(10):3851–3874, 1989. (Cited on page 77.)
- [161] Alison L. Gibbs, Francis, and Edward Su. On choosing and bounding probability metrics. *Internat. Statist.*, pages 419–435, 2002. (Cited on page 82.)
- [162] Kevin C Gross, Kenneth C Bradley, and Glen P Perram. Remote identification and quantification of industrial smokestack effluents via imaging fourier-transform spectroscopy. *Environmental science & technology*, 44(24):9390–9397, 2010. (Cited on page 87.)
- [163] A.C. Drescher, A.J. Gadgil, P.N. Price, and W.W. Nazaroff. Novel approach for tomographic reconstruction of gas concentration distributions in air: Use of smooth basis functions and simulated annealing. *Atmospheric Environment*, 30(6):929–940, 1996. (Cited on page 91.)
- [164] A. C. Kak and M. Slaney. *Principles of Computerized Tomographic Imaging*. IEEE Press, New York, 1988. (Cited on pages 91 and 92.)
- [165] L. Todd and G. Ramachandran. Evaluation of algorithms for tomographic reconstruction of chemical concentrations in indoor air. *American Industrial Hygiene Association Journal*, 55(5):403–417, 1994. (Cited on page 93.)
- [166] T. Laepple, V. Knab, K.-U. Mettendorf, and I. Pundt. Longpath doas tomography on a motorway exhaust gas plume: Numerical studies and application to data from the bab ii campaign. *Atmospheric Chemistry and Physics*, 4(5):1323–1342, 2004. (Cited on pages 93 and 109.)
- [167] W. Verkrusse and L.A. Todd. Improved method "grid translation" for mapping environmental pollutants using a two-dimensional cat scanning system. *Atmospheric Environment*, 38(12):1801–1809, 2004. (Cited on pages 93 and 94.)
- [168] A. Hartl, B.C. Song, and I. Pundt. 2-d reconstruction of atmospheric concentration peaks from horizontal long path doas tomographic measurements: Parametrisation and geometry within a discrete approach. *Atmospheric Chemistry and Physics*, 6(3):847–861, 2006. (Cited on pages 93, 94, and 112.)
- [169] W. Verkrusse and L.A. Todd. Novel algorithm for tomographic reconstruction of atmospheric chemicals with sparse sampling. *Environmental Science and Technology*, 39(7):2247–2254, 2005. (Cited on page 94.)

- [170] J. Bogner, M. Abdelrafie Ahmed, C. Diaz, A. Faaij, Q. Gao, S. Hashimoto, K. Mareckova, R. Pipatti, and T. Zhang. *Climate Change 2007: Mitigation. Contribution of Working Group III to the Fourth Assessment Report of the Intergovernmental Panel on Climate Change*. Cambridge University Press, Cambridge, United Kingdom, 2007. (Cited on page 96.)
- [171] Wang Yu-Ling, Nai Chang-Xin, Guan Shao-peng, and Jin Zhao-di. Identifying gravel layer using time-domain analysis methods for land-fill leak repair. In *Measuring Technology and Mechatronics Automation (ICMTMA), 2010 International Conference on*, volume 2, pages 406–409, March 2010. (Cited on page 97.)
- [172] Tgn 07:guidance on monitoring landfill gas surface emissions. Technical report, United Kingdom (UK), 2010. (Cited on page 97.)
- [173] T. Stoyanov, J. Saarinen, H. Andreasson, and A.J. Lilienthal. Normal distributions transform occupancy map fusion: Simultaneous mapping and tracking in large scale dynamic environments. In *Intelligent Robots and Systems (IROS), 2013 IEEE/RSJ International Conference on*, pages 4702–4708, Nov 2013. (Cited on pages 101 and 125.)
- [174] J. Saarinen, H. Andreasson, T. Stoyanov, J. Ala-Luhtala, and A.J. Lilienthal. Normal distributions transform occupancy maps: Application to large-scale online 3d mapping. In *Robotics and Automation (ICRA), 2013 IEEE International Conference on*, pages 2233–2238, May 2013. (Cited on page 101.)
- [175] J. Saarinen, H. Andreasson, T. Stoyanov, and A.J. Lilienthal. Normal distributions transform monte-carlo localization (ndt-mcl). In *Intelligent Robots and Systems (IROS), 2013 IEEE/RSJ International Conference on*, pages 382–389, Nov 2013. (Cited on page 101.)
- [176] R. Valencia, J. Saarinen, H. Andreasson, J. Vallve, J. Andrade-Cetto, and A.J. Lilienthal. Localization in highly dynamic environments using dual-timescale ndt-mcl. In *Robotics and Automation (ICRA), 2014 IEEE International Conference on*, pages 3956–3962, May 2014. (Cited on page 101.)
- [177] Todor Stoyanov, Martin Magnusson, and Achim J. Lilienthal. Fast and accurate scan registration through minimization of the distance between compact 3d ndt representations. *The International Journal of Robotics Research*, 31:1377–1393, 2012. (Cited on page 101.)
- [178] U. Desideri, D. Leonardi, and S. Proietti. Application of infra-red thermography to study behaviour of biogas captation wells. In *Eleventh*

- International Waste Management and Landfill Symposium*, pages 1–15, 2007. (Cited on page 114.)
- [179] Robots are getting closer to having humanlike abilities and senses. In <http://wapo.st/1crDt6Z>. (Cited on page 117.)
- [180] White house taps arpa-e to boost methane detection. In <http://spectrum.ieee.org/automaton/robotics/industrial-robots/gasbot-sniffs-out-climate-destruction>. (Cited on page 117.)
- [181] Researches build robot to sniff out methane at landfills. In <http://phys.org/news/2013-08-robot-methane-landfills.html>. (Cited on page 117.)
- [182] Achim J. Lilienthal. *Gas Distribution Mapping and Gas Source Localisation with a Mobile Robot*. PhD thesis, Wilhelm-Schickard Institute, University of Tübingen, December 2004. (Cited on page 118.)



PUBLICATIONS *in the series*  
ÖREBRO STUDIES IN TECHNOLOGY

1. Bergsten, Pontus (2001) *Observers and Controllers for Takagi – Sugeno Fuzzy Systems*. Doctoral Dissertation.
2. Iliev, Boyko (2002) *Minimum-time Sliding Mode Control of Robot Manipulators*. Licentiate Thesis.
3. Spännar, Jan (2002) *Grey box modelling for temperature estimation*. Licentiate Thesis.
4. Persson, Martin (2002) *A simulation environment for visual servoing*. Licentiate Thesis.
5. Boustedt, Katarina (2002) *Flip Chip for High Volume and Low Cost – Materials and Production Technology*. Licentiate Thesis.
6. Biel, Lena (2002) *Modeling of Perceptual Systems – A Sensor Fusion Model with Active Perception*. Licentiate Thesis.
7. Otterskog, Magnus (2002) *Produktionstest av mobiltelefonantennerna i mod-växlande kammare*. Licentiate Thesis.
8. Tolt, Gustav (2003) *Fuzzy-Similarity-Based Low-level Image Processing*. Licentiate Thesis.
9. Loutfi, Amy (2003) *Communicating Perceptions: Grounding Symbols to Artificial Olfactory Signals*. Licentiate Thesis.
10. Iliev, Boyko (2004) *Minimum-time Sliding Mode Control of Robot Manipulators*. Doctoral Dissertation.
11. Pettersson, Ola (2004) *Model-Free Execution Monitoring in Behavior-Based Mobile Robotics*. Doctoral Dissertation.
12. Överstam, Henrik (2004) *The Interdependence of Plastic Behaviour and Final Properties of Steel Wire, Analysed by the Finite Element Method*. Doctoral Dissertation.
13. Jennergren, Lars (2004) *Flexible Assembly of Ready-to-eat Meals*. Licentiate Thesis.
14. Jun, Li (2004) *Towards Online Learning of Reactive Behaviors in Mobile Robotics*. Licentiate Thesis.
15. Lindquist, Malin (2004) *Electronic Tongue for Water Quality Assessment*. Licentiate Thesis.
16. Wasik, Zbigniew (2005) *A Behavior-Based Control System for Mobile Manipulation*. Doctoral Dissertation.

17. Berntsson, Tomas (2005) *Replacement of Lead Baths with Environment Friendly Alternative Heat Treatment Processes in Steel Wire Production*. Licentiate Thesis.
18. Tolt, Gustav (2005) *Fuzzy Similarity-based Image Processing*. Doctoral Dissertation.
19. Munkevik, Per (2005) "Artificial sensory evaluation – appearance-based analysis of ready meals". Licentiate Thesis.
20. Buschka, Pär (2005) *An Investigation of Hybrid Maps for Mobile Robots*. Doctoral Dissertation.
21. Loutfi, Amy (2006) *Odour Recognition using Electronic Noses in Robotic and Intelligent Systems*. Doctoral Dissertation.
22. Gillström, Peter (2006) *Alternatives to Pickling; Preparation of Carbon and Low Alloyed Steel Wire Rod*. Doctoral Dissertation.
23. Li, Jun (2006) *Learning Reactive Behaviors with Constructive Neural Networks in Mobile Robotics*. Doctoral Dissertation.
24. Otterskog, Magnus (2006) *Propagation Environment Modeling Using Scattered Field Chamber*. Doctoral Dissertation.
25. Lindquist, Malin (2007) *Electronic Tongue for Water Quality Assessment*. Doctoral Dissertation.
26. Cielniak, Grzegorz (2007) *People Tracking by Mobile Robots using Thermal and Colour Vision*. Doctoral Dissertation.
27. Boustedt, Katarina (2007) *Flip Chip for High Frequency Applications – Materials Aspects*. Doctoral Dissertation.
28. Soron, Mikael (2007) *Robot System for Flexible 3D Friction Stir Welding*. Doctoral Dissertation.
29. Larsson, Sören (2008) *An industrial robot as carrier of a laser profile scanner. – Motion control, data capturing and path planning*. Doctoral Dissertation.
30. Persson, Martin (2008) *Semantic Mapping Using Virtual Sensors and Fusion of Aerial Images with Sensor Data from a Ground Vehicle*. Doctoral Dissertation.
31. Andreasson, Henrik (2008) *Local Visual Feature based Localisation and Mapping by Mobile Robots*. Doctoral Dissertation.
32. Bouguerra, Abdelbaki (2008) *Robust Execution of Robot Task-Plans: A Knowledge-based Approach*. Doctoral Dissertation.



33. Lundh, Robert (2009) *Robots that Help Each Other: Self-Configuration of Distributed Robot Systems*. Doctoral Dissertation.
34. Skoglund, Alexander (2009) *Programming by Demonstration of Robot Manipulators*. Doctoral Dissertation.
35. Ranjbar, Parivash (2009) *Sensing the Environment: Development of Monitoring Aids for Persons with Profound Deafness or Deafblindness*. Doctoral Dissertation.
36. Magnusson, Martin (2009) *The Three-Dimensional Normal-Distributions Transform – an Efficient Representation for Registration, Surface Analysis, and Loop Detection*. Doctoral Dissertation.
37. Rahayem, Mohamed (2010) *Segmentation and fitting for Geometric Reverse Engineering. Processing data captured by a laser profile scanner mounted on an industrial robot*. Doctoral Dissertation.
38. Karlsson, Alexander (2010) *Evaluating Credal Set Theory as a Belief Framework in High-Level Information Fusion for Automated Decision-Making*. Doctoral Dissertation.
39. LeBlanc, Kevin (2010) *Cooperative Anchoring – Sharing Information About Objects in Multi-Robot Systems*. Doctoral Dissertation.
40. Johansson, Fredrik (2010) *Evaluating the Performance of TEWA Systems*. Doctoral Dissertation.
41. Trincavelli, Marco (2010) *Gas Discrimination for Mobile Robots*. Doctoral Dissertation.
42. Cirillo, Marcello (2010) *Planning in Inhabited Environments: Human-Aware Task Planning and Activity Recognition*. Doctoral Dissertation.
43. Nilsson, Maria (2010) *Capturing Semi-Automated Decision Making: The Methodology of CASADEMA*. Doctoral Dissertation.
44. Dahlbom, Anders (2011) *Petri nets for Situation Recognition*. Doctoral Dissertation.
45. Ahmed, Muhammad Rehan (2011) *Compliance Control of Robot Manipulator for Safe Physical Human Robot Interaction*. Doctoral Dissertation.
46. Riveiro, Maria (2011) *Visual Analytics for Maritime Anomaly Detection*. Doctoral Dissertation.

47. Rashid, Md. Jayedur (2011) *Extending a Networked Robot System to Include Humans, Tiny Devices, and Everyday Objects*. Doctoral Dissertation.
48. Zain-ul-Abdin (2011) *Programming of Coarse-Grained Reconfigurable Architectures*. Doctoral Dissertation.
49. Wang, Yan (2011) *A Domain-Specific Language for Protocol Stack Implementation in Embedded Systems*. Doctoral Dissertation.
50. Brax, Christoffer (2011) *Anomaly Detection in the Surveillance Domain*. Doctoral Dissertation.
51. Larsson, Johan (2011) *Unmanned Operation of Load-Haul-Dump Vehicles in Mining Environments*. Doctoral Dissertation.
52. Lidström, Kristoffer (2012) *Situation-Aware Vehicles: Supporting the Next Generation of Cooperative Traffic Systems*. Doctoral Dissertation.
53. Johansson, Daniel (2012) *Convergence in Mixed Reality-Virtuality Environments. Facilitating Natural User Behavior*. Doctoral Dissertation.
54. Stoyanov, Todor Dimitrov (2012) *Reliable Autonomous Navigation in Semi-Structured Environments using the Three-Dimensional Normal Distributions Transform (3D-NDT)*. Doctoral Dissertation.
55. Daoutis, Marios (2013) *Knowledge Based Perceptual Anchoring: Grounding percepts to concepts in cognitive robots*. Doctoral Dissertation.
56. Kristoffersson, Annica (2013) *Measuring the Quality of Interaction in Mobile Robotic Telepresence Systems using Presence, Spatial Formations and Sociometry*. Doctoral Dissertation.
57. Memedi, Mevludin (2014) *Mobile systems for monitoring Parkinson's disease*. Doctoral Dissertation.
58. König, Rikard (2014) *Enhancing Genetic Programming for Predictive Modeling*. Doctoral Dissertation.
59. Erlandsson, Tina (2014) *A Combat Survivability Model for Evaluating Air Mission Routes in Future Decision Support Systems*. Doctoral Dissertation.
60. Helldin, Tove (2014) *Transparency for Future Semi-Automated Systems. Effects of transparency on operator performance, workload and trust*. Doctoral Dissertation.

61. Krug, Robert (2014) *Optimization-based Robot Grasp Synthesis and Motion Control*. Doctoral Dissertation.
62. Reggente, Matteo (2014) *Statistical Gas Distribution Modelling for Mobile Robot Applications*. Doctoral Dissertation.
63. Långkvist, Martin (2014) *Modeling Time-Series with Deep Networks*. Doctoral Dissertation.
64. Hernández Bennetts, Víctor Manuel (2015) *Mobile Robots with In-Situ and Remote Sensors for Real World Gas Distribution Modelling*. Doctoral Dissertation.

